Elements of Gas Turbine Propulsion

Jack D. Mattingly

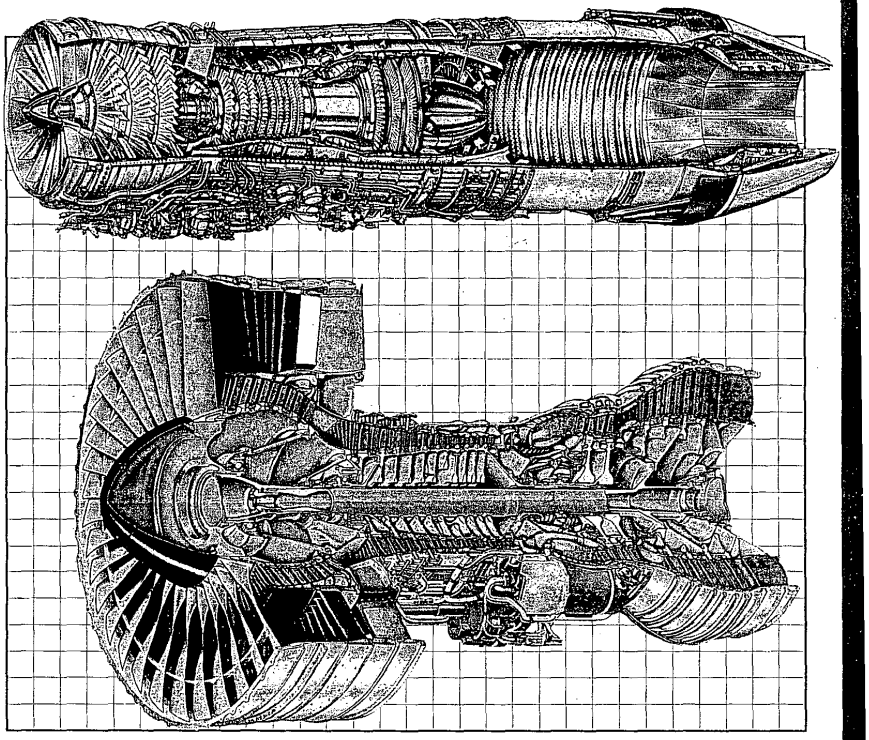

Foreword by
Hans von Ohain
German Inventor of the Jet Engine

Mattingly

Elements of Gas Turbine Propulsion

ELEMENTS OF GAS TURBINE PROPULSION

McGraw-Hill Series in Aeronautical and Aerospace Engineering

Consulting Editor

John D. Anderson, Jr., *University of Maryland*

Anderson: *Computational Fluid Dynamics: The Basics with Applications*
Anderson: *Fundamentals of Aerodynamics*
Anderson: *Hypersonic and High Temperature Gas Dynamics*
Anderson: *Introduction to Flight*
Anderson: *Modern Compressible Flow: With Historical Perspective*
Burton: *Introduction to Dynamic Systems Analysis*
D'Azzo and Houpis: *Linear Control System Analysis and Design*
Donaldson: *Analysis of Aircraft Structures: An Introduction*
Gibson: *Principles of Composite Material Mechanics*
Kane, Likins, and Levinson: *Spacecraft Dynamics*
Katz and Plotkin: *Low-Speed Aerodynamics: From Wing Theory to Panel Methods*
Mattingly: *Elements of Gas Turbine Propulsion*
Nelson: *Flight Stability and Automatic Control*
Peery and Azar: *Aircraft Structures*
Rivello: *Theory and Analysis of Flight Structures*
Schlichting: *Boundary Layer Theory*
White: *Viscous Fluid Flow*
Wiesel: *Spaceflight Dynamics*

McGraw-Hill Series in Mechanical Engineering

Consulting Editors

Anderson: *Computational Fluid Dynamics: The Basics with Applications*
Anderson: *Modern Compressible Flow: With Historical Perspective*
Arora: *Introduction to Optimum Design*
Bray and Stanley: *Nondestructive Evaluation: A Tool for Design, Manufacturing, and Service*
Burton: *Introduction to Dynamic Systems Analysis*
Culp: *Principles of Energy Conversion*
Dally: *Packaging of Electronic Systems: A Mechanical Engineering Approach*
Dieter: *Engineering Design: A Materials and Processing Approach*
Doebelin: *Engineering Experimentation: Planning, Execution, Reporting*
Driels: *Linear Control Systems Engineering*
Eckert and Drake: *Analysis of Heat and Mass Transfer*
Edwards and McKee: *Fundamentals of Mechanical Component Design*
Gebhart: *Heat Conduction and Mass Diffusion*
Gibson: *Principles of Composite Material Mechanics*
Hamrock: *Fundamentals of Fluid Film Lubrication*
Heywood: *Internal Combustion Engine Fundamentals*
Hinze: *Turbulence*
Holman: *Experimental Methods for Engineers*
Howell and Buckius: *Fundamentals of Engineering Thermodynamics*
Hutton: *Applied Mechanical Vibrations*
Juvinall: *Engineering Considerations of Stress, Strain, and Strength*
Kane and Levinson: *Dynamics: Theory and Applications*
Kays and Crawford: *Convective Heat and Mass Transfer*
Kelly: *Fundamentals of Mechanical Vibrations*
Kimbrell: *Kinematics Analysis and Synthesis*
Kreider and Rabl: *Heating and Cooling of Buildings*
Martin: *Kinematics and Dynamics of Machines*
Mattingly: *Elements of Gas Turbine Propulsion*
Modest: *Radiative Heat Transfer*
Norton: *Design of Machinery*
Phelan: *Fundamentals of Mechanical Design*
Raven: *Automatic Control Engineering*
Reddy: *An Introduction to the Finite Element Method*
Rosenberg and Karnopp: *Introduction to Physical Systems Dynamics*
Schlichting: *Boundary-Layer Theory*
Shames: *Mechanics of Fluids*
Sherman: *Viscous Flow*
Shigley: *Kinematic Analysis of Mechanisms*
Shigley and Mischke: *Mechanical Engineering Design*
Shigley and Uicker: *Theory of Machines and Mechanisms*
Stiffler: *Design with Microprocessors for Mechanical Engineers*
Stoecker and Jones: *Refrigeration and Air Conditioning*
Turns: *An Introduction to Combustion: Concepts and Applications*
Ullman: *The Mechanical Design Process*
Vanderplaats: *Numerical Optimization: Techniques for Engineering Design, with Applications*
Wark: *Advanced Thermodynamics for Engineers*
White: *Viscous Fluid Flow*
Zeid: *CAD/CAM Theory and Practice*

ELEMENTS OF GAS TURBINE PROPULSION

Jack D. Mattingly

Department of Mechanical and Manufacturing Engineering
Seattle University

With a Foreword By
Hans von Ohain

McGraw-Hill, Inc.
New York St. Louis San Francisco Auckland Bogotá Caracas
Lisbon London Madrid Mexico City Milan Montreal
New Delhi San Juan Singapore Sydney Tokyo Toronto

This book was set in Times Roman.
The editors were John J. Corrigan and James W. Bradley;
the production supervisor was Leroy A. Young.
The cover was designed by Merrill Haber.
Drawings were done by ECL Art.
R. R. Donnelley & Sons Company was printer and binder.

ELEMENTS OF GAS TURBINE PROPULSION

This book is printed on acid-free paper.

1 2 3 4 5 6 7 8 9 0 DOC DOC 9 0 9 8 7 6 5

P/N 041019-4
PART OF
ISBN 0-07-912196-9

Library of Congress Cataloging-in-Publication Data

Mattingly, Jack D. 3/13/96 dcle 31970867 dM
Elements of gas turbine propulsion / Jack D. Mattingly; with a foreword by Hans von Ohain. 3/21/96 gd.
p. cm. — (McGraw-Hill series in mechanical engineering)
(McGraw-Hill series in aeronautical and aerospace engineering)
Includes bibliographical references and index.
ISBN 0-07-912196-9 (set)
1. Airplanes—Jet propulsion. I. Title. II. Series.
III. Series: McGraw-Hill series in aeronautical and aerospace engineering.
TL709.M38 1996
629.134'353—dc20 95-897

CONTENTS

f	fuel/air ratio; function
FR	thrust ratio [Eq. (5-56)]
g	acceleration of gravity
g_c	Newton's constant
g_0	acceleration of gravity at sea level
H	enthalpy
h	enthalpy per unit mass; height
h_{PR}	low heating value of fuel
I	impulse function $[= PA(1 + \gamma M^2)]$
I_{sp}	specific impulse [Eq. (1-55)]
K	constant
L	length
M	Mach number; momentum
$\dot{M}$	time rate of change of momentum
m	mass
$\dot{m}$	mass flow rate
M	molecular weight
MFP	mass flow parameter
MR	vehicle mass ratio
N	revolutions per minute
n	load factor; burning rate exponent
n_b	number of blades
P	pressure
P_f	profile factor
P_s	weight specific excess power
P_t	total pressure
PF	pattern factor
Q	heat interaction
$\dot{Q}$	rate of heat interaction
q	heat interaction per unit mass; dynamic pressure $[=\rho V^2/(2g_c)]$
R	gas constant; extensive property; radius; additional drag
R_u	universal gas constant
r	radius; burning rate
RF	range factor [Eq. (1-43)]
$^\circ R$	degree of reaction
S	uninstalled thrust specific fuel consumption; entropy
$\dot{S}$	time rate of change of entropy
S_w	wing planform area
s	entropy per unit mass; blade spacing
T	temperature; installed thrust
T_t	total temperature
t	time; airfoil thickness
TR	throttle ratio [Eq. (8-34)]
TSFC	installed thrust specific fuel consumption

U internal energy; blade tangential or rotor velocity
u internal energy per unit mass; velocity
V absolute velocity; volume
v volume per unit mass; velocity
W weight; width
$\dot{W}$ power
w work interaction per unit mass; velocity
$\dot{w}$ weight flow rate
x, y, z coordinate system
z_e energy height [Eq. (1-25)]
Z Zweifel tangential force coefficient [Eq. (9-97)]

Greek

α bypass ratio; angle; coefficient of linear thermal expansion
β angle
Γ $= \sqrt{\gamma\left(\frac{2}{\gamma+1}\right)^{(\gamma+1)/(\gamma-1)}}$; constant
γ ratio of specific heats; angle
Δ change
δ change; dimensionless pressure ($=P/P_{ref}$); deviation
∂ partial differential
ε nozzle area ratio; rotor turning angle
η efficiency
θ angle; dimensionless temperature ($=T/T_{ref}$)
μ Mach angle
Π product
π pressure ratio defined by Eq. (5-3)
ρ density ($=1/v$)
Σ sum
σ control volume boundary; dimensionless density ($=\rho/\rho_{ref}$); tensile stress
τ temperature ratio defined by Eq. (5-4); shear stress; torque
τ_λ enthalpy ratio defined by Eq. (5-7)
ϕ installation loss coefficient; fuel equivalence ratio; function; total pressure loss coefficient
Φ function; cooling effectiveness; flow coefficient
ω angular speed

Subscripts

A air mass
a air; atmosphere

AB	afterburner
add	additive
b	burner or combustor; boattail or afterbody; blade; burning
C	core stream
c	compressor; corrected; centrifugal; chamber
DB	duct burner
d	diffuser or inlet; disk
dr	disk/rim interface
dry	afterburner not operating
e	exit; exhaust; earth
ext	external
F	fan stream
f	fan; fuel; final
fn	fan nozzle
g	gearing; gas
H	high-pressure
HP	horsepower
h	hub
i	initial; inside; ideal
int	internal
j	jet
L	low-pressure
M	mixer
m	mechanical; mean; middle
max	corresponding to maximum
N	new
n	nozzle
nac	nacelle
O	overall; output
o	overall; outer
opt	optimum
P	propulsive; products
p	propellant
pl	payload
prop	propeller
R	reference; relative; reactants
r	ram; reduced; rim; rotor
ref	reference condition
s	stage; separation; solid; stator
SL	sea-level
SLS	sea-level static
T	thermal
t	total; turbine; throat; tip; thermal
vac	vacuum
w	forebody; wing

CHAPTER 1

INTRODUCTION

1-1 PROPULSION

The *Random House College Dictionary* (Ref. 1) defines *propulsion* as "the act of propelling, the state of being propelled, a propelling force or impulse" and defines the verb *propel* as "to drive, or cause to move, forward or onward." From these definitions, we can conclude that the study of propulsion includes the study of the propelling force, the motion caused, and the bodies involved. Propulsion involves an object to be propelled plus one or more additional bodies, called *propellant.*

The study of propulsion is concerned with vehicles such as automobiles, trains, ships, aircraft, and spacecraft. The focus of this textbook is on the propulsion of aircraft and spacecraft. Methods devised to produce a thrust force for the propulsion of a vehicle in flight are based on the principle of jet propulsion (the momentum change of a fluid by the propulsion system). The fluid may be the gas used by the engine itself (e.g., turbojet), it may be a fluid available in the surrounding environment (e.g., air used by a propeller), or it may be stored in the vehicle and carried by it during the flight (e.g., rocket).

Jet propulsion systems can be subdivided into two broad categories: air-breathing and non-air-breathing. Air-breathing propulsion systems include the reciprocating, turbojet, turbofan, ramjet, turboprop, and turboshaft engines. Non-air-breathing engines include rocket motors, nuclear propulsion systems, and electric propulsion systems. We focus on gas turbine propulsion systems (turbojet, turbofan, turboprop, and turboshaft engines) in this textbook.

The material in this textbook is divided into three parts:

- Basic concepts and one-dimensional gas dynamics
- Analysis and performance of air-breathing propulsion systems
- Analysis of gas turbine engine components

This chapter introduces the types of air-breathing and rocket propulsion systems and the basic propulsion performance parameters. Also included is an introduction to aircraft and rocket performance. The material on aircraft performance shows the influence of the gas turbine engine performance on the performance of the aircraft system. This material also permits incorporation of a gas turbine engine design problem such as new engines for an existing aircraft.

Numerous examples are included throughout this book to help students see the application of a concept after it is introduced. For some students, the material on basic concepts and gas dynamics will be a review of material covered in other courses they have already taken. For other students, this may be their first exposure to this material, and it may require more effort to understand.

1-2 UNITS AND DIMENSIONS

Since the engineering world uses both the metric SI and English unit system, both will be used in this textbook. One singular distinction exists between the English system and SI—the unit of force is defined in the former but derived in the latter. Newton's second law of motion relates force to mass, length, and time. It states that the sum of the forces is proportional to the rate of change of the momentum ($\mathbf{M} = m\mathbf{V}$). The constant of proportionality is $1/g_c$.

$$\sum \mathbf{F} = \frac{1}{g_c}\frac{d(m\mathbf{V})}{dt} = \frac{1}{g_c}\frac{d\mathbf{M}}{dt} \tag{1-1}$$

The units for each term in the above equation are listed in Table 1-1 for both SI and English units. In any unit system, only four of the five items in the table can be specified, and the latter is derived from Eq. (1-1).

As a result of selecting $g_c = 1$ and defining the units of mass, length, and time in SI units, the unit of force is derived from Eq. (1-1) as

TABLE 1-1
Units and dimensions

Unit system	Force	g_c	Mass	Length	Time
SI	Derived	1	Kilogram (kg)	Meter (m)	Second (sec)
English	Pound-force (lbf)	Derived	Pound-mass (lbm)	Foot (ft)	Second (sec)

kilogram-meters per square second ($kg \cdot m/sec^2$), which is called the *newton* (N). In English units, the value of g_c is derived from Eq. (1-1) as

$$\boxed{g_c = 32.174 \text{ ft} \cdot \text{lbm}/(\text{lbf} \cdot \text{sec}^2)}$$

Rather than adopt the convention used in many recent textbooks of developing material or use with *only* SI metric units ($g_c = 1$), we will maintain g_c in all our equations. Thus g_c will also show up in the equations for *potential energy* (PE) and *kinetic energy* (KE):

$$\text{PE} = \frac{mgz}{g_c}$$

$$\text{KE} = \frac{mV^2}{2g_c}$$

The total energy per unit mass e is the sum of the specific internal energy u, specific kinetic energy ke, and specific potential energy pe.

$$e \equiv u + \text{ke} + \text{pe} = u + \frac{V^2}{2g_c} + \frac{gz}{g_c}$$

There are a multitude of engineering units for the quantities of interest in propulsion. For example, energy can be expressed in the SI unit of *joule* ($1 \text{ J} = 1 \text{ N} \cdot \text{m}$), in British thermal units (Btu's), or in foot-pound force ($\text{ft} \cdot \text{lbf}$). One must be able to use the available data in the units provided and convert the units when required. Table 1-2 is a unit conversion table provided to help you in your endeavors.

TABLE 1-2
Unit conversion table

Length	$1 \text{ m} = 3.2808 \text{ ft} = 39.37 \text{ in}$
	$1 \text{ km} = 0.621 \text{ mi}$
	$1 \text{ mi} = 5280 \text{ ft} = 1.609 \text{ km}$
	$1 \text{ nm} = 6080 \text{ ft} = 1.853 \text{ km}$
Area	$1 \text{ m}^2 = 10.764 \text{ ft}^2$
	$1 \text{ cm}^2 = 0.155 \text{ in}^2$
Volume	$1 \text{ gal} = 0.13368 \text{ ft}^3 = 3.785 \text{ L}$
	$1 \text{ L} = 10^{-3} \text{ m}^3 = 61.02 \text{ in}^3$
Time	$1 \text{ hr} = 3600 \text{ sec} = 60 \text{ min}$
Mass	$1 \text{ kg} = 1000 \text{ g} = 2.2046 \text{ lbm} = 6.8521 \times 10^{-2} \text{ slug}$
	$1 \text{ slug} = 1 \text{ lbf} \cdot \text{sec}^2/\text{ft} = 32.174 \text{ lbm}$
Density	$1 \text{ slug/ft}^3 = 512.38 \text{ kg/m}^3$
Force	$1 \text{ N} = 1 \text{ kg} \cdot \text{m/sec}^2$
	$1 \text{ lbf} = 4.448 \text{ N}$
Energy	$1 \text{ J} = 1 \text{ N} \cdot \text{m} = 1 \text{ kg} \cdot \text{m}^2/\text{sec}^2$
	$1 \text{ Btu} = 778.16 \text{ ft} \cdot \text{lbf} = 252 \text{ cal} = 1055 \text{ J}$
	$1 \text{ cal} = 4.186 \text{ J}$
	$1 \text{ kJ} = 0.947813 \text{ Btu} = 0.23884 \text{ kcal}$

Power	$1\ W = 1\ J/sec = 1\ kg \cdot m^2/sec^3$
	$1\ hp = 550\ ft \cdot lbf/sec = 2545\ Btu/hr = 745.7\ W$
	$1\ kW = 3412\ Btu/hr = 1.341\ hp$
Pressure (stress)	$1\ atm = 14.696\ lb/in^2$ or psi $= 760$ torr $= 101{,}325\ Pa$
	$1\ atm = 30.0\ inHg = 407.2\ inH_2O$
	$1\ ksi = 1000$ psi
	$1\ mmHg = 0.01934$ psi $= 1$ torr
	$1\ Pa = 1\ N/m^2$
	$1\ inHg = 3376.8\ Pa$
Energy per unit mass	$1\ kJ/kg = 0.4299\ Btu/lbm$
Specific heat	$1\ kJ/(kg \cdot °C) = 0.23884\ Btu/(lbm \cdot °F)$
Temperature	$1\ K = 1.8°R$
	$K = 273.15 + °C$
	$°R = 459.69 + °F$
Temperature change	$1°C = 1.8°F$
Specific thrust	$1\ lbf/(lbm/sec) = 9.8067\ N/(kg/sec)$
Specific power	$1\ hp/(lbm/sec) = 1.644\ kW/(kg/sec)$
Thrust specific fuel consumption (TSFC)	$1\ lbm/(lbf \cdot hr) = 28.325\ mg/(N \cdot sec)$
Power specific fuel consumption	$1\ lbm/(hp \cdot hr) = 168.97\ mg/(kW \cdot sec)$
Strength/weight ratio (σ/ρ)	$1\ ksi/(slug/ft^3) = 144\ ft^2/sec^2 = 13.38\ m^2/sec^2$

1-3 OPERATIONAL ENVELOPES AND STANDARD ATMOSPHERE

Each engine type will operate only within a certain range of altitudes and Mach numbers (velocities). Similar limitations in velocity and altitude exist for airframes. It is necessary, therefore, to match airframe and propulsion system capabilities. Figure 1-1 shows the approximate velocity and altitude limits, or *corridor of flight,* within which airlift vehicles can operate. The corridor is bounded by a *lift limit,* a *temperature limit,* and an *aerodynamic force limit.* The lift limit is determined by the maximum level-flight altitude at a given velocity. The temperature limit is set by the structural thermal limits of the material used in construction of the aircraft. At any given altitude, the maximum velocity attained is temperature-limited by aerodynamic heating effects. At lower altitudes, velocity is limited by aerodynamic force loads rather than by temperature.

The operating regions of all aircraft lie within the flight corridor. The operating region of a particular aircraft within the corridor is determined by aircraft design, but it is a very small portion of the overall corridor. Superimposed on the flight corridor in Fig. 1-1 are the operational envelopes of various powered aircraft. The operational limits of each propulsion system are determined by limitations of the components of the propulsion system and are shown in Fig. 1-2.

The analyses presented in this text use the properties of the atmosphere to determine both engine and airframe performance. Since these properties vary with location, season, time of day, etc., we will use the U.S. standard

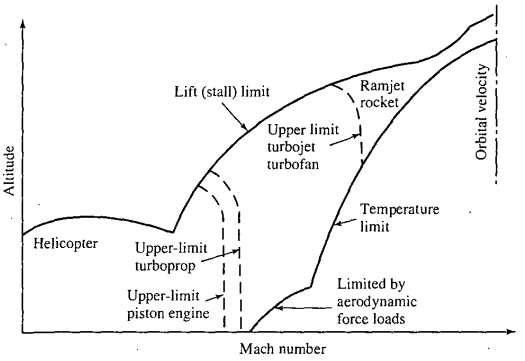

FIGURE 1-1
Flight limits.

atmosphere (Ref. 2) to give a known foundation for our analyses. Appendix A gives the properties of the U.S. standard atmosphere, 1976, in both English and SI units. Values of the pressure P, temperature T, density ρ, and speed of sound a are given in dimensionless ratios of the property at altitude to its value at sea level (SL), (the reference value). The dimensionless ratios of pressure, temperature, and density are given the symbols δ, θ, and σ,

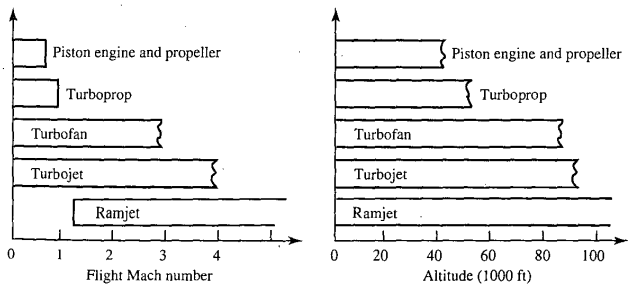

FIGURE 1-2
Engine operational limits.

respectively. These ratios are defined as follows:

$$\delta \equiv \frac{P}{P_{\text{ref}}} \tag{1-2}$$

$$\theta \equiv \frac{T}{T_{\text{ref}}} \tag{1-3}$$

$$\sigma \equiv \frac{\rho}{\rho_{\text{ref}}} \tag{1-4}$$

The reference values of pressure, temperature, and density are given for each unit system at the end of its property table.

For nonstandard conditions such as a hot day, the normal procedure is to use the standard pressure and correct the density, using the perfect gas relationship $\sigma = \delta/\theta$. As an example, we consider a 100°F day at 4-kft altitude. From App. A, we have $\delta = 0.8637$ for the 4-kft altitude. We calculate θ, using the 100°F temperature; $\theta = T/T_{\text{ref}} = (100 + 459.7)/518.7 = 1.079$. Note that absolute temperatures must be used in calculating θ. Then the density ratio is calculated using $\sigma = \delta/\theta = 0.8637/1.079 = 0.8005$.

1-4 AIR-BREATHING ENGINES

The turbojet, turbofan, turboprop, turboshaft, and ramjet engine systems are discussed in this part of Chap. 1. The discussion of these engines is in the context of providing thrust for aircraft. The listed engines are not all the engine types (reciprocating, rockets, combination types, etc.) that are used in providing propulsive thrust to aircraft, nor are they used exclusively on aircraft. The thrust of the turbojet and ramjet results from the action of a fluid jet leaving the engine; hence, the name *jet engine* is often applied to these engines. The turbofan, turboprop, and turboshaft engines are adaptations of the turbojet to supply thrust or power through the use of fans, propellers, and shafts.

Gas Generator

The "heart" of a gas turbine type of engine is the gas generator. A schematic diagram of a gas generator is shown in Fig. 1-3. The compressor, combustor, and turbine are the major components of the gas generator which is common to the turbojet, turbofan, turboprop, and turboshaft engines. The purpose of a gas generator is to supply high-temperature and high-pressure gas.

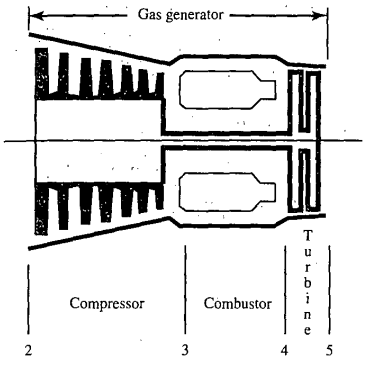

FIGURE 1-3
Schematic diagram of gas generator.

The Turbojet

By adding an inlet and a nozzle to the gas generator, a turbojet engine can be constructed. A schematic diagram of a simple turbojet is shown in Fig. 1-4*a*, and a turbojet with afterburner is shown in Fig. 1-4*b*. In the analysis of a turbojet engine, the major components are treated as sections. Also shown in Figs. 1-4*a* and 1-4*b* are the station numbers for each section.

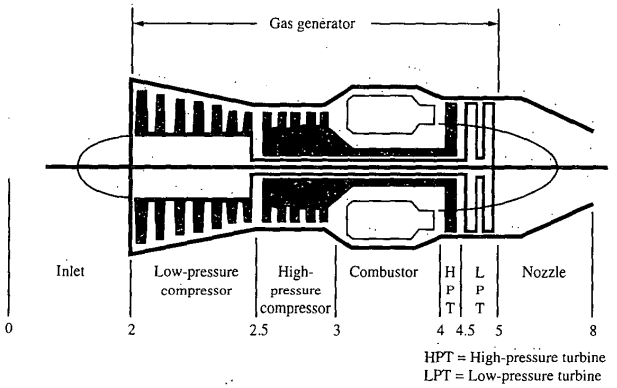

FIGURE 1-4*a*
Schematic diagram of a turbojet (dual axial compressor and turbine).

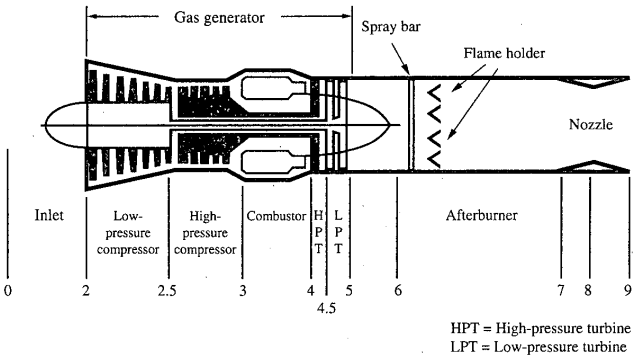

FIGURE 1-4*b*
Schematic diagram of a turbojet with afterburner.

The turbojet was first used as a means of aircraft propulsion by von Ohain (first flight August 27, 1939) and Whittle (first flight May 15, 1941). As development proceeded, the turbojet engine became more efficient and replaced some of the piston engines. A photograph of the J79 turbojet with afterburner used in the F-4 Phantom II and B-58 Hustler is shown in Fig. 1-5.

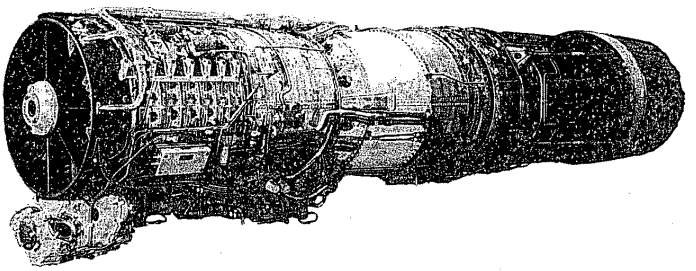

FIGURE 1-5
General Electric J79 turbojet with afterburner. (*Courtesy of General Electric Aircraft Engines.*)

The adaptations of the turbojet in the form of turbofan, turboprop, and turboshaft engines came with the need for more thrust at relatively low speeds. Some characteristics of different turbojet, turbofan, turboprop, and turboshaft engines are included in App. B.

The thrust of a turbojet is developed by compressing air in the inlet and compressor, mixing the air with fuel and burning in the combustor, and expanding the gas stream through the turbine and nozzle. The expansion of gas through the turbine supplies the power to turn the compressor. The net thrust delivered by the engine is the result of converting internal energy to kinetic energy.

The pressure, temperature, and velocity variations through a J79 engine are shown in Fig. 1-6. In the compressor section, the pressure and temperature increase as a result of work being done on the air. The temperature of the gas is further increased by burning in the combustor. In the turbine section, energy is being removed from the gas stream and converted to shaft power to turn the compressor. The energy is removed by an expansion process which results in a decrease of temperature and pressure. In the nozzle, the gas stream is further expanded to produce a high exit kinetic energy. All the sections of the engine must operate in such a way as to efficiently produce the greatest amount of thrust for a minimum of weight.

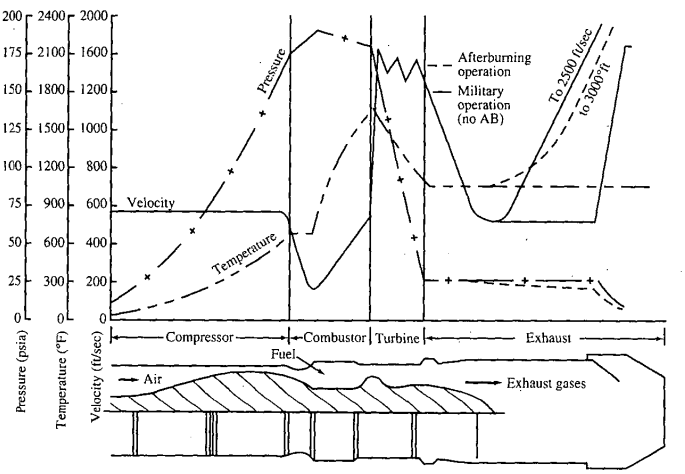

FIGURE 1-6
Property variation through the General Electric J79 afterburning turbojet engine.

The Turbofan

The turbofan engine consists of an inlet, fan, gas generator, and nozzle. A schematic diagram of a turbofan is shown in Fig. 1-7. In the turbofan, a portion of the turbine work is used to supply power to the fan. Generally the turbofan engine is more economical and efficient than the turbojet engine in a limited realm of flight. The *thrust specific fuel consumption* (TSFC, or fuel mass flow rate per unit thrust) is lower for turbofans and indicates a more economical operation. The turbofan also accelerates a larger mass of air to a lower velocity than a turbojet for a higher propulsive efficiency. The frontal area of a turbofan is quite large compared to that of a turbojet, and for this reason more drag and more weight result. The fan diameter is also limited aerodynamically when compressibility effects occur. Several of the current high-bypass-ratio turbofan engines used in subsonic aircraft are shown in Figs. 1-8*a* through 1-8*f*.

Figures 1-9*a* and 1-9*b* show the Pratt & Whitney F100 turbofan and the General Electric F110 turbofan, respectively. These afterburning turbofan engines are used in the F15 Eagle and F16 Falcon supersonic fighter aircraft. In this turbofan, the bypass stream is mixed with the core stream before passing through a common afterburner and exhaust nozzle.

The Turboprop and Turboshaft

A gas generator that drives a propeller is a turboprop engine. The expansion of gas through the turbine supplies the energy required to turn the propeller. A

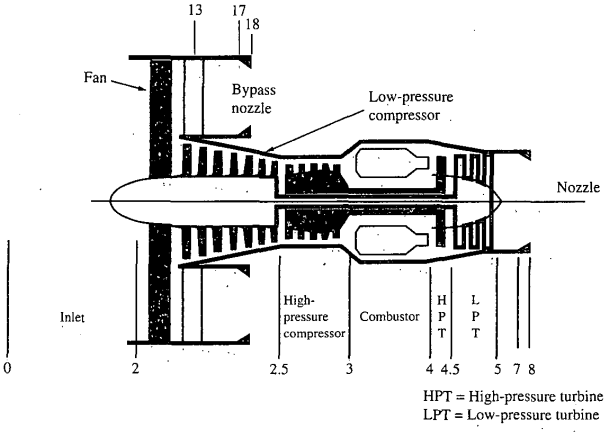

FIGURE 1-7
Schematic diagram of a high-bypass-ratio turbofan.

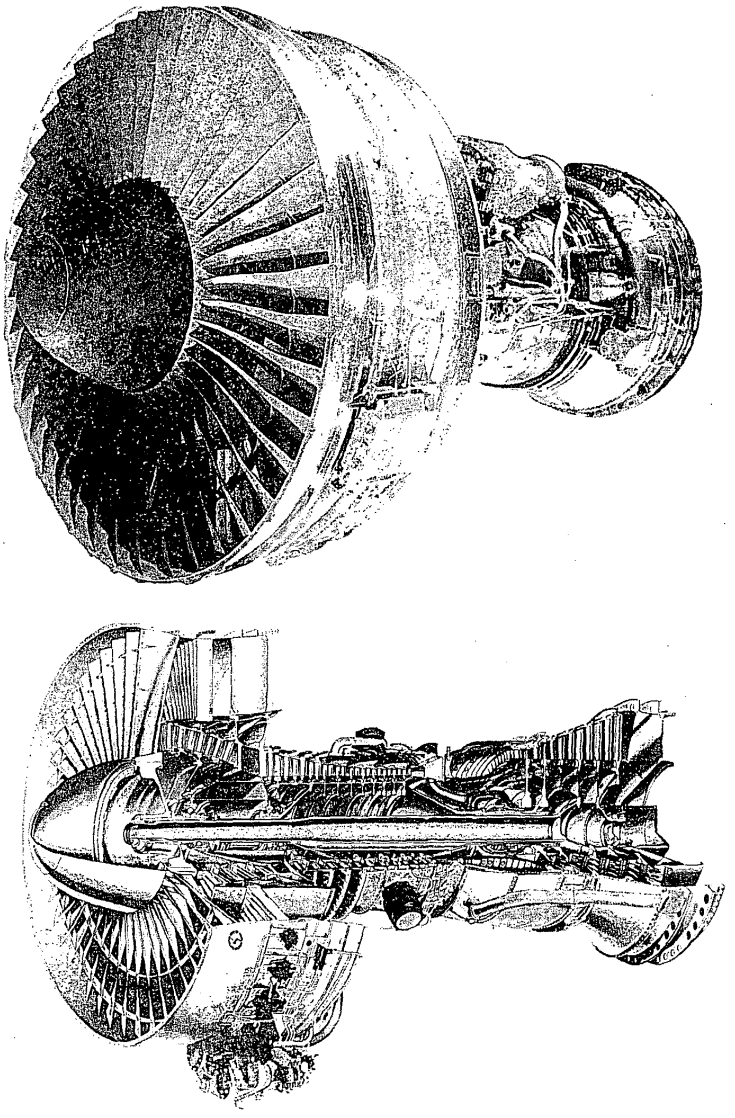

FIGURE 1-8*a*
Pratt & Whitney JT9D turbofan. (*Courtesy of Pratt & Whitney.*)

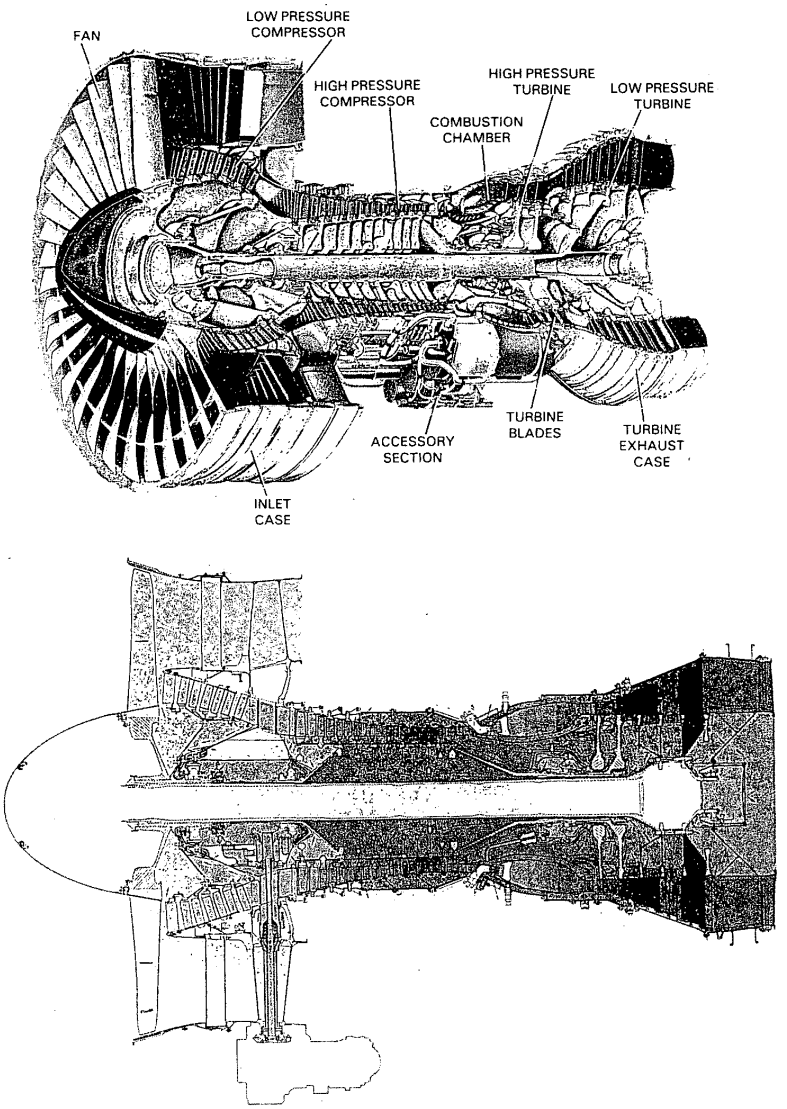

FIGURE 1-8*b*
Pratt & Whitney PW4000 turbofan. (*Courtesy of Pratt & Whitney.*)

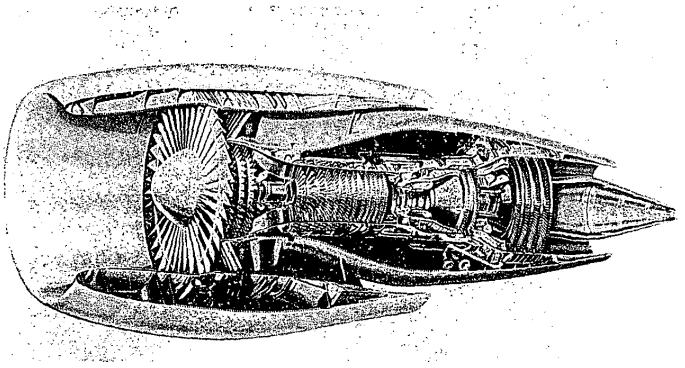

FIGURE 1-8*c*
General Electric CF6 turbofan. (*Courtesy of General Electric Aircraft Engines.*)

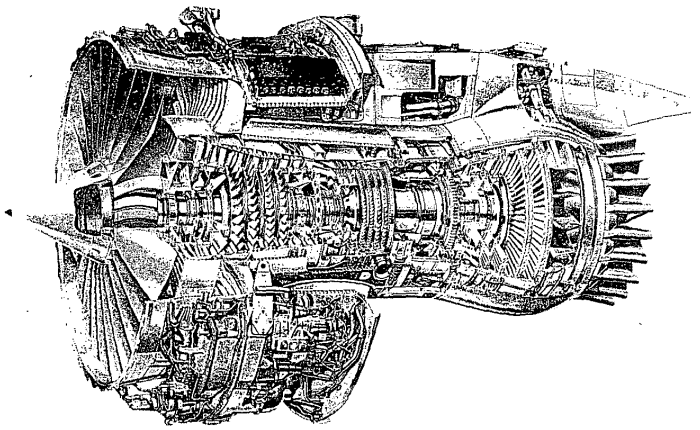

FIGURE 1-8*d*
Rolls-Royce RB-211-524G/H turbofan. (*Courtesy of Rolls-Royce.*)

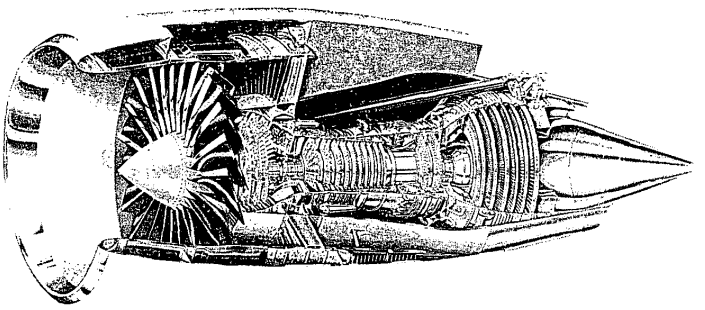

FIGURE 1-8*e*
General Electric GE90 turbofan. (*Courtesy of General Electric Aircraft Engines.*)

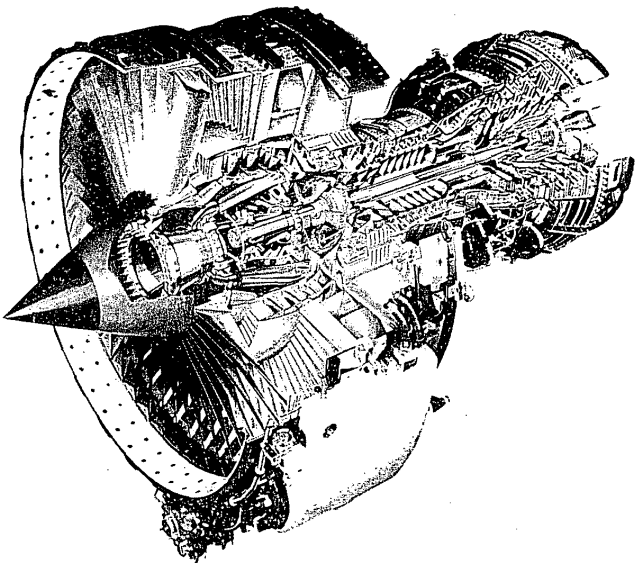

FIGURE 1-8*f*
SNECMA CFM56 turbofan. (*Courtesy of SNECMA.*)

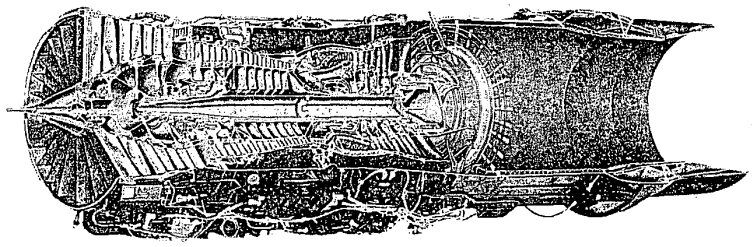

FIGURE 1-9*a*
Pratt & Whitney F100-PW-229 afterburning turbofan. (*Courtesy of Pratt & Whitney.*)

schematic diagram of the turboprop is shown in Fig. 1-10*a*. The turboshaft engine is similar to the turboprop except that power is supplied to a shaft rather than a propeller. The turboshaft engine is used quite extensively for supplying power for helicopters. The turboprop engine may find application in VTOL (vertical takeoff and landing) transporters. The limitations and advantages of the turboprop are those of the propeller. For low-speed flight and short-field takeoff, the propeller has a performance advantage. At speeds approaching the speed of sound, compressibility effects set in and the propeller loses its aerodynamic efficiency. Due to the rotation of the propeller, the propeller tip will approach the speed of sound before the vehicle approaches

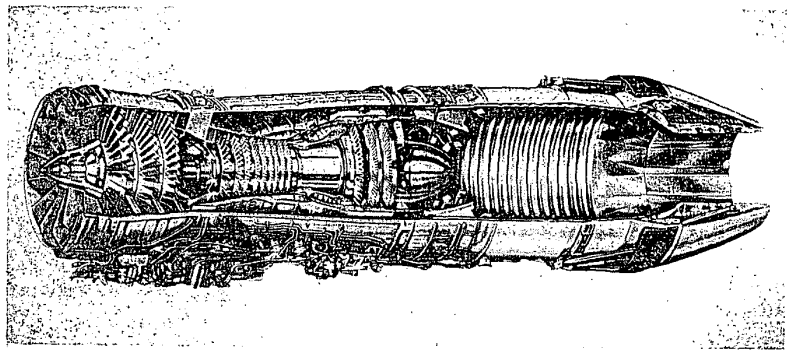

FIGURE 1-9*b*
General Electric F110-GE-129 afterburning turbofan. (*Courtesy of General Electric Aircraft Engines.*)

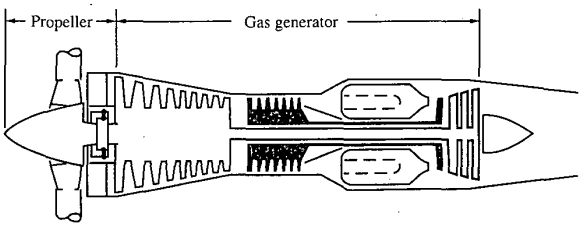

FIGURE 1-10*a*
Schematic diagram of a turboprop.

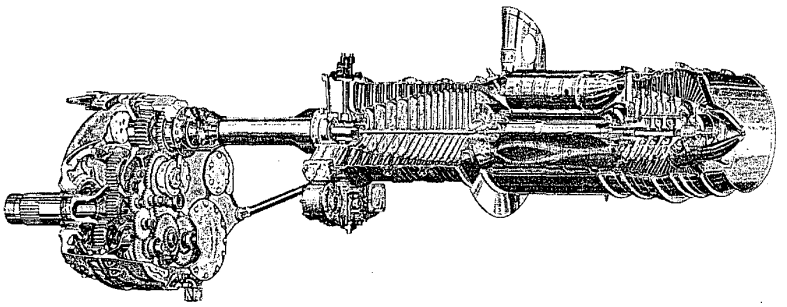

FIGURE 1-10*b*
Allison T56 turboshaft. (*Courtesy of Allison Gas Turbine Division.*)

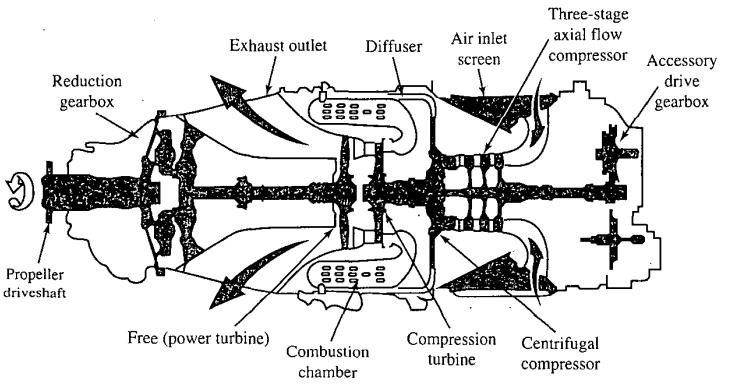

FIGURE 1-10*c*
Canadian Pratt & Whitney PT6 turboshaft. (*Courtesy of Pratt & Whitney of Canada.*)

the speed of sound. This compressibility effect when one approaches the speed of sound limits the design of helicopter rotors and propellers. At high subsonic speeds, the turbofan engine will have a better aerodynamic performance than the turboprop since the turbofan is essentially a *ducted turboprop.* Putting a duct or shroud around a propeller increases its aerodynamic performance. Examples of a turboshaft engine are the Canadian Pratt & Whitney PT6 (Fig. 1-10*c*), used in many small commuter aircraft, and the Allison T56 (Fig. 1-10*b*), used to power the C-130 Hercules and the P-3 Orion.

The Ramjet

The ramjet engine consists of an inlet, a combustion zone, and a nozzle. A schematic diagram of a ramjet is shown in Fig. 1-11. The ramjet does not have the compressor and turbine as the turbojet does. Air enters the inlet where it is compressed and then enters the combustion zone where it is mixed with the fuel and burned. The hot gases are then expelled through the nozzle, developing thrust. The operation of the ramjet depends upon the inlet to decelerate the incoming air to raise the pressure in the combustion zone. The pressure rise makes it possible for the ramjet to operate. The higher the velocity of the incoming air, the greater the pressure rise. It is for this reason that the ramjet operates best at high supersonic velocities. At subsonic velocities, the ramjet is inefficient, and to start the ramjet, air at a relatively higher velocity must enter the inlet.

The combustion process in an ordinary ramjet takes place at low subsonic velocities. At high supersonic flight velocities, a very large pressure rise is developed that is more than sufficient to support operation of the ramjet. Also, if the inlet has to decelerate a supersonic high-velocity airstream to a subsonic velocity, large pressure losses can result. The deceleration process also produces a temperature rise, and at some limiting flight speed, the temperature will approach the limit set by the wall materials and cooling methods. Thus when the temperature increase due to deceleration reaches the limit, it may not be possible to burn fuel in the airstream.

In the past few years, research and development have been done on a ramjet that has the combustion process taking place at supersonic velocities.

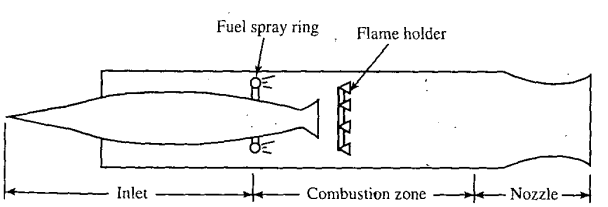

FIGURE 1-11
Schematic diagram of a ramjet.

By using a supersonic combustion process, the temperature rise and pressure loss due to deceleration in the inlet can be reduced. This ramjet with supersonic combustion is known as the *scramjet* (*s*upersonic *c*ombustion *ramjet*). Figure 1-12*a* shows the schematic of a scramjet engine similar to that proposed for the National AeroSpace Plane (NASP) research vehicle, the X-30 shown in Fig. 1-12*b*. Further development of the scramjet for other applications (e.g., the Orient Express) will continue if research and development produces a scramjet engine with sufficient performance gains. Remember that since it takes a relative velocity to start the ramjet or scramjet, another engine system is required to accelerate aircraft like the X-30 to ramjet velocities.

Turbojet/Ramjet Combined-Cycle Engine

Two of the Pratt & Whitney J58 turbojet engines (see Fig. 1-13*a*) are used to power the Lockheed SR71 Blackbird (see Fig. 1-13*b*). This was the fastest aircraft (Mach 3+) when it was retired in 1989. The J58 operates as an afterburning turbojet engine until it reaches high Mach level, at which point the six large tubes (Fig. 1-13*a*) bypass flow to the afterburner. When these tubes are in use, the compressor, burner, and turbine of the turbojet are essentially bypassed and the engine operates as a ramjet with the afterburner acting as the ramjet's burner.

Aircraft Engine Performance Parameters

This section presents several of the air-breathing engine performance parameters that are useful in aircraft propulsion. The first performance parameter is the thrust of the engine which is available for sustained flight (thrust = drag), accelerated flight (thrust > drag), or deceleration (thrust < drag).

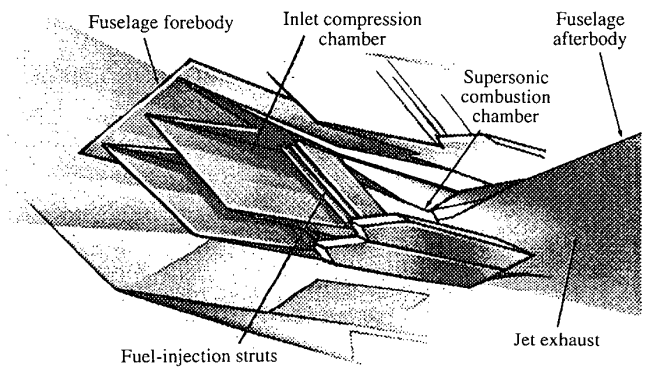

FIGURE 1-12*a*
Schematic diagram of a scramjet.

The velocity of a rocket along its trajectory can be determined from the above equation if C, D, g, and θ are known.

In the absence of drag and gravity, integration of Eq. (1-58) gives the following, assuming constant effective exhaust velocity C:

$$\boxed{\Delta V = C \ln \frac{m_i}{m_f}} \tag{1-59}$$

where ΔV is the change in velocity, m_i is the initial mass of the rocket system, and m_f is the final mass. Equation (1-59) can be solved for the mass ratio as

$$\boxed{\frac{m_i}{m_f} = \exp \frac{\Delta V}{C}} \tag{1-60}$$

Example 1-10. We want to estimate the mass ratio (final to initial) of an H_2-O_2 ($C = 4000$ m/sec) rocket for an earth orbit ($\Delta V = 8000$ m/sec), neglecting drag and gravity. Using Eq. (1-59), we obtain $m_f/m_i = e^{-2} = 0.132$, or a single-stage rocket would be about 13 percent payload and structure and 87 percent propellant.

PROBLEMS

1-1. Calculate the uninstalled thrust for Example 1-1, using Eq. (1-6).

1-2. Develop the following analytical expressions for a turbojet engine:

a. When the fuel flow rate is very small in comparison with the air mass flow rate, the exit pressure is equal to ambient pressure, and the installation loss coefficients are zero, then the installed thrust T is given by

$$T = \frac{\dot{m}_0}{g_c}(V_e - V_0)$$

b. For the above conditions, the thrust specific fuel consumption is given by

$$\text{TSFC} = \frac{Tg_c/\dot{m}_0 + 2V_0}{2\eta_T h_{PR}}$$

c. For $V_0 = 0$ and 500 ft/sec, plot the above equation for TSFC [in (lbm/hr)/lbf] versus specific thrust $T/\dot{m}_0$ [in lbf/(lbm/sec)] for values of specific thrust from 0 to 120. Use $\eta_T = 0.4$ and $h_{PR} = 18{,}400$ Btu/lbm.

d. Explain the trends.

1-3. Repeat 1-2*c*, using SI units. For $V_0 = 0$ to 150 m/sec, plot TSFC [in (mg/sec)/N] versus specific thrust $T/\dot{m}_0$ [in N/(kg/sec)] for values of specific thrust from 0 to 1200. Use $\eta_T = 0.4$ and $h_{PR} = 42{,}800$ kJ/kg.

1-4. A J57 turbojet engine is tested at sea-level, static, standard-day conditions ($P_0 = 14.696$ psia, $T_0 = 518.7$°R, and $V_0 = 0$). At one test point, the thrust is 10,200 lbf while the airflow is 164 lbm/sec and the fuel flow is 8520 lbm/hr. Using these data, estimate the exit velocity V_e for the case of exit pressure equal to ambient pressure ($P_0 = P_e$).

1-5. The thrust for a turbofan engine with separate exhaust streams is equal to the sum of the thrust from the engine core F_C and the thrust from the bypass stream F_B. The bypass ratio of the engine α is the ratio of the mass flow through the bypass stream to the core mass flow, or $\alpha \equiv \dot{m}_B/\dot{m}_C$. When the exit pressures are equal to the ambient pressure, the thrusts of the core and bypass stream are given by

$$F_C = \frac{1}{g_c}[(\dot{m}_C + \dot{m}_f)V_{Ce} - \dot{m}_C V_0]$$

$$F_B = \frac{\dot{m}_B}{g_c}(V_{Be} - V_0)$$

where V_{Ce} and V_{Be} are the exit velocities from the core and bypass, respectively, V_0 is the inlet velocity, and $\dot{m}_f$ is the mass flow rate of fuel burned in the core of the engine.

Show that the specific thrust and thrust specific fuel consumption can be expressed as

$$\frac{F}{\dot{m}_0} = \frac{1}{g_c}\left(\frac{1 + \dot{m}_f/\dot{m}_C}{1+\alpha}V_{Ce} + \frac{\alpha}{1+\alpha}V_{Be} - V_0\right)$$

$$S = \frac{\dot{m}_f}{F} = \frac{\dot{m}_f/\dot{m}_C}{(F/\dot{m}_0)(1+\alpha)}$$

where $\dot{m}_0 = \dot{m}_C + \dot{m}_B$.

1-6. The CF6 turbofan engine has a rated thrust of 40,000 lbf at a fuel flow rate of 13,920 lbm/hr at sea-level static conditions. If the core airflow rate is 225 lbm/sec and the bypass ratio is 6.0, what are the specific thrust [lbf/(lbm/sec)] and thrust specific fuel consumption [(lbm/hr)/lbf]?

1-7. The JT9D high-bypass-ratio turbofan engine at maximum static power ($V_0 = 0$) on a sea-level, standard day ($P_0 = 14.696$ psia, $T_0 = 518.7°$R) has the following data: the air mass flow rate through the core is 247 lbm/sec, the air mass flow rate through the fan bypass duct is 1248 lbm/sec, the exit velocity from the core is 1190 ft/sec, the exit velocity from the bypass duct is 885 ft/sec and the fuel flow rate into the combustor is 15,750 lbm/hr. Estimate the following for the case of exit pressures equal to ambient pressure ($P_0 = P_e$):

a. The thrust of the engine

b. The thermal efficiency of the engine (heating value of jet fuel is about 18,400 Btu/lbm)

c. The propulsive efficiency and thrust specific fuel consumption of the engine

1-8. Repeat Prob. 1-7, using SI units.

1-9. One advanced afterburning fighter engine, whose performance is depicted in Figs. 1-14*a* through 1-14*e*, is installed in the HF-1 fighter aircraft. Using the aircraft drag data of Fig. 1-26*b*, determine and plot the variation of weight specific excess power (P_s in feet per second) versus flight Mach number for level flight ($n = 1$) at 36-kft altitude. Assume the installation losses are constant with values of $\phi_{\text{inlet}} = 0.05$ and $\phi_{\text{noz}} = 0.02$.

1-10. Determine the takeoff speed of the HF-1 aircraft.

1-11. Determine the takeoff speed of the HP-1 aircraft at 90 percent of maximum gross takeoff weight.

1-12. Derive Eqs. (1-47) and (1-48) for maximum C_L/C_D. Start by taking the derivative of Eq. (1-46) with respect to C_L and finding the expression for the lift coefficient that gives maximum C_L/C_D.

1-13. Show that for maximum C_L/C_D, the corresponding drag coefficient C_D is given by

$$C_D = 2C_{D0} + K_2\sqrt{\frac{C_{D0}}{K_1}}$$

1-14. An aircraft with a wing area of 800 ft^2 is in level flight ($n = 1$) at maximum C_L/C_D. Given that the drag coefficients for the aircraft are $C_{D0} = 0.02$, $K_2 = 0$, and $K_1 = 0.2$, find

a. The maximum C_L/C_D and the corresponding values of C_L and C_D

b. The flight altitude [use Eqs. (1-29) and (1-30*b*)] and aircraft drag for an aircraft weight of 45,000 lbf at Mach 0.8

c. The flight altitude and aircraft drag for an aircraft weight of 35,000 lbf at Mach 0.8

d. The range for an installed engine thrust specific fuel consumption rate of 0.8 (lbm/hr)/lbf, if the 10,000-lbf difference in aircraft weight between parts *b* and *c* above is due only to fuel consumption

1-15. An aircraft weighing 110,000 N with a wing area of 42 m^2 is in level flight ($n = 1$) at the maximum value of C_L/C_D. Given that the drag coefficients for the aircraft are $C_{D0} = 0.03$, $K_2 = 0$, and $K_1 = 0.25$, find the following:

a. The maximum C_L/C_D and the corresponding values of C_L and C_D

b. The flight altitude [use Eqs. (1-29) and (1-30*b*)] and aircraft drag at Mach 0.5

c. The flight altitude and aircraft drag at Mach 0.75

1-16. The Breguet range equation [Eq. (1-45*b*)] applies for a cruise climb flight profile with constant range factor RF. Another range equation can be developed for a level cruise flight profile with varying RF. Consider the case where we keep C_L, C_D, and TSFC constant and vary the flight velocity with aircraft weight by the expression

$$V = \sqrt{\frac{2g_c W}{\rho C_L S_w}}$$

Using the subscripts i and f for the initial and final flight conditions, respectively, show the following:

a. Substitution of this expression for flight velocity into Eq. (1-42) gives

$$\frac{dW}{\sqrt{W}} = -\frac{\sqrt{W_i}}{\mathrm{RF}_i}\,ds$$

b. Integration of the above between the initial i and final f conditions gives

$$\frac{W_f}{W_i} = \left[1 - \frac{s}{2(\mathrm{RF}_i)}\right]^2$$

c. For a given weight fraction W_f/W_i, the maximum range s for this level cruise flight corresponds to starting the flight at the maximum altitude (minimum density) and maximum value of $\sqrt{C_L}/C_D$.

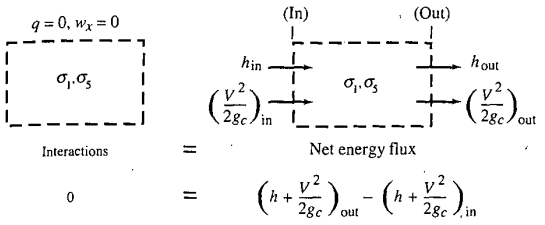

FIGURE 2-12*b*
Energy equation applied to control volumes σ_1 and σ_5.

Solution. From the steady flow energy equation with 5 and 6 the in and out stations respectively, we have

$$h_6 + \frac{V_6^2}{2g_c} = h_5 + \frac{V_5^2}{2g_c}$$

and $$V_6 = \sqrt{2g_c(h_5 - h_6) + V_5^2} = \sqrt{2c_p g_c(T_5 - T_6) + V_5^2}$$

or $$= \sqrt{2(6000)(1800 - 1200) + 400^2}$$

so $$= 2700 \text{ ft/sec}$$

b. Compressor and turbine: σ_2 and σ_4. The heat interactions at control surfaces σ_2 and σ_4 are negligibly small. Shaft work interactions are present because each control surface cuts a rotating shaft. The steady flow energy equation for the compressor or for the turbine is depicted in Fig. 2-12*c* and gives

$$-w_x = \left(h + \frac{V^2}{2g_c}\right)_{\text{out}} - \left(h + \frac{V^2}{2g_c}\right)_{\text{in}}$$

Numerical example: Compressor and turbine. For an equal mass flow† through the compressor and turbine of 185 lb/sec, determine the compressor power and

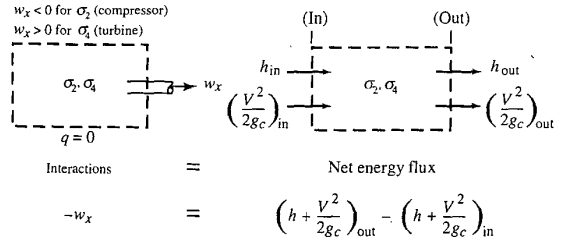

FIGURE 2-12*c*
Energy equation applied to control volumes σ_2 and σ_4.

† For a typical turbojet engine, 60 to 30 lbm of air enters for each 1 lbm of fuel consumed. It is, therefore, reasonable to assume approximately equal mass flow rates through the compressor and turbine.

the turbine exit temperature T_5 for the following conditions:

$$c_p g_c = 6000\ \text{ft}^2/(\text{sec}^2 \cdot {}^\circ\text{R})$$

Compressor	*Turbine*
$T_2 = 740^\circ\text{R}$, $T_3 = 1230^\circ\text{R}$	$T_4 = 2170^\circ\text{R}$, $T_5 = ?$
$V_2 = V_3$	$V_4 = V_5$

Solution. The compressor power $\dot{W}_c = (\dot{m}w_x)_{\sigma_2}$ is, with $V_2 = V_3$,

$$\dot{W}_c = -\dot{m}(h_3 - h_2) = -\dot{m}c_p(T_3 - T_2)$$

$$= -(185\ \text{lbm/sec})\frac{6000(\text{ft/sec})^2}{32.174\ \text{ft} \cdot \text{lbf}/(\text{lbm} \cdot \text{sec}^2)}(1230 - 740)$$

$$= -16.9 \times 10^6\ \text{ft} \cdot \text{lbf/sec} \times \frac{1\ \text{hp}}{550\ \text{ft} \cdot \text{lbf/sec}}$$

$$= -30{,}700\ \text{hp}$$

The minus sign means the compressor shaft is delivering energy to the air in σ_2.

The turbine drives the compressor so that the turbine power $\dot{W}_t = (\dot{m}w_x)_{\sigma_4}$ is equal in magnitude to the compressor power. Thus $\dot{W}_t = -\dot{W}_c$, where, from the energy equation,

$$\dot{W}_t = \dot{m}(h_4 - h_5) \quad \text{and} \quad \dot{W}_c = -\dot{m}(h_3 - h_2)$$

Thus $\dot{m}c_p(T_5 - T_4) = -\dot{m}c_p(T_3 - T_2)$

and $T_5 = T_4 - (T_3 - T_2)$

$= 2170^\circ\text{R} - (1230^\circ\text{R} - 740^\circ\text{R}) = 1680^\circ\text{R} = 1220^\circ\text{F}$

c. *Combustion chamber*: σ_3. Let us assume that the fuel and air entering the combustion chamber mix physically in a mixing zone (Fig. 2-12*d*) to form what we will call *reactants* (denoted by subscript R). The reactants then enter a combustion zone where combustion occurs, forming *products* of combustion (subscript P) which leave the combustion chamber. We apply the steady flow energy equation to combustion zone σ_3. Since the temperature in the combustion zone is higher than that of the immediate surroundings, there is a heat interaction between σ_3 and the surroundings which, per unit mass flow of reactants, is negligibly small ($q < 0$ but $q = 0$). Also the velocities of the products leaving and of the reactants entering the combustion zone are approximately equal. There is no shaft work interaction for σ_3. Hence the steady flow energy equation, as depicted in Fig. 2-12*d*, reduces to

$$\boxed{h_{R_3} = h_{P_4}}$$

We must caution the reader about two points concerning this last equation. First, we cannot use the relation $c_p\,\Delta T$ for computing the enthalpy difference between two states of a system when the chemical aggregation of the two states differs. Second, we must measure the enthalpy of each term in the equation

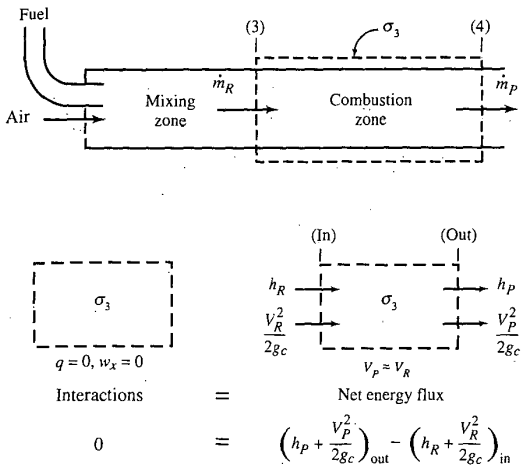

FIGURE 2-12*d*
Energy equation applied to control volume σ_3.

relative to the same datum state. To place emphasis on the first point, we have introduced the additional subscripts R and P to indicate that the chemical aggregations of states 3 and 4 are different.

To emphasize the second point, we select as our common enthalpy datum a state d having the chemical aggregation of the products at a datum temperature T_d. Then, introducing the datum state enthalpy $(h_P)_d$ into the last equation above, we have

$$\boxed{h_{R_3} - h_{P_d} = h_{P_4} - h_{P_d}} \tag{2-26}$$

Equation (2-26) can be used to determine the temperature of the products of combustion leaving an adiabatic combustor for given inlet conditions. If the combustor is not adiabatic, Eq. (2-26), adjusted to include the heat interaction term q on the left-hand side, is applicable. Let us treat the reactants and products as perfect gases and illustrate the use of Eq. (2-26) in determining the temperature of the gases at the exit of a turbojet combustion chamber via an example problem.

Numerical example: Combustion chamber. For the turbojet engine combustion chamber, 45 lbm of air enters with each 1 lbm of JP-4 (kerosene) fuel. Let us assume these reactants enter an adiabatic combustor at 1200°R. The heating value h_{PR} of JP-4 is 18,400 Btu/lbm of fuel at 298 K. [This is also called the *lower heating value* (LHV) of the fuel.] Thus the heat released $(\Delta H)_{298\,K}$ by the fuel per 1 lbm of the products is 400 Btu/lbm (18,400/46) at 298 K. The following data are known:

$$c_{pP} = 0.267 \text{ Btu/(lbm} \cdot \text{°R)} \qquad \text{and} \qquad c_{pR} = 0.240 \text{ Btu/(lbm} \cdot \text{°R)}$$

Determine the temperature of the products leaving the

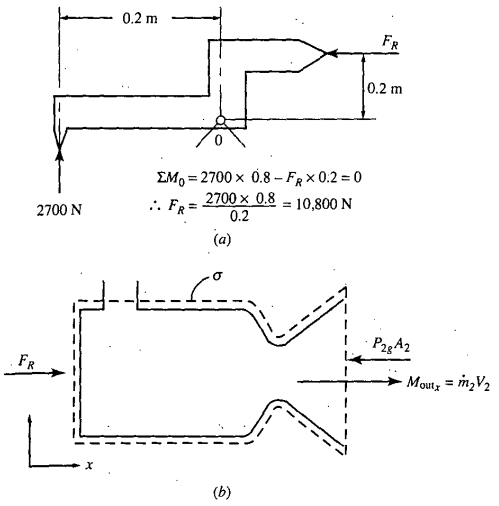

FIGURE 2-18
Moment balance and control volume σ for rocket.

2-11 SUMMARY OF LAWS FOR FLUID FLOW

Table 2-2 gives a convenient summary of the material covered so far in this chapter in the form of a tabulation of the mass, energy, entropy, and momentum equations for a system (control mass) and for control volume flow. For steady flow, all terms of the control volume equations refer to quantities evaluated at the control surface (neglecting body forces). Thus, to use the

TABLE 2-2
Summary of laws

	Closed system of mass	Control volume flow
Mass conservation	$\frac{dm}{dt} = 0$	$\frac{dm}{dt} = \frac{dm_\sigma}{dt} + \dot{m}_{\text{out}} - \dot{m}_{\text{in}}$
First law of thermodynamics	$\frac{dQ}{dt} - \frac{dW}{dt} = \frac{dE}{dt}$	$\dot{Q} - \dot{W}_x = \dot{m}(Pv + e)_{\text{out}} - \dot{m}(Pv + e)_{\text{in}} + \frac{dE_\sigma}{dt}$
Second law of thermodynamics	$\frac{dS}{dt} \geq \frac{1}{T}\frac{dQ}{dt}$	$\frac{dS_\sigma}{dt} + \dot{S}_{\text{out}} - \dot{S}_{\text{in}} \geq \frac{1}{T}\frac{dQ}{dt}$
Second law of motion	$\sum F_x = \frac{dM_x}{dt}$	$\sum F_\sigma = \frac{dM_\sigma}{dt} + \dot{M}_{\text{out}} - \dot{M}_{\text{in}}$

control volume equations for steady flow, one need only examine the boundary of the control region and identify the applicable terms of the equations. To paraphrase Prandtl and Tiejens concerning the theorem of momentum from their *Fundamentals of Hydro and Aeromechanics* (Ref. 14):

> The undoubted value of the steady flow control volume equations lies in the fact that their application enables one to obtain results in physical problems from just a knowledge of the boundary conditions. There is no need to be told anything about the state of fluid, or the mechanism of the motion, interior to the control volume.

Needless to say, the first step in analyzing a fluid flow problem is a clear statement or understanding of the control volume and its surface. In this respect, note that the mass in the control volume need not be restricted to that of a flowing fluid. The control volumes of Figs. 2-12*a* and 2-17 illustrate this point.

The flows analyzed in this chapter have generally been through volumes of other than infinitesimal size. The control volume equations apply also to infinitesimally sized control volumes as long as the fluid is a continuum. Examples of the use of an infinitesimal control volume will be given in Chap. 3.

The basic laws discussed in this chapter represent a powerful set of analytical tools which form the starting point in the analysis of any continuum fluid flow problem. Equations (2-8) through (2-11), or Eqs. (2-20), (2-24), (2-28), and (2-29) plus an equation of state relating the thermodynamic properties of the substance under consideration will form the basis of all the analytical work to follow.

Definitions of new quantities may be introduced, but no further fundamental laws will be required. Since the relations presented in this chapter form the starting point of all analytical studies to follow, time spent on the homework problems of this chapter, which are designed to bring out a basic understanding of the fundamental equations, will be well invested.

2-12 PERFECT GAS

General Characteristics

The thermodynamic equations of state for a perfect gas are

$$\boxed{P = \rho RT} \tag{2-30}$$

$$\boxed{u = u(T)} \tag{2-31}$$

where P is the thermodynamic pressure, ρ is the density, R is the gas constant, T is the thermodynamic temperature, and u is the internal energy per unit mass

and a function of temperature only. The gas constant R is related to the universal gas constant R_u and the molecular weight of the gas M by

$$R = \frac{R_u}{M}$$

Values of the gas constant and molecular weight for typical gases are presented in Table 2-3 in several unit systems; $R_u = 8.31434\ \text{kJ/(kmol} \cdot \text{K)} = 1.98718\ \text{Btu/(mol} \cdot {}^\circ\text{R)}$.

From the definition of enthalpy per unit mass h of a substance in Eq. (2-3), this simplifies for a perfect gas to

$$h = u + RT \tag{2-32}$$

Equations (2-31) and (2-32) combined show that the enthalpy per unit mass is also only a function of temperature $h = h(T)$. Differentiating Eq. (2-32) gives

$$dh = du + R\,dT \tag{2-33}$$

The differentials dh and du in Eq. (2-33) are related to the specific heat at constant pressure and specific heat at constant volume [see definitions in Eqs. (2-4) and (2-5)], respectively, as follows:

$$dh = c_p\,dT$$

$$du = c_v\,dT$$

Note that both specific heats can be functions of temperature. These equations can be integrated from state 1 to state 2 to give

$$u_2 - u_1 = \int_{T_1}^{T_2} c_v\,dT \tag{2-34}$$

$$h_2 - h_1 = \int_{T_1}^{T_2} c_p\,dT \tag{2-35}$$

Substitution of the equations for dh and du into Eq. (2-33) gives the relationship between specific heats for a perfect gas

$$\boxed{c_p = c_v + R} \tag{2-36}$$

And γ is the ratio of the specific heat at constant pressure to the specific heat at constant volume, or

$$\boxed{\gamma \equiv \frac{c_p}{c_v}} \tag{2-6}$$

TABLE 2-3
Properties of ideal gases at 298.15 K (536.67°R)

Gas	Molecular weight	c_p [kJ/(kg · K)]	c_p [Btu/(lbm · °R)]	R [kJ/(kg · K)]	R [(ft · lbf)/(lbm · °R)]	γ
Air	28.07	1.004	0.240	0.286	53.34	1.40
Argon	39.94	0.523	0.125	0.208	38.69	1.67
Carbon dioxide	44.01	0.845	0.202	0.189	35.1	1.29
Carbon monoxide	28.01	1.042	0.249	0.297	55.17	1.40
Hydrogen	2.016	14.32	3.42	4.124	766.5	1.40
Nitrogen	28.02	1.038	0.248	0.296	55.15	1.40
Oxygen	32.00	0.917	0.217	0.260	48.29	1.39
Sulfur dioxide	64.07	0.644	0.154	0.130	24.1	1.25
Water vapor	18.016	1.867	0.446	0.461	85.78	1.33

The following relationships result from using Eqs. (2-36) and (2-6):

$$\boxed{\frac{R}{c_v} = \gamma - 1} \tag{2-37}$$

$$\boxed{\frac{R}{c_p} = \frac{\gamma - 1}{\gamma}} \tag{2-38}$$

The Gibbs equation relates the entropy per unit mass s to the other thermodynamic properties of a substance. It can be written as

$$ds = \frac{du + P\,d(1/\rho)}{T} = \frac{dh - (1/\rho)\,dP}{T} \tag{2-39}$$

For a perfect gas, the Gibbs equation can be written simply as

$$\boxed{ds = c_v \frac{dT}{T} + R\frac{d(1/\rho)}{1/\rho}} \tag{2-40}$$

or

$$\boxed{ds = c_p \frac{dT}{T} - R\frac{dP}{P}} \tag{2-41}$$

These equations can be integrated between states 1 and 2 to yield the following expressions for the change in entropy $s_2 - s_1$:

$$s_2 - s_1 = \int_{T_1}^{T_2} c_v \frac{dT}{T} + R \ln \frac{\rho_1}{\rho_2} \tag{2-42}$$

$$s_2 - s_1 = \int_{T_1}^{T_2} c_p \frac{dT}{T} - R \ln \frac{P_2}{P_3} \tag{2-43}$$

f the specific heats are known functions of temperature for a perfect gas, then qs. (2-34), (2-35), (2-42), and (2-43) can be integrated from a reference state nd tabulated for further use in what are called *gas tables.*

The equation for the speed of sound in a perfect gas is easily obtained by se of Eqs. (2-7) and (2-30) to give

$$\boxed{a = \sqrt{\gamma R g_c T}}$$

Calorically Perfect Gas

A *calorically perfect gas* is a perfect gas with constant specific heats (c_p and c_v). In this case, the expressions for changes in internal energy u, enthalpy h, and entropy s simplify to the following:

$$u_2 - u_1 = c_v(T_2 - T_1) \tag{2-45}$$

$$h_2 - h_1 = c_p(T_2 - T_1) \tag{2-46}$$

$$s_2 - s_1 = c_v \ln \frac{T_2}{T_1} - R \ln \frac{\rho_2}{\rho_1} \tag{2-47}$$

$$s_2 - s_1 = c_p \ln \frac{T_2}{T_1} - R \ln \frac{P_2}{P_1} \tag{2-48}$$

Equations (2-47) and (2-48) can be rearranged to give the following equations for the temperature ratio T_2/T_1:

$$\frac{T_2}{T_1} = \left(\frac{\rho_2}{\rho_1}\right)^{R/c_v} \exp \frac{s_2 - s_1}{c_v}$$

$$\frac{T_2}{T_1} = \left(\frac{P_2}{P_1}\right)^{R/c_p} \exp \frac{s_2 - s_1}{c_p}$$

From Eqs. (2-37) and (2-38), these expressions become

$$\frac{T_2}{T_1} = \left(\frac{\rho_2}{\rho_1}\right)^{\gamma-1} \exp \frac{s_2 - s_1}{c_v} \tag{2-49}$$

$$\frac{T_2}{T_1} = \left(\frac{P_2}{P_1}\right)^{(\gamma-1)/\gamma} \exp \frac{s_2 - s_1}{c_p} \tag{2-50}$$

Isentropic Process

For an isentropic process ($s_2 = s_1$), Eqs. (2-49), (2-50), and (2-30) yield the following equations:

$$\boxed{\frac{T_2}{T_1} = \left(\frac{P_2}{P_1}\right)^{(\gamma-1)/\gamma}} \tag{2-51}$$

$$\boxed{\frac{T_2}{T_1} = \left(\frac{\rho_2}{\rho_1}\right)^{\gamma-1}} \tag{2-52}$$

$$\boxed{\frac{P_2}{P_1} = \left(\frac{\rho_2}{\rho_1}\right)^{\gamma}} \tag{2-53}$$

Note that Eqs. (2-51), (2-52), and (2-53) apply only to a calorically perfect gas undergoing an isentropic process.

Example 2-5. Air initially at 20°C and 1 atm is compressed reversibly and adiabatically to a final pressure of 15 atm. Find the final temperature.

Solution. Since the process is isentropic from initial to final state, Eq. (2-51) can be used to solve for the final temperature. The ratio of specific heats for air is 1.4.

$$T_2 = T_1\left(\frac{P_2}{P_1}\right)^{(\gamma-1)/\gamma} = (20 + 273.15)\left(\frac{15}{1}\right)^{0.4/1.4}$$

$$= 293.15 \times 2.1678 = 635.49 \text{ K } (362.34°\text{C})$$

Example 2-6. Air is expanded isentropically through a nozzle from $T_1 = 3000°\text{R}$, $V_1 = 0$, and $P_1 = 10$ atm to $V_2 = 3000$ ft/sec. Find the exit temperature and pressure.

Solution. Application of the first law of thermodynamics to the nozzle gives the following for a calorically perfect gas:

$$c_p T_1 + \frac{V_1^2}{2g_c} = c_p T_2 + \frac{V_2^2}{2g_c}$$

This equation can be rearranged to give T_2:

$$T_2 = T_1 - \frac{V_2^2 - V_1^2}{2g_c c_p} = 3000 - \frac{3000^2}{2 \times 32.174 \times 186.76}$$

$$= 3000 - 748.9 = 2251.1°\text{R}$$

Solving Eq. (2-51) for P_2 gives

$$P_2 = P_1\left(\frac{T_2}{T_1}\right)^{\gamma/(\gamma-1)} = 10\left(\frac{2251.1}{3000}\right)^{3.5} = 3.66 \text{ atm}$$

Mollier Diagram for a Perfect Gas

The Mollier diagram is a thermodynamic state diagram with the coordinates of enthalpy and entropy s. Since the enthalpy of a perfect gas depends upon temperature alone,

$$dh = c_p\, dT$$

temperature can replace enthalpy as the coordinate of a Mollier diagram for a perfect gas. When temperature T and

Mollier diagram, we call it a *T-s diagram.* We can construct lines of constant pressure and density in the *T-s* diagram by using Eqs. (2-42) and (2-43). For a calorically perfect gas, Eqs. (2-47) and (2-48) can be written between any state and the entropy reference state ($s = 0$) as

$$s = c_v \ln \frac{T}{T_{\text{ref}}} - R \ln \frac{\rho}{\rho_{\text{ref}}}$$

$$s = c_p \ln \frac{T}{T_{\text{ref}}} - R \ln \frac{P}{P_{\text{ref}}}$$

where T_{ref}, P_{ref}, and ρ_{ref} are the values of temperature, pressure, and density, respectively, when $s = 0$. Since the most common working fluid in gas turbine engines is air, Fig. 2-19 was constructed for air by using the above equations with these data:

$$c_p = 1.004 \text{ kJ/(kg} \cdot \text{K)} \qquad T_{\text{ref}} = 288.2 \text{ K} \qquad \rho_{\text{ref}} = 1.225 \text{ kg/m}^3$$

$$R = 0.286 \text{ kJ/(kg} \cdot \text{K)} \qquad P_{\text{ref}} = 1 \text{ atm} = 101{,}325 \text{ Pa}$$

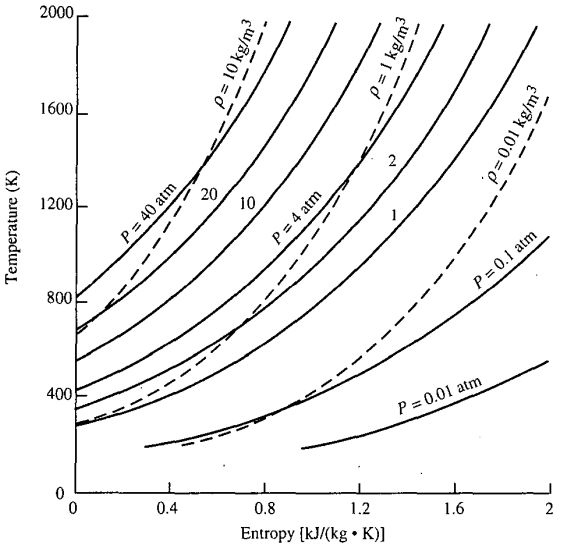

FIGURE 2-19
A *T-s* diagram for air as a calorically perfect gas.

Mixtures of Perfect Gases

We consider a mixture of perfect gases, each obeying the perfect gas equation

$$PV = NR_u T$$

where N is the number of moles and R_u is the universal gas constant. The mixture is idealized as independent perfect gases, each having the temperature T and occupying the volume V. The partial pressure of gas i is

$$P_i = N_i R_u \frac{T}{V}$$

According to the Gibbs-Dalton law, the pressure of the gas mixture of n constituents is the sum of the partial pressures of each constituent:

$$P = \sum_{i=1}^{n} P_i \tag{2-54}$$

The total number of moles N of the gas is

$$N = \sum_{i=1}^{n} N_i \tag{2-55}$$

The ratio of the number of moles of constituent i to the total number of moles in the mixture is called the *mole fraction* χ_i. By using the above equations, the mole fraction of constituent i can be shown to equal the ratio of the partial pressure of constituent i to the pressure of the mixture:

$$\chi_i = \frac{N_i}{N} = \frac{P_i}{P} \tag{2-56}$$

The Gibbs-Dalton law also states that the internal energy, enthalpy, and entropy of a mixture are equal, respectively, to the sum of the internal energies, the enthalpies, and the entropies of the constituents when each alone occupies the volume of the mixture at the mixture temperature. Thus we can write for a mixture of n constituents:

Energy $$U = \sum_{i=1}^{n} U_i = \sum_{i=1}^{n} m_i u_i \tag{2-57}$$

Enthalpy $$H = \sum_{i=1}^{n} H_i = \sum_{i=1}^{n} m_i h_i \tag{2-58}$$

Entropy $$S = \sum_{i=1}^{n} S_i = \sum_{i=1}^{n} m_i s_i \tag{2-59}$$

where m_i is the mass of constituent i

The specific heats of the mixture follow directly the definitions of c_p and c_v and the above equations. For a mixture of n constituents, the specific heats are

$$c_p = \frac{\sum_{i=1}^{n} m_i c_{pi}}{m} \quad \text{and} \quad c_v = \frac{\sum_{i=1}^{n} m_i c_{vi}}{m} \tag{2-60}$$

where m is the total mass of the mixture.

Gas Tables

In the case of a perfect gas with nonconstant specific heats, the variation of the specific heat at constant pressure c_p is normally modeled by several terms of a power series in temperature T. This expression is used in conjunction with the general equations presented above and the new equations that are developed below to generate a gas table for a particular gas (see Ref. 15).

For convenience, we define

$$h \equiv \int_{T_{\text{ref}}}^{T} c_p \, dT \tag{2-61}$$

$$\phi \equiv \int_{T_{\text{ref}}}^{T} c_p \frac{dT}{T} \tag{2-62}$$

$$P_r \equiv \exp \frac{\phi - \phi_0}{R} \tag{2-63}$$

$$v_r \equiv \exp\left(-\frac{1}{R} \int_{T_0}^{T} c_v \frac{dT}{T} \right) \tag{2-64}$$

where P_r and v_r are called the *reduced pressure* and *reduced volume*, respectively. Using the definition of ϕ from Eq. (2-62) in Eq. (2-43) gives

$$s_2 - s_1 = \phi_2 - \phi_1 - R \ln \frac{P_2}{P_1} \tag{2-65}$$

For an isentropic process between states 1 and 2, Eq. (2-65) reduces to

$$\phi_2 - \phi_1 = R \ln \frac{P_2}{P_1}$$

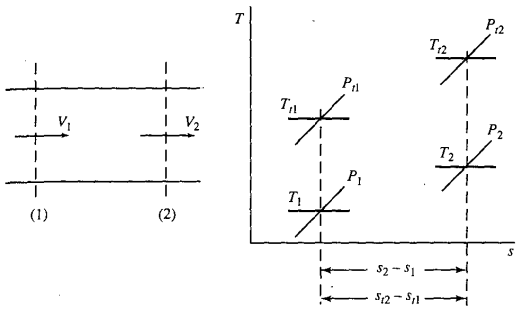

FIGURE 3-6
Entropy change in terms of the stagnation properties T_t and P_t.

on modern high-speed airplanes, and these properties are used to determine speed and Mach number and to provide other data for many aircraft subsystems.

Consider a gas flowing in a duct in which P and T may change due to heat interaction and friction effects. The flow total state points t_1 and t_2 and the static state points 1 and 2, each of which corresponds to flow stations 1 and 2, are located in the T-s diagram of Fig. 3-6. By definition, the entropy of the total state at any given point in a gas flow has the same value as the entropy of the static state properties at that point. Therefore, $s_{t1} = s_1$ and $s_{t2} = s_2$.

From the entropy equation of state of a perfect gas, the entropy change between 1 and 2 is

$$s_2 - s_1 = c_p \ln \frac{T_2}{T_1} - R \ln \frac{P_2}{P_1}$$

The entropy change between total state points t_1 and t_2 is

$$\boxed{s_{t2} - s_{t1} = c_p \ln \frac{T_{t2}}{T_{t1}} - R \ln \frac{P_{t2}}{P_{t1}}} \tag{3-8}$$

Since $s_{t1} = s_1$ and $s_{t2} = s_2$, we have

$$s_{t2} - s_{t1} = s_2 - s_1$$

Therefore, the change of entropy between two states of a flowing gas can be determined by using total properties in place of static properties.

Equation (3-8) indicates that in an adiabatic and no-shaft-work constant-T_t flow (such as exists in an airplane engine inlet or flow through a shock wave), we have

$$s_2 - s_1 = -R \ln \frac{P_{t2}}{P}$$

By virtue of this equation and the entropy control volume equation for adiabatic flow, $s_2 - s_1 \geq 0$. Thus, in a constant-T_t flow,

$$\frac{P_{t2}}{P_{t1}} \leq 1$$

Hence the total pressure of air passing through an engine inlet or a shock wave cannot increase and must, in fact, decrease because of the irreversible effects of friction.

T/T_t and P/P_t as Functions of Mach Number

The speed of sound a in a perfect gas is given by

$$a = \sqrt{\gamma g_c RT}$$

Using this relation for the speed of sound, we can write the Mach number in the following form:

$$M^2 = \frac{V^2}{\gamma g_c RT}$$

With the help of this expression for the Mach number, we can obtain many useful relations that give gas flow property ratios in terms of the flow Mach number alone. Two such relations for T/T_t and P/P_t are

$$\boxed{\frac{T}{T_t} = \left(1 + \frac{\gamma - 1}{2} M^2\right)^{-1}} \tag{3-9}$$

$$\boxed{\frac{P}{P_t} = \left(1 + \frac{\gamma - 1}{2} M^2\right)^{-\gamma/(\gamma-1)}} \tag{3-10}$$

Equations (3-9) and (3-10) appear graphically in Fig. 3-7 and are tabulated in App. E for γ values of 1.4 and 1.3. These equations show that for each free stream Mach number (hence, for each flight Mach number of an airplane), the ratios P/P_t and T/T_t have unique values.

Both Fig. 3-7 and the corresponding equations provide Mach numbers and ambient temperatures for known values of P, P_t, and T_t. For example, we are given the following in-flight measurements:

$$P = 35.4 \text{ kPa} \qquad T_t = 300 \text{ K} \qquad \text{and} \qquad P_t = 60.0 \text{ kPa}$$

From these data, $P/P_t = 0.59$. If we enter Fig. 3-7 with this value of P/P_t, we

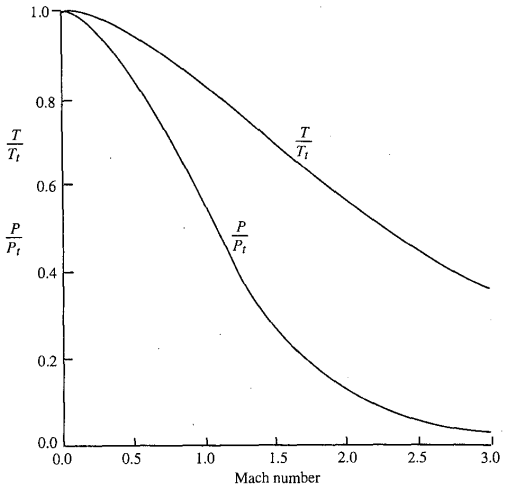

FIGURE 3-7
T/T_t and P/P_t versus Mach number ($\gamma = 1.4$).

find $M = 0.9$ and $T/T_t = 0.86$. Then we obtain the ambient temperature by using $T = (T/T_t)T_t = 0.86(300) = 258°\text{R}$.

Figure 3-7 shows that in a sonic ($M = 1.0$) stream of gas with $\gamma = 1.4$,

$$\frac{P}{P_t} = 0.528 \quad \text{and} \quad \frac{T}{T_t} = 0.833$$

and for supersonic flow,

$$\frac{P}{P_t} < 0.528 \quad \text{and} \quad \frac{T}{T_t} < 0.833$$

Consider the one-dimensional steady flow of a gas in a duct with T_t and P_t constant at all stations along the duct. This means a total temperature probe will measure the same value of T_t at each duct station, and an isentropic total pressure probe will measure the same value of P_t at each station. The path line of α of the flow is a vertical line in the T-s diagram. The state points on the path line can be categorized as follows:

Subsonic	$T > 0.883T_t$	$P > 0.528P_t$
Sonic	$T = 0.833T_t$	$P = 0.528P_t$
Supersonic	$T < 0.833T_t$	$P < 0.528P_t$

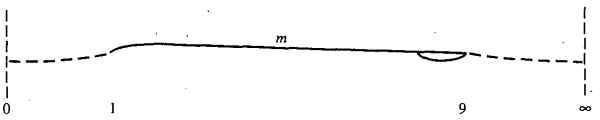

FIGURE 4-7
Ideal long nacelle.

drag associated with the forebody (front half of nacelle) D_w and the drag associated with the afterbody (rear half of nacelle) D_b. This is usually a reasonable approach because often lip separation dominates near the inlet and boat-tail drag near the exit. Assuming the division of nacelle drag to be meaningful, we can interpret the two drag terms by considering the nacelle to be very long and parallel in the middle, as shown in Fig. 4-7.

In this case, perfect flow would give us P_0, etc., at the middle. Application of the momentum equation to a control volume from 0 to m containing all the fluid outside the engine's stream tube will give

$$\int_0^1 (P - P_0)\, dA_y + \int_1^m (P - P_0)\, dA_y = 0$$

That is, in perfect flow,

$$D_{\text{add}} + D_w = 0 \tag{4-13}$$

Similarly, application of the momentum equation to a control from m to ∞ containing all the fluid outside the engine's stream tube will give

$$D_b + \int_9^\infty (P - P_0)\, dA_y = 0 \tag{4-14}$$

4-3 NOTE ON PROPULSIVE EFFICIENCY

The kinetic energy of the fluid flowing through an aircraft propulsion system is increased by an energy-transfer mechanism consisting of a series of processes constituting an engine cycle. From the point of view of an observer riding on the propulsion unit (see Fig. 4-8*a*), the engine cycle output is the increase of

FIGURE 4-8*a*
Velocity change by observer on aircraft.

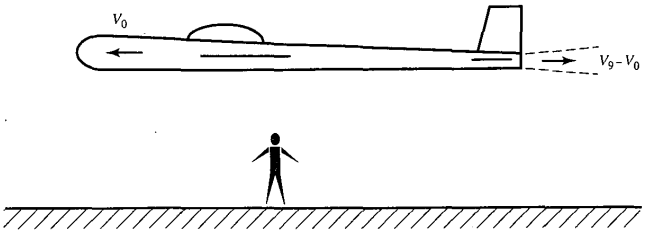

FIGURE 4-8*b*
Velocity change by observer on ground.

kinetic energy received by the air passing through the engine, which is $(V_9^2 - V_0^2)/(2g_c)$. From this observer's point of view, the total power output of the engine is the kinetic energy increase imparted to the air per unit time. On the other hand, from the point of view of an observer on the ground (see Fig. 4-8*b*), one sees the aircraft propulsion system's thrust moving at a velocity V_0 and observes the still air to receive an increase in kinetic energy, after passing through the engine, by an amount $(V_9 - V_0)^2/(2g_c)$. From this point of view, therefore, the total effect of the engine (and its output) is the sum of the propulsive power FV_0 and the kinetic energy per unit time imparted to the air passing through the engine. The sole purpose of the engine is to produce a propulsive power, and this is called the *useful power output* of the propulsion system. The ratio of the useful power output to the total power output of the propulsion system is called the *propulsive efficiency* [see Eq. (1-14)].

4-4 GAS TURBINE ENGINE COMPONENTS

The inlet, compressor, combustor, turbine, and nozzle are the main components of the gas turbine engine. The purpose and operation of these components and two thrust augmentation techniques are discussed in this section.

Inlets

An inlet reduces the entering air velocity to a level suitable for the compressor. The air velocity is reduced by a compression process which increases the air pressure. The operation and design of the inlet are described in terms of the efficiency of the compression process, the external drag of the inlet, and the mass flow into the inlet. The design and operation of the inlet depend on whether the air entering the duct is subsonic or supersonic. As the aircraft approaches the speed of sound, the air tends to be compressed more, and at

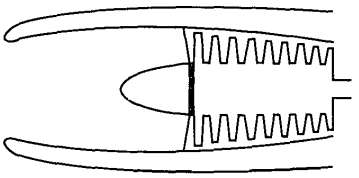

FIGURE 4-9
Subsonic inlet.

Mach 1, shock waves occur. Shock waves are compression waves, and at higher Mach numbers, these compression waves are stronger. Compression by shock waves is inefficient. In subsonic flow, there are no shock waves, and the air compression takes place quite efficiently. In supersonic flow, there are shock waves present. Shock waves and the compressibility of air then influence the design of inlets.

SUBSONIC INLET. The subsonic inlet can be a divergent duct, as shown in Fig. 4-9. This duct is satisfactory until the Mach number becomes greater than 1, at which time a shock wave occurs at the mouth and the compression process becomes inefficient. The subsonic divergent duct operates best at one velocity (design point), and at other velocities, the compression process is less efficient and the external drag is greater. The airflow patterns for the subsonic inlet are shown in Fig. 4-10.

SUPERSONIC INLET. Since shock waves will occur in supersonic flow, the geometry of supersonic inlets is designed to obtain the most efficient compression with a minimum of weight. If the velocity is reduced from a supersonic speed to a subsonic speed with one normal shock wave, the compression process is relatively inefficient. If several oblique shock waves are employed to reduce the velocity, the compression process is more efficient. Two typical supersonic inlets are the *ramp* (two-dimensional wedge) and the

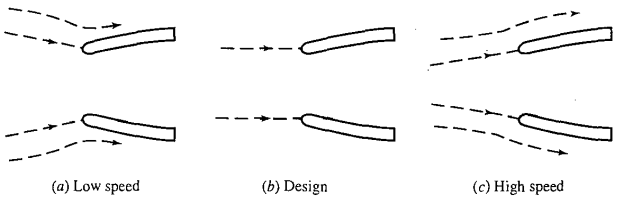

(*a*) Low speed (*b*) Design (*c*) High speed

FIGURE 4-10
Subsonic inlet flow patterns.

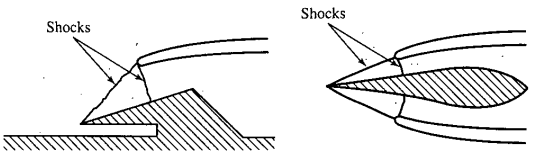

FIGURE 4-11
Supersonic inlets.

centerbody (three-dimensional spike), which are shown in Fig. 4-11. The shock wave positions in Fig. 4-11 are for the design condition of the inlet. At off-design Mach numbers, the positions of the shock waves change, thus affecting the external drag and the efficiency of compression. A more efficient ramp or centerbody inlet can be designed by using more than two shock waves to compress the entering air. Also, if the geometry is designed to be variable, the inlet operates more efficiently over a range of Mach numbers.

Compressors

The function of the compressor is to increase the pressure of the incoming air so that the combustion process and the power extraction process after combustion can be carried out more efficiently. By increasing the pressure of the air, the volume of the air is reduced, which means that the combustion of the fuel/air mixture will occur in a smaller volume.

CENTRIFUGAL COMPRESSOR. The compressor was the main stumbling block during the early years of turbojet engine development. Great Britain's Sir Frank Whittle solved the problem by using a centrifugal compressor. This type of compressor is still being used in many of the smaller gas turbine engines. A typical single-stage centrifugal compressor is shown in Fig. 4-12. The compressor consists of three main parts: an impeller, a diffuser, and a compressor manifold. Air enters the compressor near the hub of the impeller and is then compressed by the rotational motion of the impeller. The compression occurs by first increasing the velocity of the air (through rotation) and then diffusing the air where the velocity decreases and the pressure increases. The diffuser also straightens the flow, and the manifold serves as a collector to feed the air into the combustor. The single-stage centrifugal compressor has a low efficiency and a maximum compression ratio of 4 : 1 or 5 : 1. Multistage centrifugal compressors are somewhat better, but an axial compressor offers more advantages.

AXIAL COMPRESSORS. An axial compressor is shown in Fig. 4-13. The air in an axial compressor flows in an axial direction through a series of rotating

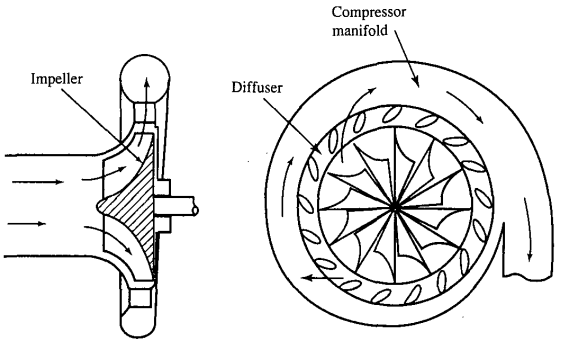

FIGURE 4-12
Single-stage centrifugal compressor.

rotor blades and stationary *stator* vanes which are concentric with the axis of rotation. Each set of rotor blades and stator vanes is known as a *stage.* The flow path in an axial compressor decreases in the cross-sectional area in the direction of flow. The decrease of area is in proportion to the increased density of the air as the compression progresses from stage to stage. Figure 4-13 contains a schematic of an axial compressor. Each stage of an axial compressor produces a small compression pressure ratio (1.1 : 1 to 1.2 : 1) at a high efficiency. Therefore, for high pressure ratios (12 : 1), multiple stages are used. Axial compressors are also more compact and have a smaller frontal area than a centrifugal compressor, which are added advantages. For the best axial compressor efficiency, the compressor operates at a constant axial velocity, as shown in Fig. 1-6. At high compression ratios, multistaging a single axial compressor does not produce as efficient an operation as a dual axial compressor would (see Fig. 1-4*a*). For a single rotational speed, there is a limit in the balance operation between the first and last stages of the compressor. To obtain more flexibility and a more uniform loading of each compressor stage,

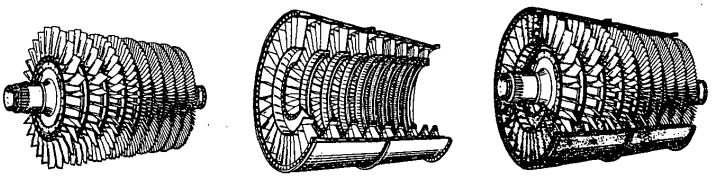

FIGURE 4-13
Multistage axial compressor.

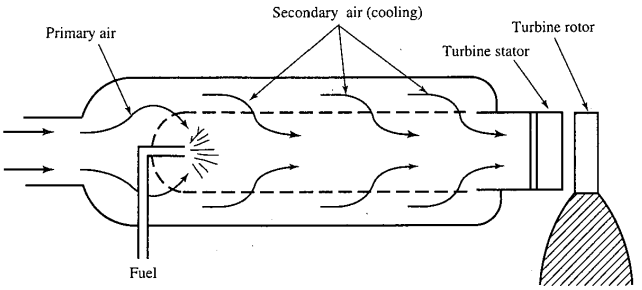

FIGURE 4-14
Straight-through flow combustor.

a dual compressor with two different rotational speeds is generally used in high-compression-ratio axial compressors.

Combustor or Main Burner

The combustor is designed to burn a mixture of fuel and air and to deliver the resulting gases to the turbine at a uniform temperature. The gas temperature must not exceed the allowable structural temperature of the turbine. A schematic of a combustor is shown in Fig. 4-14. Less than one-half of the total volume of air entering the burner mixes with the fuel and burns. The rest of the air—secondary air—is simply heated or may be thought of as cooling the products of combustion and cooling the burner surfaces. The ratio of total air to fuel varies among the different types of engines from 30 to 60 parts of air to 1 part of fuel by weight. The average ratio in new engine designs is about 40 : 1, but only 15 parts are used for burning (since the combustion process demands that the number of parts of air to fuel must be within certain limits at a given pressure for combustion to occur). Combustion chambers may be of the can, the annular, or the can-annular type, as shown in Fig. 4-15.

For an acceptable burner design, the pressure loss as the gases pass through the burner must be held to a minimum, the combustion efficiency must be high, and there must be no tendency for the burner to blow out (flameout). Also, combustion must take place entirely within the burner.

Turbines

The turbine extracts kinetic energy from the expanding gases which flow from the combustion chamber. The kinetic energy is converted to shaft horsepower to drive the compressor and the accessories. Nearly three-fourths of all the energy available from the products of combustion is required to drive the

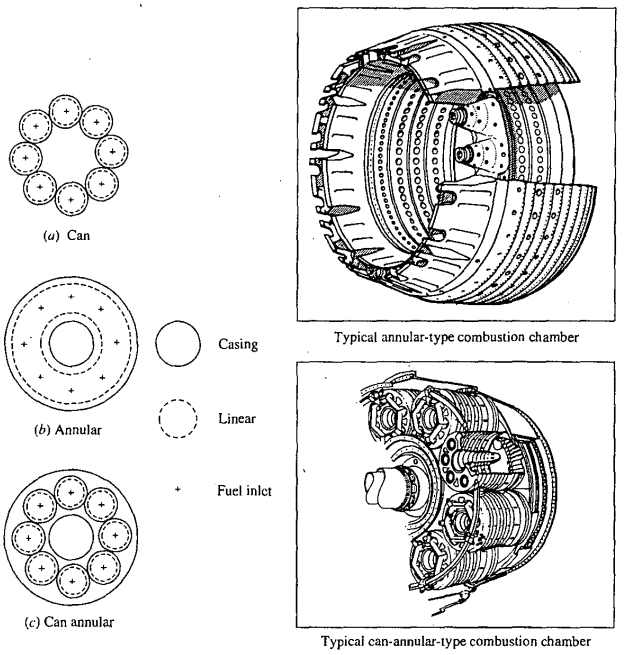

FIGURE 4-15
Cross sections of combustion chambers.

compressor. The axial-flow turbine consists of a turbine wheel *rotor* and a set of stationary vanes *stator,* as shown in Fig. 4-16. The set of stationary vanes of the turbine is a plane of vanes (concentric with the axis of the turbine) that are set at an angle to form a series of small nozzles which discharge the gases onto

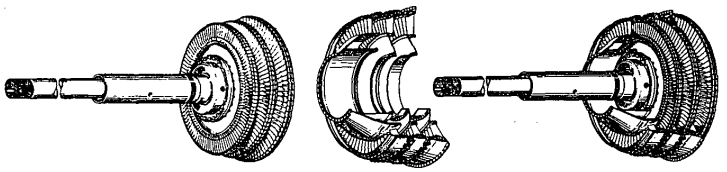

FIGURE 4-16
Axial-flow turbine components.

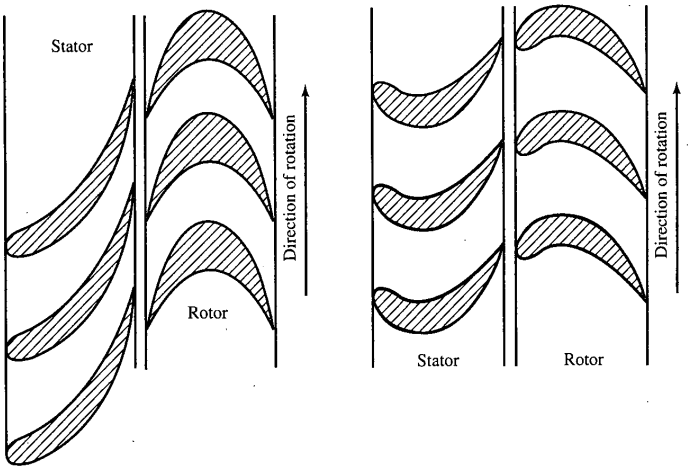

(*a*) Impulse (*b*) Reaction

FIGURE 04-17
Impulse and reaction stages.

the blades of the turbine wheel. The discharge of the gases onto the rotor allows the kinetic energy of the gases to be transformed to mechanical shaft energy.

Like the axial compressor, the axial turbine is usually multistaged. There are generally fewer turbine stages than compressor stages since in the turbine the pressure is decreasing (expansion process) whereas, in the compressor the pressure is increasing (compression process). In each of the processes (expansion or compression), the blades of the axial turbine or axial compressor act as airfoils, and the airflow over the airfoil is more favorable in the expansion process.

IMPULSE TURBINE. The impulse turbine and the reaction turbine are the two basic types of axial turbines, as shown in Fig. 4-17. In the impulse type, the relative discharge velocity of the rotor is the same as the relative inlet velocity since there is no net change in pressure between the rotor inlet and rotor exit. The stator nozzles of the impulse turbine are shaped to form passages which increase the velocity and reduce the pressure of the escaping gases.

REACTION TURBINE. In the reaction turbine, the relative discharge velocity of the rotor increases and the pressure decreases in the passages between rotor blades. The stator nozzle passages of the reaction turbine merely alter the direction of the flow.

Most turbines in jet engines are a combination of impulse and reaction

turbines. In the design of turbines, the following items must be considered: (1) shaft rotational speed, (2) gas flow rate, (3) inlet and outlet temperatures, (4) inlet and outlet pressures, (5) exhaust velocity, and (6) required power output. If the jet engine is equipped with a dual compressor, the turbine must also be dual or split.

Exhaust Nozzle

The purpose of the exhaust nozzle is to increase the velocity of the exhaust gas before discharge from the nozzle and to collect and straighten gas flow from the turbine. In operating, the gas turbine engine converts the internal energy of the fuel to kinetic energy in the exhaust gas stream. The net thrust (or force) of the engine is the result of this operation, and it can be calculated by applying Newton's second law of motion (see Chap. 2). For large values of specific thrust, the kinetic energy of the exhaust gas must be high, which implies a high exhaust velocity. The nozzle supplies a high exit velocity by expanding the exhaust gas in an expansion process which requires a decrease in pressure. The pressure ratio across the nozzle controls the expansion process, and the maximum thrust for a given engine is obtained when the exit pressure equals the ambient pressure. Nozzles and their operation are discussed further in Chaps. 3 and 10. The two basic types of nozzles used in jet engines are the convergent and convergent-divergent nozzles.

CONVERGENT NOZZLE. The convergent nozzle is a simple convergent duct, as shown in Fig. 4-18. When the nozzle pressure ratio (turbine exit pressure to nozzle exit pressure) is low (less than about 2), the convergent nozzle is used. The convergent nozzle has generally been used in low thrust engines for subsonic aircraft.

CONVERGENT-DIVERGENT NOZZLE. The convergent-divergent nozzle can be a convergent duct followed by a divergent duct. Where the cross-sectional

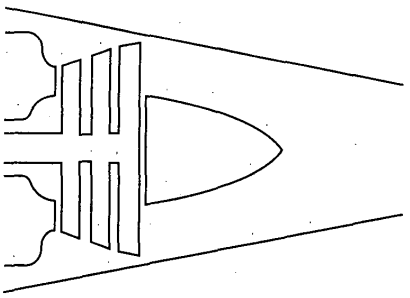

FIGURE 4-18
Convergent exhaust nozzle.

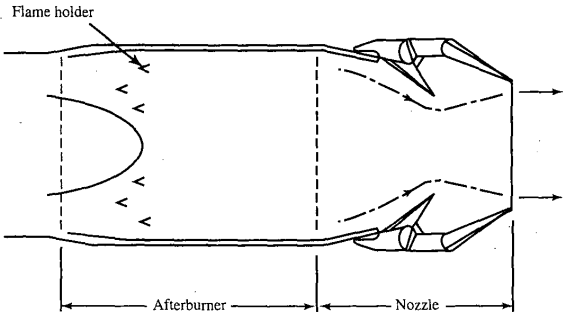

FIGURE 4-19
Convergent-divergent ejector exhaust nozzle.

area of the duct is a minimum, the nozzle is said to have a *throat* at that position. Most convergent-divergent nozzles used in supersonic aircraft are not simple ducts, but incorporate variable geometry and other aerodynamic features, as shown in Fig. 4-19. Only the throat area and exit area of the nozzle in Fig. 4-19 are set mechanically, the nozzle walls being determined aerodynamically by the gas flow. The convergent-divergent nozzle is used if the nozzle pressure ratio is high. High-specific-thrust engines in supersonic aircraft generally have some form of convergent-divergent nozzle. If the engine incorporates an afterburner, the nozzle throat and exit area must be varied to match the different flow conditions and to produce the maximum available thrust.

Thrust Augmentation

Thrust augmentation can be accomplished by either water injection or afterburning.

WATER INJECTION. Thrust augmentation by water injection (or by water/alcohol mixture) is achieved by injecting water into either the compressor or the combustion chamber. When water is injected into the inlet of the compressor, the mass flow rate increases and a higher combustion chamber pressure results if the turbine can handle the increased mass flow rate. The higher pressure and the increase in mass flow combine to increase the thrust. Injection of water into the combustion chamber produces the same effect, but to a lesser degree and with greater consumption of water. Water injection on a hot day can increase the takeoff thrust by as much as 50 percent because the original mass of air entering the jet engine is less for a hot day. The amount of air entering any turbomachine is determined by its volumetric constraints;

therefore, it follows that the mass flow on a hot day will be less since the air is less dense on a hot day.

AFTERBURNING. Another method of thrust augmentation is by burning additional fuel in the afterburner. The afterburner is a section of duct between the turbine and exhaust nozzle. The schematic diagram in Fig. 4-19 shows the afterburner section. The afterburner consists of the duct section, fuel injectors, and flame holders. It is possible to have afterburning because, in the main burner section, the combustion products are air-rich. The effect of the afterburning operation is to raise the temperature of the exhaust gases which, when exhausted through the nozzle, will reach a higher exit velocity. The pressure/temperature velocity profile for afterburning is also shown in Fig. 1-6. The J79 for afterburner operation has a thrust of 17,900 lbf and a *thrust specific fuel consumption* (TSFC) of 1.965 [(lbm/hr)/lbf]/hr, and for military operation (no afterburning) it has a thrust of 11,870 lbf and a TSFC of 0.84 [(lbm/hr)/lbf]/hr. We then see that afterburning produces large thrust gains at the expense of fuel economy.

4-5 BRAYTON CYCLE

The Brayton power cycle is a model used in thermodynamics for an ideal gas turbine power cycle. It is composed of the four following processes, which are also shown in Fig. 4-20(*a*):

1. Isentropic compression (2 to 3)
2. Constant-pressure heat addition (3 to 4)

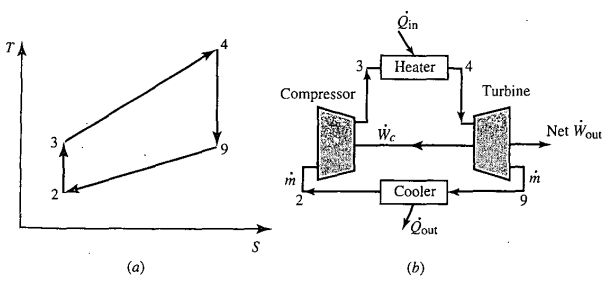

FIGURE 4-20
Brayton cycle.

3. Isentropic expansion (4 to 9)
4. Constant-pressure heat rejection (9 to 2)

The basic components of the Brayton cycle are shown to the right in Fig. 4-20(*b*). In the ideal cycle, the processes through both the compressor and the turbine are considered to be reversible and adiabatic (isentropic). The processes through the heater and cooler are considered to be constant-pressure in the ideal cycle.

For a calorically perfect gas, thermodynamic analysis of the ideal Brayton cycle gives the following equations for the rate of energy transfer of each component:

$$\dot{W}_c = \dot{m}c_p(T_3 - T_2) \qquad \dot{Q}_{\text{in}} = \dot{m}c_p(T_4 - T_3)$$
$$\dot{W}_t = \dot{m}c_p(T_4 - T_9) \qquad \dot{Q}_{\text{out}} = \dot{m}c_p(T_9 - T_2)$$
$$\text{Net } \dot{W}_{\text{out}} = \dot{W}_t - \dot{W}_c = \dot{m}c_p[T_4 - T_9 - (T_3 - T_2)]$$

Now, the thermal efficiency of the cycle is $\eta_T = \text{net } \dot{W}_{\text{out}}/\dot{Q}_{\text{in}}$. Noting that $(P_3/P_2)^{(\gamma-1)/\gamma} = T_3/T_2 = T_4/T_9$, we see that the thermal efficiency for the ideal Brayton cycle can be shown to be given by

$$\boxed{\eta_T = 1 - \left(\frac{1}{\text{PR}}\right)^{(\gamma-1)/\gamma}} \tag{4-15}$$

where PR is the *pressure ratio* P_3/P_2. The thermal efficiency is plotted in Fig. 4-21 as a function of the compressor pressure ratio for two ratios of specific heats.

For an ideal Brayton cycle with fixed compressor inlet temperature T_2 and heater exit temperature T_4, simple calculus yields an expression for the pressure ratio P_3/P_2 and associated temperature ratio T_3/T_2 giving the maximum net work output per unit mass. This optimum compressor pressure, or temperature ratio, corresponds to the maximum area within the cycle on a T-s diagram, as shown in Fig. 4-22. One can show that the optimum compressor temperature ratio is given by

$$\left(\frac{T_3}{T_2}\right)_{\text{max work}} = \sqrt{\frac{T_4}{T_2}} \tag{4-16}$$

and the corresponding net work output per unit mass is given by

$$\frac{\text{Net } \dot{W}_{\text{out}}}{\dot{m}} = c_p T_2\left(\sqrt{\frac{T_4}{T_2}} - 1\right)^2 \tag{4-17}$$

which is plotted in Fig. 4-23 versus T_4 for air with $T_2 = 288$ K.

Three variations in the basic Brayton cycle are shown in Figs. 4-24 through 4-26. Figure 4-24 shows the cycle with a *high-pressure* (HP) turbine driving the compressor and a free-power turbine providing the output power. This cycle has the same thermal efficiency as the ideal Brayton cycle of Fig.

The *total* or *stagnation pressure* P_t is defined as the pressure reached when a steady flowing stream is brought to rest adiabatically and reversibly (i.e., isentropically). Since $P_t/P = (T_t/T)^{(\gamma-1)/\gamma}$, then

$$P_t = P\left(1 + \frac{\gamma - 1}{2} M^2\right)^{\gamma/(\gamma-1)} \tag{5-2}$$

Ratios of total temperatures and pressures will be used extensively in this text, and a special notation is adopted for them. We denote a *ratio of total pressures* across a component by π, with a subscript indicating the component: d for diffuser (inlet), c for compressor, b for burner, t for turbine, n for nozzle, and f for fan:

$$\boxed{\pi_a = \frac{\text{total pressure leaving component } a}{\text{total pressure entering component } a}} \tag{5-3}$$

Similarly, the *ratio of total temperatures* is denoted by τ, and

$$\boxed{\tau_a = \frac{\text{total temperature leaving component } a}{\text{total temperature entering component } a}} \tag{5-4}$$

Exceptions

1. We define the total/static temperature and pressure ratios of the free stream (τ_r and π_r) by

$$\boxed{\tau_r = \frac{T_{t0}}{T_0} = 1 + \frac{\gamma - 1}{2} M_0^2} \tag{5-5}$$

$$\boxed{\pi_r = \frac{P_{t0}}{P_0} = \left(1 + \frac{\gamma - 1}{2} M_0^2\right)^{\gamma/(\gamma-1)}} \tag{5-6}$$

Thus the total temperature and pressure of the free stream can be written as

$$T_{t0} = T_0 \tau_r \qquad P_{t0} = P_0 \pi_r$$

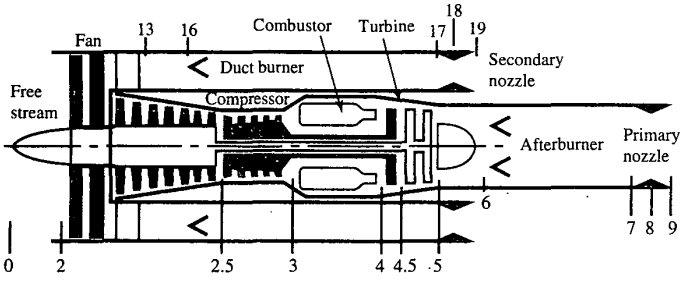

FIGURE 5-1
Station numbering for gas turbine engines.

2. Also, τ_λ is defined as the ratio of the burner exit enthalpy $c_p T_t$ to the ambient enthalpy $c_p T_0$:

$$\tau_\lambda = \frac{h_{t\,\text{burner exit}}}{h_0} = \frac{(c_p T_t)_{\text{burner exit}}}{(c_p T)_0} \tag{5-7}$$

Figure 5-1 shows the cross section and station numbering of a turbofan engine with both afterburning and duct burning. This station numbering is in accordance with Aerospace Recommended Practice (ARP) 755A (Ref. 27). Note that the station numbers 13 through 19 are used for the bypass stream and decimal numbers such as station number 4.5 are used to indicate an intermediate station.

Table 5-1 contains most of the short-form notation temperature ratios (τ's) and pressure ratios (π's) that we will use in our analysis. (Note that the τ_λ's are expressed for calorically perfect gases.) These ratios are shown in terms of the standard station numbering (Ref. 26).

5-3 DESIGN INPUTS

The total temperature ratios, total pressure ratios, etc., can be classified into one of four categories:

1. Flight conditions $P_0, T_0, M_0, c_p, \tau_r, \pi_r$

2. Design limits $(c_p T_t)_{\text{burner exit}}$

TABLE 5-1
Temperature and pressure relationships for all τ and π

Free stream			
$\tau_r = 1 + \frac{\gamma - 1}{2} M_0^2$		$\pi_r = \left(1 + \frac{\gamma - 1}{2} M_0^2\right)^{\gamma/(\gamma-1)}$	
Core stream		**Bypass stream**	
$\tau_\lambda = \frac{c_{pt} T_{t4}}{c_{pc} T_0}$	$\tau_{\lambda AB} = \frac{c_{pAB} T_{t7}}{c_{pc} T_0}$	$\tau_{\lambda DB} = \frac{c_{pDB} T_{t17}}{c_{pc} T_0}$	
$\tau_d = \frac{T_{t2}}{T_{t0}}$	$\pi_d = \frac{P_{t2}}{P_{t0}}$	$\tau_f = \frac{T_{t13}}{T_{t2}}$	$\pi_f = \frac{P_{t13}}{P_{t2}}$
$\tau_c = \frac{T_{t3}}{T_{t2}}$	$\pi_c = \frac{P_{t3}}{P_{t2}}$	$\tau_{DB} = \frac{T_{t17}}{T_{t13}}$	$\pi_{DB} = \frac{P_{t17}}{P_{t13}}$
$\tau_b = \frac{T_{t4}}{T_{t3}}$	$\pi_b = \frac{P_{t4}}{P_{t3}}$	$\tau_{fn} = \frac{T_{t19}}{T_{t17}}$	$\pi_{fn} = \frac{P_{t19}}{P_{t17}}$
$\tau_t = \frac{T_{t5}}{T_{t4}}$	$\pi_t = \frac{P_{t5}}{P_{t4}}$		
$\tau_{AB} = \frac{T_{t7}}{T_{t5}}$	$\pi_{AB} = \frac{P_{t7}}{P_{t5}}$		
$\tau_n = \frac{T_{t9}}{T_{t7}}$	$\pi_n = \frac{P_{t9}}{P_{t7}}$		

3. Component performance π_d, π_b, π_n, etc.
4. Design choices π_c, π_f, etc.

5-4 STEPS OF ENGINE PARAMETRIC CYCLE ANALYSIS

The steps of engine parametric cycle analysis listed below are based on a jet engine with a single inlet and single exhaust. Thus these steps will use only the station numbers for the core engine flow (from 0 to 9) shown in Fig. 5-1. We will use these steps in this chapter and Chap. 7. When more than one exhaust stream is present (e.g., high-bypass-ratio turbofan engine), the steps will be modified.

Parametric cycle analysis desires to determine how the engine performance (specific thrust and fuel consumption) varies with changes in the flight conditions (e.g., Mach number), design limits (e.g., main burner exit temperature), component performance (e.g., turbine efficiency), and design choices (e.g., compressor pressure ratio).

1. Starting with an equation for uninstalled engine thrust, we rewrite this equation in terms of the total pressure and total temperature ratios: the ambient pressure P_0, temperature T_0, and speed of sound a_0, and the flight

Mach number M_0 as follows:

$$F = \frac{1}{g_c}(\dot{m}_9 V_e - \dot{m}_0 V_0) + A_9(P_9 - P_0)$$

$$\frac{F}{\dot{m}_0} = \frac{a_0}{g_c}\left(\frac{\dot{m}_9}{\dot{m}_0}\frac{V_9}{a_0} - M_0\right) + \frac{A_9 P_9}{\dot{m}_0}\left(1 - \frac{P_0}{P_9}\right)$$

2. Next express the velocity ratio(s) V_9/a_0 in terms of Mach numbers, temperatures, and gas properties of states 0 and 9:

$$\left(\frac{V_9}{a_0}\right)^2 = \frac{a_9^2 M_9^2}{a_0^2} = \frac{\gamma_9 R_9 g_c T_9}{\gamma_0 R_0 g_c T_0} M_9^2$$

3. Find the exit Mach number M_9. Since

$$P_{t9} = P_9\left(1 + \frac{\gamma - 1}{2} M_9^2\right)^{\gamma/(\gamma-1)}$$

then

$$M_9^2 = \frac{2}{\gamma - 1}\left[\left(\frac{P_{t9}}{P_9}\right)^{(\gamma-1)/\gamma} - 1\right]$$

where

$$\frac{P_{t9}}{P_9} = \frac{P_0}{P_9}\frac{P_{t0}}{P_0}\frac{P_{t2}}{P_{t0}}\frac{P_{t3}}{P_{t2}}\frac{P_{t4}}{P_{t3}}\frac{P_{t5}}{P_{t4}}\frac{P_{t7}}{P_{t5}}\frac{P_{t9}}{P_{t7}}$$

$$= \frac{P_0}{P_9}\pi_r \pi_d \pi_c \pi_b \pi_t \pi_{AB} \pi_n$$

4. Find the temperature ratio T_9/T_0:

$$\frac{T_9}{T_0} = \frac{T_{t9}/T_0}{T_{t9}/T_9} = \frac{T_{t9}/T_0}{(P_{t9}/P_9)^{\gamma-1)/\gamma}}$$

where

$$\frac{T_{t9}}{T_0} = \frac{T_{t0}}{T_0}\frac{T_{t2}}{T_{t0}}\frac{T_{t3}}{T_{t2}}\frac{T_{t4}}{T_{t3}}\frac{T_{t5}}{T_{t4}}\frac{T_{t7}}{T_{t5}}\frac{T_{t9}}{T_{t7}} = \tau_r \tau_d \tau_c \tau_b \tau_t \tau_{AB} \tau_n$$

5. Apply the first law of thermodynamics to the burner (combustor), and find an expression for the fuel/air ratio f in terms of τ's, etc:

$$\dot{m}_0 c_p T_{t3} + \dot{m}_f h_{PR} = \dot{m}_0 c_p T_{t4}$$

6. When applicable, find an expression for the total temperature ratio across the turbine τ_t by relating the turbine power output to the compressor, fan, and/or propeller power requirements. This allows us to find τ_t in terms of other variables.

7. Evaluate the specific thrust, using the above results.

8. Evaluate the thrust specific fuel consumption S, using the results for specific thrust and fuel/air ratio:

$$S = \frac{f}{F/\dot{m}_0} \tag{5-8}$$

9. Develop expressions for the thermal and propulsive efficiencies.

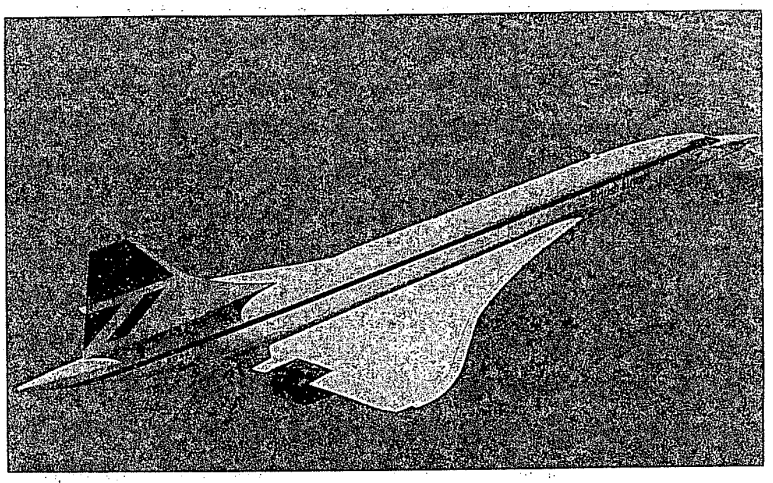

FIGURE 5-18*c*
Concorde supersonic transport. (*Courtesy of Rolls-Royce.*)

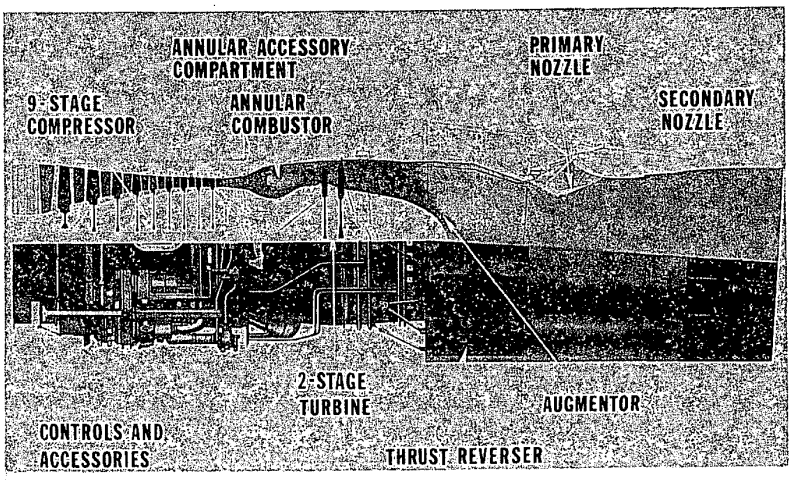

FIGURE 5-19
General Electric GE4 turbojet engine (developed for Boeing SST). (*Courtesy of General Electric.*)

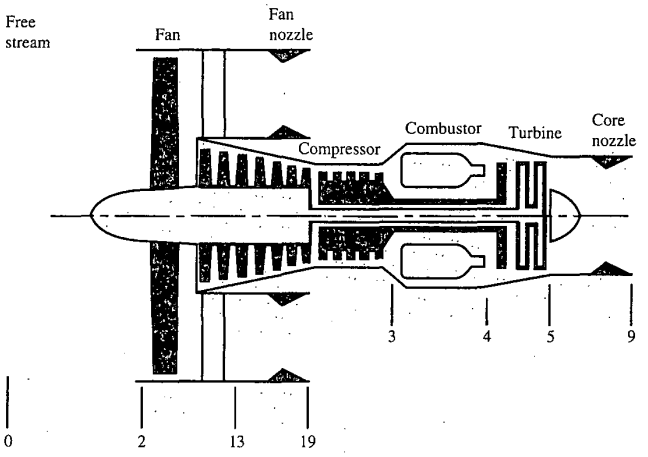

FIGURE 5-20
Station numbering of a turbofan engine.

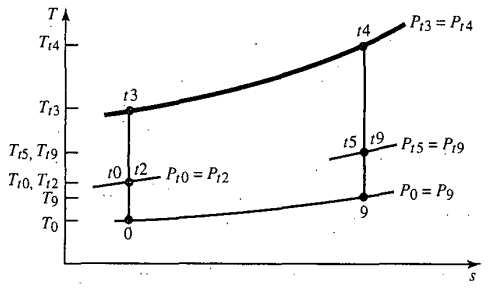

FIGURE 5-21
The T-s diagram for core stream of ideal turbofan engine.

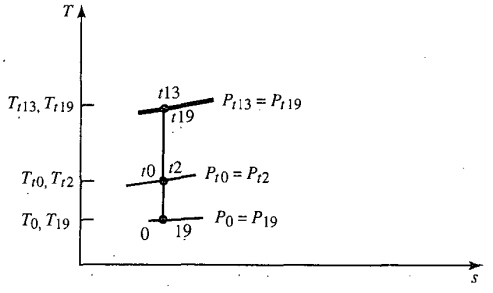

FIGURE 5-22
The T-s diagram for fan stream of ideal turbofan engine.

is $\dot{m}_F$. The ratio of the fan flow to the core flow is defined as the *bypass ratio* and given the symbol alpha α. Thus

$$\boxed{\text{Bypass ratio } \alpha = \frac{\dot{m}_F}{\dot{m}_C}} \tag{5-46}$$

the total gas flow is $\dot{m}_C + \dot{m}_F$, or $(1 + \alpha)\dot{m}_C$. We will also use $\dot{m}_0$ for the total gas flow. Thus

$$\boxed{\dot{m}_0 = \dot{m}_C + \dot{m}_F = (1 + \alpha)\dot{m}_C} \tag{5-47}$$

In the analysis of the ideal turbofan engine, we will assume that the mass flow rate of fuel is much less than the mass flow rate of gas through the engine core. We will also assume that both the engine core nozzle and the fan nozzle are designed so that $P_0 = P_9 = P_{19}$.

Cycle Analysis

Application of the steps of cycle analysis to the ideal turbofan engine of Figs. 5-20 and 5-21 is presented below in the order listed in Sec. 5-4.

Step 1. The thrust of the ideal turbofan engine is

$$F = \frac{\dot{m}_C}{g_c}(V_9 - V_0) + \frac{\dot{m}_F}{g_c}(V_{19} - V_0)$$

Thus

$$\boxed{\frac{F}{\dot{m}_0} = \frac{a_0}{g_c}\frac{1}{1+\alpha}\left[\frac{V_9}{a_0} - M_0 + \alpha\left(\frac{V_{19}}{a_0} - M_0\right)\right]} \tag{5-48}$$

Steps 2 through 4. First, the core stream of the turbofan encounters the same engine components as the ideal turbojet, and we can use its results. We have, from the analysis of the ideal turbojet,

$$\left(\frac{V_9}{a_0}\right)^2 = \frac{T_9}{T_0}M_9^2 \qquad \frac{T_9}{T_0} = \tau_b = \frac{\tau_\lambda}{\tau_r\tau_c} \qquad \text{and} \qquad M_9^2 = \frac{2}{\gamma - 1}(\tau_r\tau_c\tau_t - 1)$$

Thus

$$\boxed{\left(\frac{V_9}{a_0}\right)^2 = \frac{T_9}{T_0}M_9^2 = \frac{2}{\gamma - 1}\frac{\tau_\lambda}{\tau_r\tau_c}(\tau_r\tau_c\tau_t - 1)} \tag{5-49}$$

Second, compared to the core stream, the fan stream of the turbofan contains a fan rather than a compressor and does not have either a combustor or a turbine. Thus the above equations for the core stream of the ideal turbofan can be adapted for the fan stream as follows:

$$\left(\frac{V_{19}}{a_0}\right)^2 = \frac{T_{19}}{T_0} M_{19}^2 \qquad \boxed{T_{19} = T_0} \qquad \text{and} \qquad M_{19}^2 = \frac{2}{\gamma - 1}(\tau_r \tau_f - 1)$$

$$\boxed{\left(\frac{V_{19}}{a_0}\right)^2 = M_{19}^2 = \frac{2}{\gamma - 1}(\tau_r \tau_f - 1)} \tag{5-50}$$

Step 5. Application of the steady flow energy equation to the burner gives

$$\dot{m}_C c_p T_{t3} + \dot{m}_f h_{PR} = (\dot{m}_C + \dot{m}_f) c_p T_{t4}$$

We define the fuel/air ratio f in terms of the mass flow rate of air through the burner $\dot{m}_C$, and we obtain

$$\boxed{f = \frac{\dot{m}_f}{\dot{m}_C} = \frac{c_p T_0}{h_{PR}}(\tau_\lambda - \tau_r \tau_c)} \tag{5-51}$$

Step 6. The power out of the turbine is

$$\dot{W}_t = (\dot{m}_C + \dot{m}_f) c_p (T_{t4} - T_{t5}) \cong \dot{m}_C c_p T_{t4}(1 - \tau_t)$$

The power required to drive the compressor is

$$\dot{W}_c = \dot{m}_C c_p (T_{t3} - T_{t2}) = \dot{m}_C c_p T_{t2}(\tau_c - 1)$$

The power required to drive the fan is

$$\dot{W}_f = \dot{m}_F c_p (T_{t13} - T_{t2}) = \dot{m}_F c_p T_{t2}(\tau_f - 1)$$

Since $\dot{W}_t = \dot{W}_c + \dot{W}_f$ for the ideal turbofan, then

$$T_{t4}(1 - \tau_t) = T_{t2}(\tau_c - 1) + \alpha T_{t2}(\tau_f - 1)$$

$$\tau_t = 1 - \frac{T_{t2}}{T_{t4}}[\tau_c - 1 + \alpha(\tau_f - 1)]$$

$$\boxed{\tau_t = 1 - \frac{\tau_r}{\tau_\lambda}[\tau_c - 1 + \alpha(\tau_f - 1)]} \tag{5-52}$$

Step 7. Combining Eqs. (5-49) and (5-52), we get

$$\left(\frac{V_9}{a_0}\right)^2 = \frac{2}{\gamma - 1}\frac{\tau_\lambda}{\tau_r \tau_c}\left(\tau_r \tau_c\left\{1 - \frac{\tau_r}{\tau_\lambda}[\tau_c - 1 + \alpha(\tau_f - 1)]\right\} - 1\right)$$

which can be simplified to

$$\boxed{\left(\frac{V_9}{a_0}\right)^2 = \frac{2}{\gamma - 1}\left\{\tau_\lambda - \tau_r[\tau_c - 1 + \alpha(\tau_f - 1)] - \frac{\tau_\lambda}{\tau_r \tau_c}\right\}} \tag{5-53}$$

Thus the specific thrust of the ideal turbojet is given by Eqs. (5-48), (5-50), and (5-53).

Step 8

$$S = \frac{\dot{m}_f}{F} = \frac{f}{F/\dot{m}_C} = \frac{f}{(\dot{m}_0/\dot{m}_C)(F/\dot{m}_0)}$$

$$\boxed{S = \frac{f}{(1+\alpha)(F/\dot{m}_0)}} \tag{5-54}$$

Step 9. The thermal efficiency of an ideal turbofan engine is the same as that of an ideal turbojet engine. That is,

$$\eta_T = 1 - \frac{1}{\tau_r \tau_c} \tag{5-22}$$

This may seem surprising since the net power out of a turbojet is $\dot{m}_0(V_9^2 - V_0^2)/(2g_c)$, while for a turbofan it is $\dot{m}_C(V_9^2 - V_0^2)/(2g_c) + \dot{m}_F(V_{19}^2 - V_0^2)/(2g_c)$. The reason that the thermal efficiency is the same is that power extracted from the core stream of the turbofan engine is added to the bypass stream without loss in the ideal case. Thus the net power out remains the same.

One can easily show that the propulsive efficiency of the ideal turbofan engine is given by

$$\boxed{\eta_P = 2\frac{V_9/V_0 - 1 + \alpha(V_{19}/V_0 - 1)}{V_9^2/V_0^2 - 1 + \alpha(V_{19}^2/V_0^2 - 1)}} \tag{5-55}$$

A useful performance parameter for the turbofan engine is the ratio of the specific thrust per unit mass flow of the core stream to that of the fan stream. We give this *thrust ratio* the symbol FR and define

$$\boxed{\text{FR} \equiv \frac{F_C/\dot{m}_C}{F_F/\dot{m}_F}} \tag{5-56}$$

For the ideal turbofan engine, the thrust ratio FR can be expressed as

$$\text{FR} = \frac{V_9/a_0 - M_0}{V_{19}/a_0 - M_0} \tag{5-57}$$

We will discover in the analysis of optimum turbofan engines that we will want a certain thrust ratio for minimum thrust specific fuel consumption.

Summary of Equations—Ideal Turbofan

INPUTS: M_0, T_0(K, °R), γ, $c_p\left(\frac{\text{kJ}}{\text{kg}\cdot\text{K}}, \frac{\text{Btu}}{\text{lbm}\cdot\text{°R}}\right)$, $h_{PR}\left(\frac{\text{kJ}}{\text{kg}}, \frac{\text{Btu}}{\text{lbm}}\right)$, T_{t4}(K, °R), π_c, π_f, α

OUTPUTS: $\frac{F}{\dot{m}_0}\left(\frac{\text{N}}{\text{kg/sec}}, \frac{\text{lbf}}{\text{lbm/sec}}\right)$, f, $S\left(\frac{\text{mg/sec}}{\text{N}}, \frac{\text{lbm/hr}}{\text{lbf}}\right)$, η_T, η_P, η_O, FR

EQUATIONS:

$$R = \frac{\gamma - 1}{\gamma} c_p \tag{5-58a}$$

$$a_0 = \sqrt{\gamma R g_c T_0} \tag{5-58b}$$

$$\tau_r = 1 + \frac{\gamma - 1}{2} M_0^2 \tag{5-58c}$$

$$\tau_\lambda = \frac{T_{t4}}{T_0} \tag{5-58d}$$

$$\tau_c = (\pi_c)^{(\gamma-1)/\gamma} \tag{5-58e}$$

$$\tau_f = (\pi_f)^{(\gamma-1)/\gamma} \tag{5-58f}$$

$$\frac{V_9}{a_0} = \sqrt{\frac{2}{\gamma - 1}\left\{\tau_\lambda - \tau_r[\tau_c - 1 + \alpha(\tau_f - 1)] - \frac{\tau_\lambda}{\tau_r \tau_c}\right\}} \tag{5-58g}$$

$$\frac{V_{19}}{a_0} = \sqrt{\frac{2}{\gamma - 1}(\tau_r \tau_f - 1)} \tag{5-58h}$$

$$\frac{F}{\dot{m}_0} = \frac{a_0}{g_c} \frac{1}{1 + \alpha}\left[\frac{V_9}{a_0} - M_0 + \alpha\left(\frac{V_{19}}{a_0} - M_0\right)\right] \tag{5-58i}$$

$$f = \frac{c_p T_0}{h_{PR}}(\tau_\lambda - \tau_r \tau_c) \tag{5-58j}$$

$$S = \frac{f}{(1 + \alpha)(F/\dot{m}_0)} \tag{5-58k}$$

$$\eta_T = 1 - \frac{1}{\tau_r \tau_c} \tag{5-58l}$$

$$\eta_P = 2M_0 \frac{V_9/a_0 - M_0 + \alpha(V_{19}/a_0 - M_0)}{V_9^2/a_0^2 - M_0^2 + \alpha(V_{19}^2/a_0^2 - M_0^2)} \tag{5-58m}$$

$$\eta_O = \eta_T \eta_P \tag{5-58n}$$

$$\text{FR} = \frac{V_9/a_0 - M_0}{V_{19}/a_0 - M_0} \tag{5-58o}$$

Example 5-4. The turbofan engine has three design variables:

- Compressor pressure ratio π_c
- Fan pressure ratio π_f
- Bypass ratio α

Since this engine has two more design variables than the turbojet, this section contains many more plots of engine performance than were required for the turbojet. First, we will look at the variation of each of the three design variables for an engine that will operate at a flight Mach number of 0.9. Then we will look at the variation of design performance with flight Mach number. In all the calculations for this section, the following values are held constant:

$$T_0 = 216.7\,\text{K} \quad \gamma = 1.4 \quad c_p = 1.004\,\text{kJ/(kg}\cdot\text{K)} \quad h_{PR} = 42{,}800\,\text{kJ/kg} \quad T_{t4} = 1670\,\text{K}$$

Figures 5-23*a* through 5-23*e*. Specific thrust and thrust specific fuel consumption are plotted versus the compressor pressure ratio for different values of the bypass ratio in Figs. 5-23*a* and 5-23*b*. The fan pressure ratio is held constant in these plots. Figure 5-23*a* shows that specific thrust remains essentially constant with respect to the compressor pressure ratio for values of π_c from 15 to 25, and that specific thrust decreases with increasing bypass ratio. Figure 5-23*b* shows that thrust specific fuel consumption decreases with increasing compressor pressure ratio π_c and increasing bypass ratio α.

Figure 5-23*c* shows that the fuel/air ratio decreases with compressor pressure ratio, the thermal efficiency increases with compressor pressure ratio, and both are independent of the engine bypass ratio. From Fig. 5-23*d*, we can see that the propulsive efficiency increases with engine bypass ratio and varies very little with compressor pressure ratio. The overall efficiency, shown also in Fig. 5-23*d*, increases with both compressor pressure ratio and bypass ratio.

The thrust ratio is plotted versus compressor pressure ratio and bypass ratio in Fig. 5-23*e*. As can be seen, the thrust ratio decreases with increasing bypass ratio and varies very little with compressor pressure ratio.

Figures 5-24*a* through 5-24*e*. Specific thrust and thrust specific fuel consumption are plotted versus the compressor pressure ratio π_c for different values of the fan pressure ratio π_f. The bypass ratio α is held constant in these plots. Figure 5-24*a* shows that the specific thrust remains essentially constant with respect to the compressor pressure ratio for values of π_c from 15 to 25, and that the specific thrust has a maximum with respect to the fan pressure ratio π_f. Figure 5-24*b* shows that thrust specific fuel consumption decreases with increasing compressor pressure ratio π_c and that S has a minimum with respect to fan pressure ratio π_f. We will look at this optimum fan pressure ratio in more detail in another section of this chapter.

Propulsive and overall efficiencies are plotted versus compressor pressure ratio and fan pressure ratio in Figs. 5-24*c* and 5-24*d*. Figure 5-24*c* shows that propulsive efficiency increases with fan pressure ratio until a value of $\pi_f = 3.5$ and then decreases. There is a fan pressure ratio giving maximum propulsive efficiency. Propulsive efficiency is essentially constant for values of the compressor pressure ratio above 15. Also from Fig. 5-24*d*, we can see that overall efficiency increases with compressor pressure ratio and increases with fan pressure ratio until a value of $\pi_f = 3.5$ and then decreases. There is a fan pressure ratio giving maximum overall efficiency.

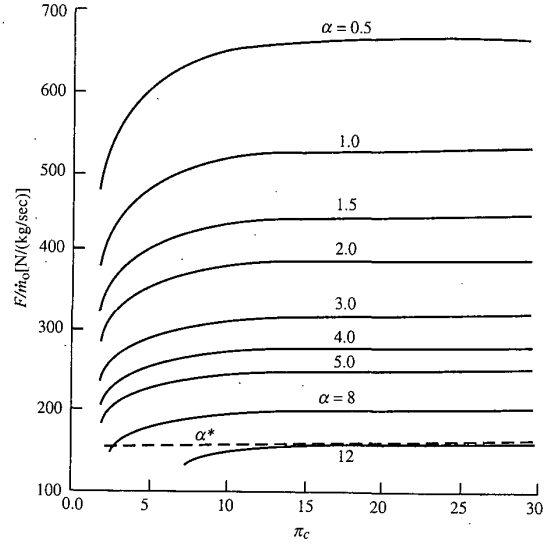

FIGURE 5-23*a*
Ideal turbofan performance versus π_c, for $\pi_f = 2$ and $M_0 = 0.9$: specific thrust.

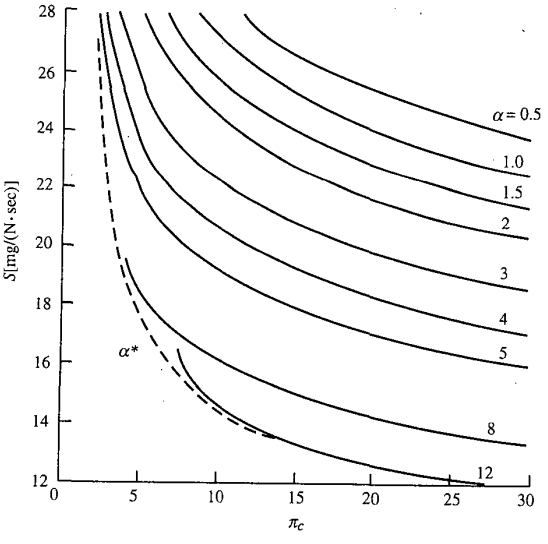

FIGURE 5-23*b*
Ideal turbofan performance versus π_c, for $\pi_f = 2$ and $M_0 = 0.9$: thrust specific fuel consumption.

Summary of Equations—Optimum-Bypass-Ratio Ideal Turbofan

INPUTS: M_0, T_0(K, °R), γ, $c_p\left(\frac{\text{kJ}}{\text{kg}\cdot\text{K}}, \frac{\text{Btu}}{\text{lbm}\cdot\text{°R}}\right)$, $h_{PR}\left(\frac{\text{kJ}}{\text{kg}}, \frac{\text{Btu}}{\text{lbm}}\right)$, T_{t4}(K, °R), π_c, π_f

OUTPUTS: $\frac{F}{\dot{m}_0}\left(\frac{\text{N}}{\text{kg/sec}}, \frac{\text{lbf}}{\text{lbm/sec}}\right)$, f, $S\left(\frac{\text{mg/sec}}{\text{N}}, \frac{\text{lbm/hr}}{\text{lbf}}\right)$, η_T, η_P, η_O, α^*

EQUATIONS: Equations (5-58*a*) through (5-58*h*) plus

$$\alpha^* = \frac{1}{\tau_r(\tau_f - 1)}\left[\tau_\lambda - \tau_r(\tau_c - 1) - \frac{\tau_\lambda}{\tau_r\tau_c} - \frac{1}{4}(\sqrt{\tau_r\tau_f - 1} + \sqrt{\tau_r - 1})^2\right] \tag{5-63a}$$

$$\frac{F}{\dot{m}_0} = \frac{a_0}{g_c}\frac{1 + 2\alpha^*}{2(1 + \alpha^*)}\left[\sqrt{\frac{2}{\gamma - 1}(\tau_r\tau_f - 1)} - M_0\right] \tag{5-63b}$$

$$\eta_P = \frac{4(1 + 2\alpha^*)M_0}{(3 + 4\alpha^*)M_0 + (1 + 4\alpha^*)(V_{19}/a_0)} \tag{5-63c}$$

and Eqs. (5-58*j*), (5-58*k*), (5-58*l*), (5-58*n*)

Example 5-5. The engine we looked at in Sec. 5-9 is used again in this section for an example. The following values are held constant for all plots:

$T_0 = 216.7$ K $\quad \gamma = 1.4 \quad c_p = 1.004$ kJ/(kg · K)

$h_{PR} = 42{,}800$ kJ/kg $\quad T_{t4} = 1670$ K

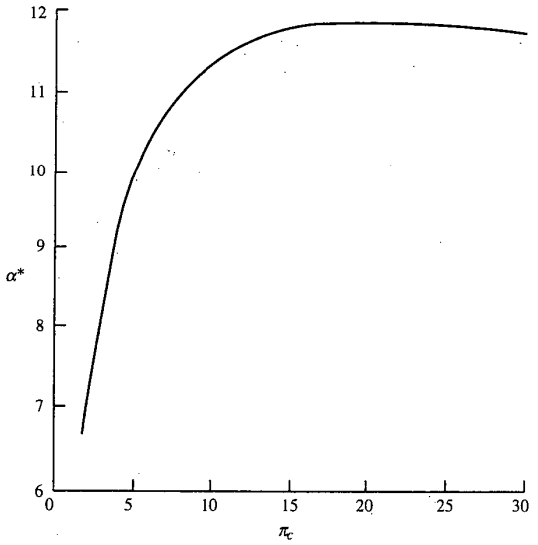

FIGURE 5-29*a*
α^* versus π_c, for $\pi_f = 2$ and $M_0 = 0.9$.

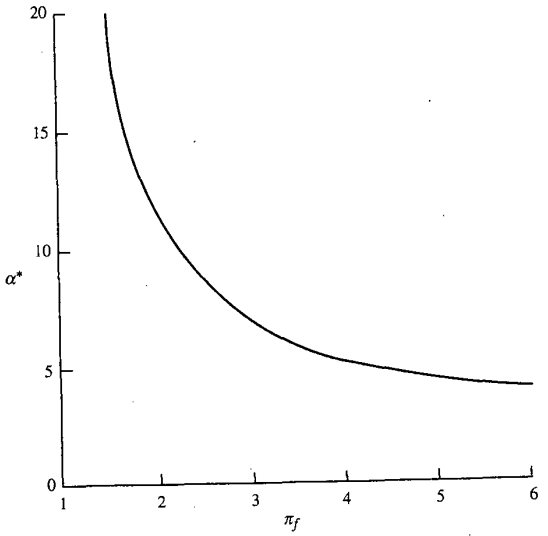

FIGURE 5-29*b*
α^* versus π_f, for $\pi_c = 24$ and $M_0 = 0.9$.

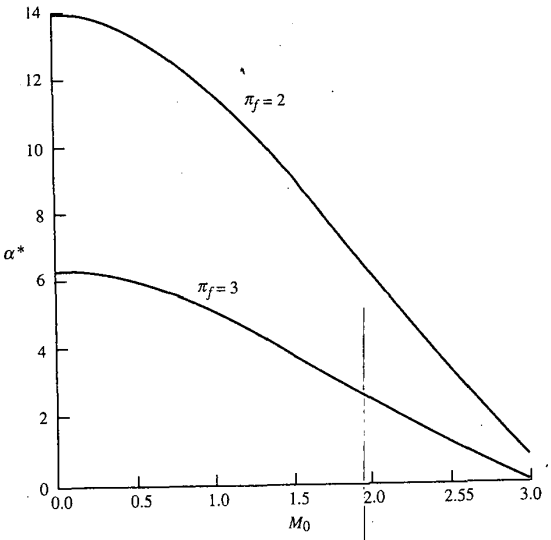

FIGURE 5-29*c*
α^* versus M_0, for $\pi_c = 24$ and $\pi_f = 2$ and 3.

The optimum bypass ratio is plotted in Fig. 5-29*a* versus the compressor pressure ratio for a flight Mach number of 0.9 and fan pressure ratio of 2. From this plot, we can see that the optimum bypass ratio increases with the compressor pressure ratio. The optimum bypass ratio is plotted in Fig. 5-29*b* versus the fan pressure ratio, and this figure shows that optimum bypass ratio decreases with fan pressure ratio.

The optimum bypass ratio versus the flight Mach number is plotted in Fig. 5-29*c* for fan pressure ratios of 2 and 3. From these plots, we can see that the optimum bypass ratio decreases with the flight Mach number. Note that the optimum engine is a turbojet at a Mach number of about 3.0 for a fan pressure ratio of 3.

The plots of specific thrust and thrust specific fuel consumption for an ideal turbofan engine with optimum bypass ratio versus compressor pressure ratio are superimposed on Figs. 5-23*a* through 5-23*e* by a dashed line marked α^*. The optimum-bypass-ratio ideal turbofan has the minimum thrust specific fuel consumption.

The plots of specific thrust and thrust specific fuel consumption for the optimum-bypass-ratio ideal turbofan versus fan pressure ratio are superimposed on Figs. 5-25*a* through 5-25*d* by a dashed line marked α^*. As shown in these figures, the plot for α^* is the locus of the minimum value of S for each π_f.

The plots of specific thrust and thrust specific fuel consumption for the optimum-bypass-ratio ideal turbofan versus flight Mach number are superimposed on Figs. 5-27*a* through 5-27*e* for a fan pressure ratio of 2 and on Figs. 5-28*a* through 5-28*e* for a fan pressure ratio of 3. As shown in these figures, the plots for α^* are the locus of the minimum value of S for fixed values of π_c and π_f.

The thermal efficiency of an optimum-bypass-ratio ideal turbofan is the same as that of an ideal turbojet. The bypass ratio of an ideal turbofan affects only the propulsive efficiency. The propulsive efficiency of an optimum-bypass-ratio ideal turbofan is superimposed on those of Figs. 5-23*d*, 5-25*c*, 5-27*c*, and 5-28*c*. As can be seen, the optimum bypass ratio gives the maximum propulsive efficiency. Likewise, as shown in Figs. 5-23*d*, 5-25*c*, 5-27*d*, and 5-28*d*, the optimum bypass ratio gives the maximum overall efficiency. The thrust ratio of an optimum-bypass-ratio ideal turbofan is superimposed on those of Figs. 5-23*e*, 5-25*d*, 5-27*e*, and 5-28*e* and is equal to 0.5.

5-11 IDEAL TURBOFAN WITH OPTIMUM FAN PRESSURE RATIO

Figures 5-25*a* and 5-25*b* show that for given flight conditions T_0 and M_0, design limit τ_λ, compressor pressure ratio π_c, and bypass ratio α, there is an optimum fan pressure ratio π_f which gives the minimum specific fuel consumption and maximum specific thrust. As will be shown, the optimum fan pressure ratio corresponds to the exit velocity V_{19} of the fan stream, being equal to the exit velocity of the core stream V_9. It is left, as a reader exercise, to show that equal exit velocities ($V_9 = V_{19}$) correspond to maximum propulsive efficiency.

Optimum Fan Pressure Ratio π_f^*

For a given set of prescribed variables (τ_r, π_c, τ_λ, V_0, α), we may locate the optimum fan pressure ratio by taking the partial derivative of the specific

thrust with respect to the fan total temperature ratio. The derivation of an expression for the optimum fan total temperature ratio and, by Eq. (5-58*f*), the optimum fan pressure ratio follows. From Eq. (5-54), we have

$$\frac{\partial S}{\partial \tau_f} = \frac{-f}{[(1+\alpha)(F/\dot{m}_0)]^2} \frac{\partial}{\partial \tau_f}\left[(1+\alpha)\left(\frac{F}{\dot{m}_0}\right)\right] = 0$$

Thus $\dfrac{\partial S}{\partial \tau_f} = 0$ is satisfied by $\dfrac{\partial}{\partial \tau_f}\left[\dfrac{g_c}{V_0}(1+\alpha)\left(\dfrac{F}{\dot{m}_0}\right)\right] = 0$

where $$\frac{g_c}{V_0}(1+\alpha)\left(\frac{F}{\dot{m}_0}\right) = \frac{V_9}{V_0} - 1 + \alpha\left(\frac{V_{19}}{V_0} - 1\right)$$

Hence the optimum fan pressure ratio is given by solution of

$$\frac{\partial}{\partial \tau_f}\left[\frac{V_9}{V_0} - 1 + \alpha\left(\frac{V_{19}}{V_0} - 1\right)\right] = \frac{\partial}{\partial \tau_f}\left(\frac{V_9}{V_0}\right) + \alpha \frac{\partial}{\partial \tau_f}\left(\frac{V_{19}}{V_0}\right) = 0 \tag{i}$$

Since $$\frac{\partial}{\partial \tau_f}\left(\frac{V_9}{V_0}\right) = \frac{1}{2V_9/V_0} \frac{\partial}{\partial \tau_f}\left[\left(\frac{V_9}{V_0}\right)^2\right]$$

and $$\frac{\partial}{\partial \tau_f}\left(\frac{V_{19}}{V_0}\right) = \frac{1}{2V_{19}/V_0} \frac{\partial}{\partial \tau_f}\left[\left(\frac{V_{19}}{V_0}\right)^2\right]$$

Eq. (i) becomes

$$\frac{1}{2V_9/V_0} \frac{\partial}{\partial \tau_f}\left[\left(\frac{V_9}{V_0}\right)^2\right] + \alpha \frac{1}{2V_{19}/V_0} \frac{\partial}{\partial \tau_f}\left[\left(\frac{V_{19}}{V_0}\right)^2\right] = 0 \tag{ii}$$

To determine the first term of Eq. (ii), we start with

$$\left(\frac{V_9}{V_0}\right)^2 = \frac{1}{M_0^2}\left(\frac{V_9}{a_0}\right)^2 = \frac{1}{[(\gamma-1)/2](\tau_r - 1)}\left(\frac{V_9}{a_0}\right)^2$$

$$= \frac{\tau_\lambda - \tau_r[\tau_c - 1 + \alpha(\tau_f - 1)] - \tau_\lambda/(\tau_r \tau_c)}{\tau_r - 1} \tag{iii}$$

Thus $$\frac{\partial}{\partial \tau_f}\left[\left(\frac{V_9}{V_0}\right)^2\right] = \frac{-\alpha \tau_r}{\tau_r - 1} \tag{iv}$$

To determine the second term of Eq. (ii), we start with

$$\left(\frac{V_{19}}{V_0}\right)^2 = \frac{1}{M_0^2}\left(\frac{V_{19}}{a_0}\right)^2 = \frac{1}{[(\gamma-1)/2](\tau_r - 1)}\left(\frac{V_{19}}{a_0}\right)^2 = \frac{\tau_r \tau_f - 1}{\tau_r - 1} \tag{v}$$

Thus $$\frac{\partial}{\partial \tau_f}\left[\left(\frac{V_{19}}{V_0}\right)^2\right] = \frac{\tau_r}{\tau_r - 1} \tag{vi}$$

Substitution of Eqs. (iv) and (vi) into Eq. (ii) gives

$$\frac{1}{2V_9/V_0}\left(\frac{-\alpha\tau_r}{\tau_r-1}\right)+\alpha\frac{1}{2V_{19}/V_0}\frac{\tau_r}{\tau_r-1}=0 \tag{vii}$$

Thus we can conclude from Eq. (vii) that the optimum fan pressure ratio corresponds to that value of τ_f yielding

$$\boxed{V_9 = V_{19}} \tag{5-64}$$

Also

$$\boxed{\text{FR} = 1} \tag{5-65}$$

To solve for the optimum fan temperature ratio, we equate Eqs. (iii) and (v):

$$\left(\frac{V_9}{V_0}\right)^2 = \frac{\tau_\lambda - \tau_r[\tau_c - 1 + \alpha(\tau_f - 1)] - \tau_\lambda/(\tau_r\tau_c)}{\tau_r - 1}$$

$$= \left(\frac{V_{19}}{V_0}\right)^2 = \frac{\tau_r\tau_f - 1}{\tau_r - 1}$$

giving

$$\boxed{\tau_f^* = \frac{\tau_\lambda\tau_r(\tau_c - 1) - \tau_\lambda/(\tau_r\tau_c) + \alpha\tau_r + 1}{\tau_r(1+\alpha)}} \tag{5-66}$$

An equation for the specific thrust of an optimum-fan-pressure-ratio turbofan can be obtained by starting with the simplified expression

$$\left(\frac{F}{\dot{m}_0}\right)_{\tau_f^*} = \frac{a_0}{g_c}\left(\frac{V_{19}}{a_0} - M_0\right)$$

which becomes

$$\boxed{\left(\frac{F}{\dot{m}_0}\right)_{\tau_f^*} = \frac{a_0}{g_c}\left[\sqrt{\frac{2}{\gamma-1}(\tau_r\tau_f^* - 1)} - M_0\right]} \tag{5-67}$$

The propulsive efficiency for the optimum-fan-pressure-ratio turbofan engine is simply

$$\boxed{(\eta_P)_{\tau_f^*} = \frac{2}{V_{19}/V_0 + 1}} \tag{5-68}$$

Summary of Equations—Optimum-Fan-Pressure-Ratio Ideal Turbofan

INPUTS: M_0, T_0(K, °R), γ, $c_p\left(\frac{\text{kJ}}{\text{kg}\cdot\text{K}}, \frac{\text{Btu}}{\text{lbm}\cdot\text{°R}}\right)$, $h_{PR}\left(\frac{\text{kJ}}{\text{kg}}, \frac{\text{Btu}}{\text{lbm}}\right)$, T_{t4}(K, °R), π_c, α

OUTPUTS: $\frac{F}{\dot{m}_0}\left(\frac{\text{N}}{\text{kg/sec}}, \frac{\text{lbf}}{\text{lbm/sec}}\right)$, f, $S\left(\frac{\text{mg/sec}}{\text{N}}, \frac{\text{lbm/hr}}{\text{lbf}}\right)$, η_T, η_P, η_O, π_f^*

EQUATIONS: Equations (5-58*a*) through (5-58*e*), (5-58*j*), (5-58*l*), plus

$$\tau_f^* = \frac{\tau_\lambda - \tau_r(\tau_c - 1) - \tau_\lambda/(\tau_r\tau_c) + \alpha\tau_r + 1}{\tau_r(1+\alpha)} \tag{5-69a}$$

$$\pi_f^* = (\tau_f^*)^{\gamma/(\gamma-1)} \tag{5-69b}$$

$$\frac{V_{19}}{a_0} = \sqrt{\frac{2}{\gamma-1}(\tau_r\tau_f^* - 1)} \tag{5-69c}$$

$$\frac{F}{\dot{m}_0} = \frac{a_0}{g_c}\left(\frac{V_{19}}{a_0} - M_0\right) \tag{5-69d}$$

$$\eta_P = \frac{2M_0}{V_{19}/a_0 + M_0} \tag{5-69e}$$

and Eqs. (5-58*k*) and (5-58*n*)

Effect of Bypass Ratio on Specific Thrust and Fuel Consumption

Data for several turbofan engines are listed in Table 5-2. The bypass ratio ranges from 0.76 for the engine in the smaller A-7D fighter attack airplane to 5 for engines in the commercial transports, to 8 for the C-5A/B heavy logistics military transport engine. The specific thrust and specific fuel consumption for the fighter are about twice their values for the three transport-type airplanes. Let us look at the interrelationship between the bypass ratio, specific thrust,

TABLE 5-2

Engine	Bypass ratio α	$F/\dot{m}_0$ {[N/(kg/sec) [lbf/(lbm/sec)]}	S {[(mg/sec)/N] [(lbm/hr)/lbf]}	π_f	π_c	Aircraft
TF-39	8.0	251.8 (25.68)	8.87 (0.313)	1.45	22.0	C5A/B
JT9D	5.1	253.4 (25.84)	9.80 (0.346)	1.54	22.3	Boeing 747
CF6	4.32	255.6 (26.06)	9.86 (0.348)	1.71	30.2	DC-10
TF-41	0.76	498.0 (50.78)	17.8 (0.629)	2.45	21.0	A-7D

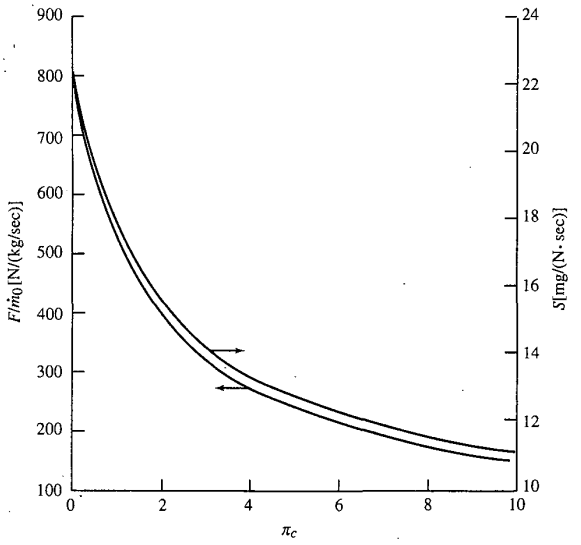

FIGURE 5-30
Performance at π_f^* versus α, for $\pi_c = 24$ and $M_0 = 0.8$.

and specific fuel consumption to help explain the trends in the values of these quantities, as exhibited by the table.

We can examine how these quantities interact for the ideal turbofan with optimum fan pressure ratio by plotting specific thrust and thrust specific fuel consumption versus bypass ratio. Such plots are given in Fig. 5-30 for $M_0 = 0.8$, $T_0 = 216.7\,\text{K}$, $\tau_\lambda = 6.5$, $\pi_c = 24$, $h_{PR} = 42{,}800\,\text{kJ/kg}$, $\gamma = 1.4$, and $c_p = 1.004\,\text{kJ/(kg} \cdot \text{K)}$. The optimum fan pressure ratio which gives $V_9 = V_{19}$ is plotted versus the bypass ratio α in Fig. 5-31.

We can see, in Fig. 5-30, a sharp reduction in specific fuel consumption as α increases from zero. An equally marked, but unfavorable, decrease in thrust per unit mass flow occurs. A large fraction of the beneficial decrease in S is obtained by selecting an α of about 5, as was done for the engines in the DC-10 and 747 transports. At a bypass ratio of 8, corresponding to the C-5A engines, a further decrease in specific fuel consumption is realized. Since engine weight is a small fraction of the takeoff gross weight for these airplanes, it is of secondary importance compared to fuel weight and hence specific fuel consumption. Thus we find a relatively large bypass ratio for the engines in the transporters tabulated compared to the 0.76 value of the A-7D engine.

Example 5-6. The engine that we looked at in Sec. 5-9 is used again in this section for an example. The following values are held constant for all plots:

$T_0 = 216.7\,\text{K}$ $\gamma = 1.4$ $c_p = 1.004\,\text{kJ/(kg K)}$ $h_{PR} = 42{,}800\,\text{kJ/kg}$ $T_{t4} = 1670\,\text{K}$

engines, and it is wise to review such reasons so that we can comprehend why similar concepts are again gaining in popularity.

A major reason for the success of the turbofan was its high (subsonic) Mach number capability. In a turboprop, the propeller tip Mach numbers became very large above approximately $M = 0.7$, and the resultant loss in propeller efficiency limits the turboprop use to Mach numbers less than 0.7. With a turbofan, the onset of high-Mach-number effects is reduced by the diffusion within the duct. In addition, the individual blade loading can be much reduced by utilizing many blades. A second important benefit of conventional turbofans is that they require no gearbox to reduce the tip speeds of their relatively short blades. (Note, of course, that usually a turbofan engine has multiple spools.) Turboprop gearboxes have, to date, been heavy and subject to reliability problems. Finally, the high tip speed of the turboprops led to high noise levels, both in the airport vicinity and within the aircraft at flight speeds.

Recent studies of the very-high-bypass-ratio engines have, however, suggested some compromise designs that show high promise. Thus if a bypass ratio of, say, 25 is selected, the corresponding cowl could have identified with it both weight penalties and drag penalties that do not compensate for the benefits of the inlet diffusion and of the reduction in tip losses. By considering this "in between" bypass ratio, the required shaft speed reduction will be reduced with the result that a lighter and simpler gearbox may be utilized. The effects of tip losses and noise production may be somewhat curtailed by utilizing many (about eight) of the smaller blades and by sweeping the blades to reduce the relative Mach numbers. An additional benefit is available in that the blades may be made variable-pitch which will allow high propeller efficiencies to be maintained over a wide operating range. Recall [Eq. (1-16)] that the propulsive efficiency of a single-exhaust engine is $\eta_P = 2V_0/(V_j + V_0)$, where V_0 = flight speed and V_j = jet speed.

This expression is appropriate for a propeller also, and it serves to emphasize that we want a large propeller [to reduce V_j for a given thrust $F = \dot{m}_0(V_j - V_0)/g_c$] if the propulsive efficiency is to be high. The *propulsive efficiency* represents the ideal limit of the propeller efficiency and is defined as

$$\eta_{\text{prop}} = \frac{\text{power to vehicle}}{\text{power to propeller}} = \frac{F_{\text{prop}} V_0}{\dot{W}_{\text{prop}}} \tag{5-87}$$

Thus

$$\eta_{\text{prop}} = \frac{F_{\text{prop}} V_0}{\dot{W}_{\text{prop}}} = \frac{\dot{m}_{\text{prop}}(V_j - V_0)}{\frac{1}{2}\dot{m}_{\text{prop}}(V_j^2 - V_0^2)} \frac{\frac{1}{2}\dot{m}_{\text{prop}}(V_j^2 - V_0^2)}{\dot{W}_{\text{prop}}}$$

$$\equiv \eta_P \eta_L \tag{5-88}$$

where $\dot{W}_{\text{prop}}$ = propeller power in, η_P is the propulsive efficiency and

$$\eta_L = \frac{\frac{1}{2}\dot{m}_{\text{prop}}(V_j^2 - V_0^2)}{\dot{W}_{\text{prop}}} \tag{5-89}$$

represents the power output of the propeller to the stream divided by the power input to the propeller.

Thus we expect the propeller efficiency to increase with propeller size simply because the ideal propeller efficiency (i.e., the propulsive efficiency) increases. This, of course, relates the propeller efficiency and bypass ratio. The propeller size will, in practice, be limited by the onset of tip Mach number losses, etc., which would be reflected in a reduced η_L.

Cycle Analysis

It is appropriate in analyzing the turboprop class of engine to consider the work supplied to the vehicle, rather than the thrust. To facilitate this, we introduce the dimensionless *work output coefficient C,* defined as

$$C = \frac{\text{power interaction/mass flow of air through engine core}}{h_0} \tag{5-90}$$

For the thrust of the core stream, we define its work output coefficient as

$$C_C = \frac{F_C V_0}{\dot{m}_0 c_p T_0} \tag{5-91}$$

Thus the work output coefficient for the total turboprop engine is

$$C_{\text{tot}} = C_{\text{prop}} + C_C \tag{5-92}$$

and the corresponding thrust is

$$F = F_{\text{prop}} + F_C = \frac{C_{\text{tot}}\dot{m}_0 c_p T_0}{V_0} \tag{5-93}$$

It is usual, with turboprop engines, to have the core stream exit nozzles unchoked, so the pressure imbalance term will not contribute in the expression for the thrust. We consider the numbering stations indicated in Figs.

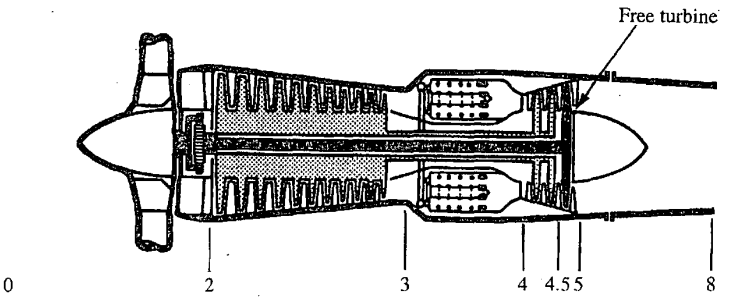

FIGURE 5-40*a*
Station numbering of turboprop engine. (*Courtesy of Pratt & Whitney.*)

5-40*a* and 5-40*b*, and we proceed with the analysis in much the same way as with the previously considered engine types.

For a turboprop engine, we have two design variables—the compressor pressure ratio and the low-pressure (free or power) turbine temperature ratio. We want to develop the cycle equations in terms of the pressure and temperature ratios across both the high-pressure turbine (drives the compressor) and the low-pressure turbine. With station number 4.5 between the high- and low-pressure turbines, we define

$$\pi_{tH} = \frac{P_{t4.5}}{P_{t4}} \qquad \tau_{tH} = \frac{T_{t4.5}}{T_{t4}} \qquad \pi_{tL} = \frac{T_{t5}}{T_{t4.5}} \qquad \tau_{tL} = \frac{T_{t5}}{T_{t4.5}} \tag{5-94}$$

Step 1. We have for the engine core

$$\frac{F_C}{\dot{m}_0} = \frac{a_0}{g_c}\left(\frac{V_9}{a_0} - M_0\right)$$

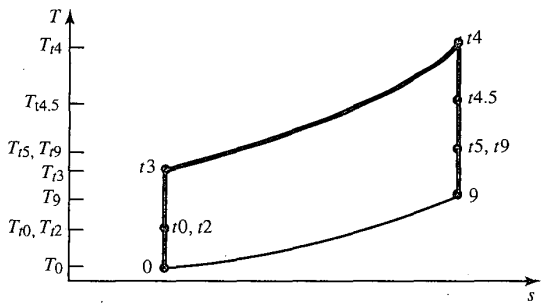

FIGURE 5-40*b*
The *T*-*s* diagram of ideal turboprop engine.

Then
$$C_C = \frac{V_0}{c_p T_0}\frac{a_0}{g_c}\left(\frac{V_9}{a_0} - M_0\right)$$

Thus
$$\boxed{C_C = (\gamma - 1)M_0\left(\frac{V_9}{a_0} - M_0\right)} \tag{5-95}$$

Step 2. Now $V_9/a_0 = \sqrt{T_9/T_0}M_9$, where

$$M_9 = \sqrt{\frac{2}{\gamma - 1}\left[\left(\frac{P_{t9}}{P_9}\right)^{(\gamma-1)/\gamma} - 1\right]} \tag{5-96}$$

Step 3.
$$\frac{P_{t9}}{P_9} = \frac{P_0}{P_9}\pi_r\pi_d\pi_c\pi_b\pi_{tH}\pi_{tL}\pi_n = \pi_r\pi_c\pi_{tH}\pi_{tL}$$

$$\boxed{M_9 = \sqrt{\frac{2}{\gamma - 1}(\tau_r\tau_c\tau_{tH}\tau_{tL} - 1)}} \tag{5-97}$$

Step 4.
$$\frac{T_9}{T_0} = \frac{T_{t9}/T_0}{T_{t9}/T_9} = \frac{T_{t9}/T_0}{(P_{t9}/P_9)^{(\gamma-1)/\gamma}}$$

where
$$\frac{T_{t9}}{T_0} = \tau_\lambda\tau_{tH}\tau_{tL}\tau_n = \tau_\lambda\tau_{tH}\tau_{tL}$$

and
$$\left(\frac{P_{t9}}{P_9}\right)^{(\gamma-1)/\gamma} = (\pi_r\pi_c\pi_{tH}\pi_{tL})^{(\gamma-1)/\gamma} = \tau_r\tau_c\tau_{tH}\tau_{tL}$$

Thus
$$\boxed{\frac{T_9}{T_0} = \frac{\tau_\lambda}{\tau_r\tau_c}} \tag{5-98}$$

Step 5. From the energy balance of the ideal turbojet's burner, we have

$$f = \frac{c_p T_0}{h_{PR}}(\tau_\lambda - \tau_r\tau_c) \tag{5-25}$$

Step 6. For the high-pressure turbine, we have from the ideal turbojet analysis

$$\boxed{\tau_{tH} = 1 - \frac{\tau_r}{\tau_\lambda}(\tau_c - 1)} \tag{5-99}$$

For the low-pressure turbine (also called *free turbine*), we equate the power out of this turbine to the power into the propeller. Thus

$$\dot{m}_{4.5}c_p(T_{t4.5} - T_{t5}) = \dot{W}_{\text{prop}}$$

or
$$\boxed{C_{\text{prop}} = \frac{\eta_{\text{prop}}\dot{W}_{\text{prop}}}{\dot{m}_0 c_p T_0} = \eta_{\text{prop}}\tau_\lambda\tau_{tH}(1 - \tau_{tL})} \tag{5-100}$$

TABLE 8-1
Comparison of analysis variables

Variable	Parametric cycle	Engine performance
Flight condition (M_0, T_0, and P_0)	Independent	Independent
Compressor pressure ratio π_c	Independent	Dependent
Main burner exit temperature T_{t4}	Independent	Independent
Turbine temperature ratio τ_t	Dependent	Constant

conditions were specified via the design inputs: T_{t4}, M_0, T_0, and P_0. In addition, the engine cycle was selected along with the compressor pressure atio, the polytropic efficiency of turbomachinery components, etc. For the combination of design input values, the resulting calculations yielded the specific performance of the engine (specific thrust and thrust specific fuel consumption), required turbine temperature ratio, and the efficiencies of the turbomachinery (fan, compressor, and turbine). The specific combination or design input values is referred to as the engine *design point* or *reference point.* The resulting specific engine thrust and fuel consumption are valid only for the given engine cycle and values of T_{t4}, M_0, T_0, π_c, τ_t, η_c, etc. When we changed any of these values in parametric cycle analysis, we were studying a "rubber" engine, i.e., one which changes its shape and component design to meet the thermodynamic, fluid dynamic, etc., requirements.

When a gas turbine engine is designed and built, the degree of variability of an engine depends upon available technology, the needs of the principal application for the engine, and the desires of the designers. Most gas turbine engines have constant-area flow passages and limited variability (variable T_{t4}; *and sometimes variable* T_{t7} and exhaust nozzle throat area). In a simple constant-flow-area turbojet engine, the performance (pressure ratio and mass flow rate) of its compressor depends upon the power from the turbine and the inlet conditions to the compressor. As we will see in this chapter, a simple analytical expression can be used to express the relationship between the compressor performance and the independent variables: throttle setting (T_{t4}) and flight condition (M_0, T_0, P_0).

When a gas turbine engine is installed in an aircraft, its performance varies with flight conditions and throttle setting and is limited by the engine control system. In flight, the pilot controls the operation of the engine directly through the throttle and indirectly by changing flight conditions. The thrust and fuel consumption will thereby change. In this chapter, we will look at how specific engine cycles perform at conditions other than their design (or reference) point.

There are several ways to obtain this engine performance. One way is to look at the interaction and performance of the compressor-burner-turbine combination, known as the *pumping characteristics* of the gas generator. In this case, the performance of the components is known since the gas generator exists. However, in a preliminary design, the gas generator has not been built,

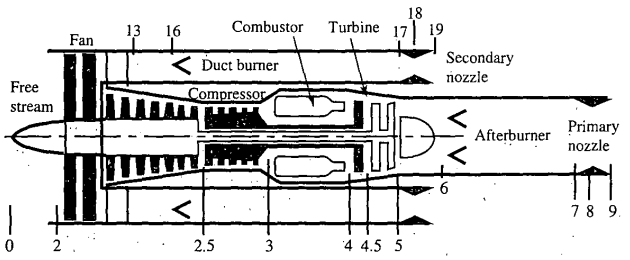

FIGURE 8-1
Station numbering for two-spool gas turbine engine.

and the pumping characteristics are not available. In such a case, the gas generator performance can be estimated by using first principles and estimates of the variations in component efficiencies. In reality, the principal effects of engine performance occur because of the changes in propulsive efficiency and thermal efficiency (rather than because of changes in component efficiency). Thus a good approximation of an engine's performance can be obtained by simply assuming that the component efficiencies remain constant.

The analysis of engine performance requires a model for the behavior of each engine component over its actual range of operation. The more accurate and complete the model, the more reliable the computed results. Even though the approach (constant efficiency of rotating components and constant total pressure ratio of the other components) used in this textbook gives answers that are perfectly adequate for preliminary design, it is important to know that the usual industrial practice is to use data or correlations having greater accuracy and definition in the form of component "maps." The principal values of the maps are to improve the understanding of component behavior and to slightly increase the accuracy of the results.

Nomenclature

The station numbering used for the performance analysis of the turbojet and turbofan is shown in Fig. 8-1. Note that the turbine is divided into a high-pressure turbine (station 4 to 4.5) and a low-pressure turbine (station 4.5 to 5). The high-pressure turbine drives the high-pressure compressor (station 2.5 to 3), and the low-pressure turbine drives the fan (station 2 to 13) and low-pressure compressor (station 2 to 2.5).

The assembly containing the high-pressure turbine, high-pressure compressor, and connecting shaft is called the *high-pressure spool.* That containing the low-pressure turbine, fan or low-pressure compressor, and connecting shaft is called the *low-pressure spool.* In addition to the τ and π values defined in Table 5-1, the component total temperature ratios and total pressure ratios listed in Table 8-2 are required for analysis of the above gas turbine engine with high- and low-pressure spools.

TABLE 8-2
Additional temperature and pressure relationships

$\tau_{cH} = \frac{T_{t3}}{T_{t2.5}}$	$\pi_{cH} = \frac{P_{t3}}{P_{t2.5}}$	$\tau_{tH} = \frac{T_{t4.5}}{T_{t4}}$	$\pi_{tH} = \frac{P_{t4.5}}{P_{t4}}$
$\tau_{cL} = \frac{T_{t2.5}}{T_{t2}}$	$\pi_{cL} = \frac{P_{t2.5}}{P_{t2}}$	$\tau_{tL} = \frac{T_{t5}}{T_{t4.5}}$	$\pi_{tL} = \frac{P_{t5}}{P_{t4.5}}$
$\tau_c = \tau_{cL}\tau_{cH}$	$\pi_c = \pi_{cL}\pi_{cH}$	$\tau_t = \tau_{tH}\tau_{tL}$	$\pi_t = \pi_{tH}\pi_{tL}$

Reference Values and Engine Performance Analysis Assumptions

Functional relationships are used to predict the performance of a gas turbine engine at different flight conditions and throttle settings. These relationships are based on the application of mass, energy, momentum, and entropy considerations to the one-dimensional steady flow of a perfect gas at an engine steady-state operating point. Thus, if

$$f(\tau, \pi) = \text{constant}$$

represents a relationship between the two engine variables τ and π at a steady-state operating point, then the constant can be evaluated at a reference condition (subscript R) so that

$$f(\tau, \pi) = f(\tau_R, \pi_r) = \text{constant}$$

since $f(\tau, \pi)$ applies to the engine at all operating points. *Sea-level static* (*SLS*) *is the normal reference condition* (*design point*) *for the value of the gas turbine engine variables.* This technique for replacing constants with reference conditions is frequently used in the analysis to follow.

For conventional turbojet, turbofan, and turboprop engines, we will consider the simple case where the high-pressure turbine entrance nozzle, low-pressure turbine entrance nozzle, and primary exit nozzle (and bypass duct nozzle for the separate-exhaust turbofan) are choked. In addition, we assume that the throat areas where choking occurs in the high-pressure turbine entrance nozzle and the low-pressure turbine entrance nozzle are constant. This type of turbine is known as a *fixed-area turbine* (FAT) engine. These assumptions are true over a wide operating range for modern gas turbine engines. The following performance analyses also include the case(s) of unchoked engine exit nozzle(s).

The following assumptions will be made in the turbojet and turbofan performance analysis:

1. The flow is choked at the high-pressure turbine entrance nozzle, low-pressure turbine entrance nozzle, and the primary exit nozzle. Also the bypass duct nozzle for the turbofan is choked.

2. The total pressure ratios of the main burner, primary exit nozzle, and bypass stream exit nozzle (π_b, π_n, and π_{fn}) do not change from their reference values.
3. The component efficiencies (η_c, η_f, η_b, η_{tH}, η_{tL}, η_{mH}, and η_{mL}) do not change from their reference values.
4. Turbine cooling and leakage effects are neglected.
5. No power is removed from the turbine to drive accessories (or alternately, η_{mH} or η_{mL} includes the power removed but is still constant).
6. Gases will be assumed to be calorically perfect both upstream and downstream of the main burner, and γ_t and c_{pt} do not vary with the power setting (T_{t4}).
7. The term unity plus the fuel/air ratio $(1+f)$ will be considered as a constant.

Assumptions 4 and 5 are made to simplify the analysis and increase understanding. Reference 12 includes turbine cooling air, compressor bleed air, and power takeoff in the performance analysis. Assumptions 6 and 7 permit easy analysis which results in a set of algebraic expressions for an engine's performance. The performance analysis of an engine with variable gas properties is covered in Sec. 8-8.

Dimensionless and Corrected Component Performance Parameters

Dimensional analysis identifies correlating parameters that allow data taken under one set of conditions to be extended to other conditions. These parameters are useful and necessary because it is always impractical to accumulate experimental data for the bewildering number of possible operating conditions, and because it is often impossible to reach many of the operating conditions in a single, affordable facility.

The quantities of pressure and temperature are normally made dimensionless by dividing each by its respective standard sea-level static values. The dimensionless pressure and temperature are represented by δ and θ, respectively. When total (stagnation) properties are nondimensionalized, a subscript is used to indicate the station number of that property. The only static properties made dimensionless are free stream, the symbols for which carry no subscripts. Thus

$$\boxed{\delta_i \equiv \frac{P_{ti}}{P_{\text{ref}}}} \tag{8-1a}$$

and

$$\boxed{\theta_i \equiv \frac{T_{ti}}{T_{\text{ref}}}} \tag{8-1b}$$

where $P_{\text{ref}} = 14.696$ psia (101,300 Pa) and $T_{\text{ref}} = 518.69°\text{R}$ (288.2 K).

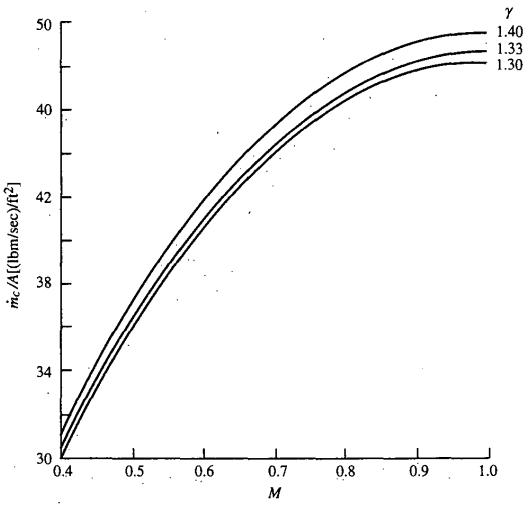

FIGURE 8-2
Variation of corrected mass flow per area.

Dimensionless analysis of engine components yields many useful dimensionless and/or modified component performance parameters. Some examples of these are the compressor pressure ratio, adiabatic efficiency, Mach number at the compressor face, ratio of blade (tip) speed to the speed of sound, and the Reynolds number.

The *corrected mass flow rate* at engine station i used in this analysis is defined as

$$\dot{m}_{ci} \equiv \frac{\dot{m}_i \sqrt{\theta_i}}{\delta_i} \tag{8-2}$$

and is related to the Mach number at station i as shown below. From the definition of the mass flow parameter [Eq. (3-12)], we can write the mass flow at station i as

$$\dot{m}_i = \frac{P_{ti}}{\sqrt{T_{ti}}} A_i \times \text{MFP}(M_i)$$

Then

$$\frac{\dot{m}_{ci}}{A_i} = \frac{\dot{m}_i \sqrt{T_{ti}}}{P_{ti}} \frac{P_{\text{ref}}}{\sqrt{T_{\text{ref}}}} = \frac{P_{\text{ref}}}{\sqrt{T_{\text{ref}}}} \text{MFP}(M_i) \tag{8-3}$$

and the corrected mass flow rate per unit area is a function of the Mach number alone for a gas. Equation (8-3) is plotted versus Mach number in Fig. 8-2 for three different γ values. Aircraft gas turbine engines need high thrust or

power per unit weight which requires high corrected mass flow rates per unit area.

At the entrance to the fan or compressor (station 2), the design Mach number is about 0.56 which corresponds to a corrected mass flow rate per unit area of about 40 lbm/(sec · ft^2). A reduction in engine power will lower the corrected mass flow rate and the corresponding Mach number into the fan or compressor.

The flow is normally choked at the entrance to the turbine (station 4) and the throat of the exhaust nozzle (station 8) for most steady-state operating conditions of interest (the flow is typically unchoked at these stations during engine start-up). When the flow is choked at station 4, the corrected mass flow rate per unit area entering the turbine is constant, which helps define the pumping characteristics of the gas generator. As shown later in this chapter, choked flow at both stations 4 and 8 limits the turbine operation. Even if the flow unchokes at a station and the Mach number drops from 1.0 to 0.9, the corrected mass flow rate is reduced less than 1 percent. Thus the corrected mass flow rate is considered constant when the flow is near or at choking conditions.

Choked flow at station 8 is desired in convergent-only exhaust nozzles to obtain high exit velocity and is required in a convergent-divergent exhaust nozzle to reach supersonic exit velocities. When the afterburner is operated on a turbojet or turbofan engine with choked exhaust nozzle, T_{t8} increases—this requires an increase in the nozzle throat area A_8 to maintain the correct mass flow rate/area ratio corresponding to choked conditions. If the nozzle throat is not increased, the pressure increases and the mass flow rate decreases, which can adversely impact the upstream engine components.

The *corrected engine speed* at engine station i used in this analysis is defined as

$$N_{ci} \equiv \frac{N}{\sqrt{\theta_i}} \tag{8-4}$$

and is related to the *blade* Mach number.

These four parameters represent a first approximation of the complete set necessary to reproduce nature for the turbomachinery. These extremely useful parameters have become a standard in the gas turbine industry and are summarized in Table 8-3.

Three additional corrected quantities have found common acceptance for describing the performance of gas turbine engines: corrected thrust F_c, corrected thrust specific fuel consumption S_c, and correct fuel mass flow rate $\dot{m}_{fc}$.

The *corrected thrust* is defined as

$$F_c \equiv \frac{F}{\delta_0} \tag{8-5}$$

TABLE 8-3
Corrected parameters

Parameter	Symbol	Corrected parameter
Total pressure	P_{ti}	$\delta_i = \frac{P_{ti}}{P_{\text{ref}}}$
Total temperature	T_{ti}	$\theta_i = \frac{T_{ti}}{T_{\text{ref}}}$
Rotational speed	N = RPM	$N_{ci} = \frac{N}{\sqrt{\theta_i}}$
Mass flow rate	$\dot{m}_i$	$\dot{m}_{ci} = \frac{\dot{m}_i\sqrt{\theta_i}}{\delta_i}$
Thrust	F	$F_c = \frac{F}{\delta_0}$
Thrust specific fuel consumption	S	$S_c = \frac{S}{\sqrt{\theta_0}}$
Fuel mass flow rate	$\dot{m}_f$	$\dot{m}_{fc} = \frac{\dot{m}_f}{\delta_2\sqrt{\theta_2}}$

For many gas turbine engines operating at maximum T_{t4}, the corrected thrust is essentially a function of only the corrected free-stream total temperature θ_0.

The *corrected thrust specific fuel consumption* is defined as

$$S_c \equiv \frac{S}{\sqrt{\theta_0}} \tag{8-6}$$

and the *corrected fuel mass flow rate* is defined as

$$\dot{m}_{fc} \equiv \frac{\dot{m}_f}{\delta_2\sqrt{\theta_2}} \tag{8-7}$$

Like the corrected thrust, these two corrected quantities collapse the variation in fuel consumption with flight condition and throttle setting.

These three corrected quantities are closely related. By using the equation for thrust specific fuel consumption

$$S = \frac{\dot{m}_f}{F}$$

$\pi_d = P_{t2}/P_{t0}$, and the fact that $\theta_2 = \theta_0$, the following relationship results between these corrected quantities:

$$S_c = \pi_d \frac{\dot{m}_{fc}}{F_c} \tag{8-8}$$

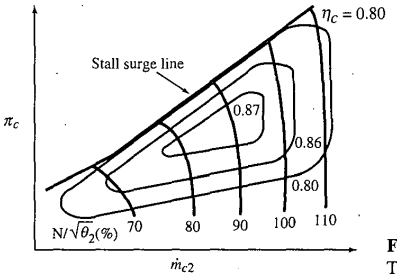

FIGURE 8-3
Typical compressor performance map.

These extremely useful corrected engine performance parameters have also become a standard in the gas turbine industry and are included in Table 8-3.

Component Performance Maps

COMPRESSOR AND FAN PERFORMANCE MAPS. The performance of a compressor or fan is normally shown by using the total pressure ratio, corrected mass flow rate, corrected engine speed, and component efficiency. Most often this performance is presented in one map showing the interrelationship of all four parameters, like that depicted in Fig. 8-3. Sometimes, for clarity, two maps are used, with one showing the pressure ratio versus corrected mass flow rate/corrected speed and the other showing compressor efficiency versus corrected mass flow rate/corrected speed.

A limitation on fan and compressor performance of special concern is the *stall* or *surge line*. Steady operation above the line is impossible, and entering the region even momentarily is dangerous to the gas turbine engine.

MAIN BURNER MAPS. The performance of the main burner is normally presented in terms of its performance parameters that are most important to engine performance: total pressure ratio of the main burner π_b and its combustion efficiency η_b. The total pressure ratio of the main burner is normally plotted versus the corrected mass flow rate through the burner ($\dot{m}_3\sqrt{\theta_3}/\delta_3$) for different fuel/air ratios f, as shown in Fig. 8-4*a*. The efficiency of the main burner can be represented as a plot versus the temperature rise in the main burner $T_{t4} - T_{t3}$ or fuel/air ratio f for various values of inlet pressures P_{t3}, as shown in Fig. 8-4*b*.

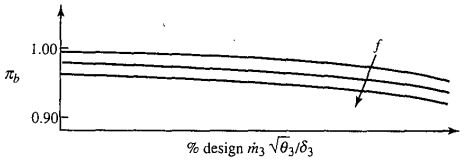

FIGURE 8-4*a*
Combustor pressure ratio.

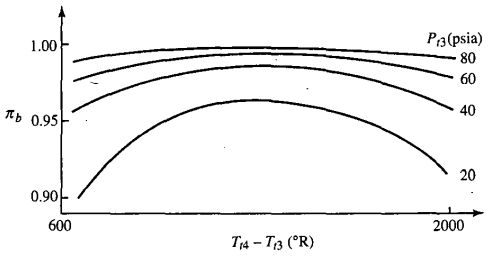

FIGURE 8-4*b*
Combustor efficiency.

TURBINE MAPS. The flow through a turbine first passes through stationary airfoils (often called *inlet guide vanes* or *nozzles*) which turn and accelerate the fluid, increasing its tangential momentum. The flow then passes through rotating airfoils (called *rotor blades*) that remove energy from the fluid as they change its tangential momentum. Successive pairs of stationary airfoils followed by rotating airfoils remove additional energy from the fluid. To obtain a high output power/weight ratio from a turbine, the flow entering the first-stage turbine rotor is normally supersonic which requires the flow to pass through sonic conditions at the minimum passage area in the inlet guide vanes (nozzles). By using Eq. (8-3), the corrected inlet mass flow rate based on this minimum passage area (throat) will be constant for fixed-inlet-area turbines. This flow characteristic is shown in the typical turbine flow map (Fig. 8-5*a*) when the expansion ratio across the turbine $[(P_{t4}/P_{t5}) = 1/\pi_t)]$ is greater than about 2 and the flow at the throat is choked.

The performance of a turbine is normally shown by using the total pressure ratio, corrected mass flow rate, corrected turbine speed, and component efficiency. This performance can be presented in two maps or a combined map (similar to that shown for the compressor in Fig. 8-3). When two maps are used, one map shows the interrelationship of the total pressure

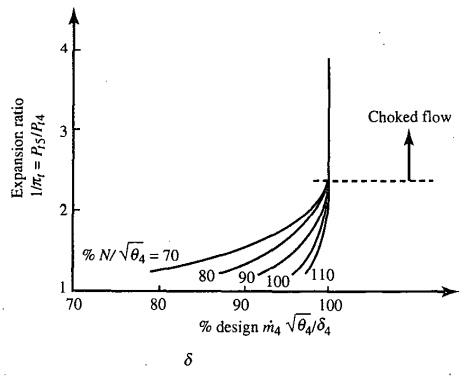

FIGURE 8-5*a*
Typical turbine flow map.

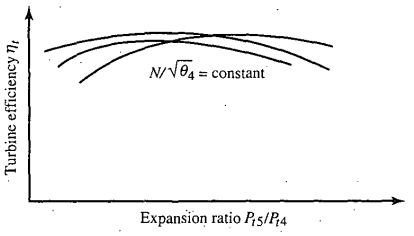

FIGURE 8-5*b*
Typical turbine efficiency map.

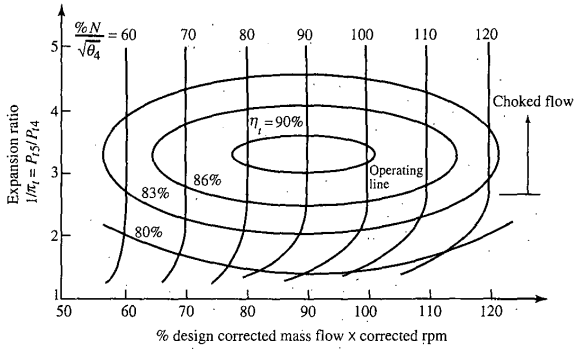

FIGURE 8-5*c*
Combined turbine performance map.

ratio, corrected mass flow rate, and corrected turbine speed, like that depicted in Fig. 8-5*a*. The other map shows the interrelationship of turbine efficiency versus corrected mass flow rate/expansion ratio, like that shown in Fig. 8-5*b*. When a combined map is used, the total pressure ratio of the turbine is plotted versus the product of corrected mass flow rate and the corrected speed, as shown in Fig. 8-5*c*. This spreads out the lines of constant corrected speed from those shown in Fig. 8-5*a*, and the turbine efficiency can now be shown. If we tried to add these lines of constant turbine efficiency to Fig. 8-5*a*, many would coincide with the line for choked flow.

For the majority of aircraft gas turbine engine operation, the turbine efficiency varies very little. In the analysis of this chapter, we consider that the turbine efficiency is constant.

8-2 GAS GENERATOR

The performance of a gas turbine engine depends on the operation of its gas generator. In this section, algebraic expressions for the pumping characteristics of a simple gas turbine engine are developed.

Conservation of Mass

We consider the flow through a single-spool turbojet engine with constant inlet area to the turbine (A_4 = constant). The mass flow rate into the turbine is equal to the sum of the mass flow rate through the compressor and the fuel flow rate into the main burner. Using the *mass flow parameter* (MFP), we can write

$$\dot{m}_2 + \dot{m}_f = (1+f)\dot{m}_2 = \dot{m}_4 = \frac{P_{t4}A_4}{\sqrt{T_{t4}}}\text{MFP}(M_4)$$

With the help of Eq. (8-3), the above equation yields the following expression for the compressor corrected mass flow rate:

$$\dot{m}_{c2} = \sqrt{\frac{T_{t2}}{T_{\text{ref}}}}\frac{P_{\text{ref}}}{P_{t2}}\frac{P_{t4}}{\sqrt{T_{t4}}}\frac{A_4}{1+f}\,\text{MFP}(M_4)$$

Noting that $P_{t4} = \pi_c\pi_b P_{t2}$, we see that

$$\boxed{\dot{m}_{c2} = \left(\frac{T_{t2}}{T_{t4}}\right)^{1/2}\pi_c\pi_b\frac{P_{\text{ref}}}{\sqrt{T_{\text{ref}}}}\frac{A_4}{1+f}\,\text{MFP}(M_4)} \tag{8-9}$$

Equation (8-9) is a straight line on a compressor map for constant values of T_{t4}/T_{t2}, A_4, f, and M_4. Lines of constant T_{t2}/T_{t4} are plotted on a typical compressor map in Figs. 8-6*a* and 8-6*b* for constant values of A_4 and f. Note

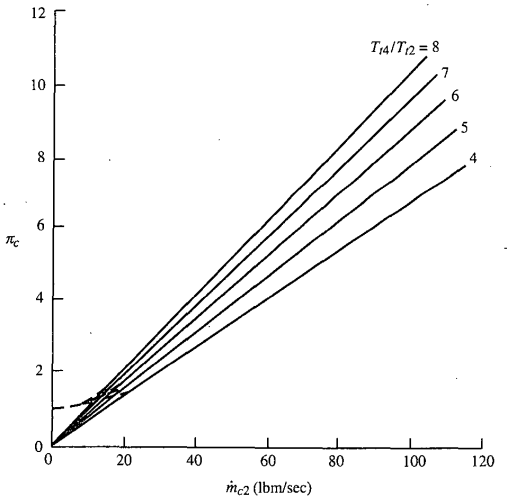

FIGURE 8-6*a*
Compressor map with lines of constant T_{t4}/T_{t2}.

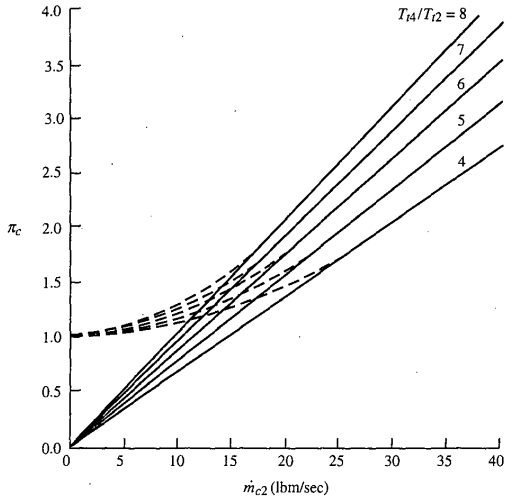

FIGURE 8-6*b*
Compressor map origin with lines of constant T_{t4}/T_{t2}.

that these lines start at a pressure ratio of 1 and corrected mass flow rate of 0 and are curved for low compressor pressure ratios (see Fig. 8-6*b*) because station 4 is unchoked. Station 4 chokes at a pressure ratio of about 2. At pressure ratios above 2, these lines are straight and appear to start at the origin (pressure ratio of 0 and mass flow rate of 0). The lines of constant T_{t2}/T_{t4} show the general characteristics required to satisfy conservation of mass and are independent of the turbine. For a given T_{t4}/T_{t2}, any point on that line will satisfy mass conservation for engine stations 2 and 4. The actual operating point of the compressor depends on the turbine and exhaust nozzle.

Equation (8-9) can be written simply for the case when station 4 is choked (the normal situation in gas turbine engines) as

$$\boxed{\dot{m}_{c2} = C_1 \frac{\pi_c}{\sqrt{T_{t4}/T_{t2}}}} \tag{8-10}$$

For an engine or gas generator, the specific relationship between the compressor pressure ratio and corrected mass flow rate is called the *compressor operating line* and depends on the characteristics of the turbine. The equation for the operating line is developed later in this section.

Turbine Characteristics

Before developing the equations that predict the operating characteristics of the turbine, we write the mass flow parameter at any station i in terms of the mass flow rate, total pressure, total temperature, area, and Mach number. Since

$$\frac{\dot{m}_i\sqrt{T_{ti}}}{P_{ti}A_i} = \text{MFP}(M_i) = \sqrt{\frac{\gamma_i g_c}{R_i}}\, M_i\left(1 + \frac{\gamma_i - 1}{2} M_i^2\right)^{-(\gamma_i+1)/[2(\gamma_i-1)]}$$

Then, for $M_i = 1$,

$$\boxed{\frac{\dot{m}_i\sqrt{T_{ti}}}{P_{ti}A_i} = \text{MFP}(M_i = 1) = \sqrt{\frac{\gamma_i g_c}{R_i}}\left(\frac{2}{\gamma_i + 1}\right)^{(\gamma_i+1)/[2(\gamma_i-1)]} = \frac{\Gamma_i}{\sqrt{R_i/g_c}}} \tag{8-11a}$$

where

$$\boxed{\Gamma_i \equiv \sqrt{\gamma_i}\left(\frac{2}{\gamma_i + 1}\right)^{(\gamma_i+1)/[2(\gamma_i-1)]}} \tag{8-11b}$$

For a turbojet engine, the flow is choked ($M = 1$) in the turbine inlet guide vanes (station 4) and nearly at the throat of the exhaust nozzle (station 8). Thus the corrected mass flow rate per unit area is constant at station 4 and

$$\dot{m}_4 = \frac{P_{t4}A_4}{\sqrt{T_{t4}}}\frac{\Gamma_4}{\sqrt{R_4}} \qquad \dot{m}_8 = \frac{P_{t8}A_8}{\sqrt{T_{t8}}}\text{MFP}(M_8) \tag{i}$$

For a simple turbojet engine, the mass flow rate through the turbine is equal to that through the exhaust nozzle, or

$$\boxed{\dot{m}_8 = \dot{m}_4}$$

Using Eq. (i), then, we have

$$\frac{\sqrt{T_{t8}/T_{t4}}}{P_{t8}/P_{t4}} = \frac{A_8}{A_4}\frac{\text{MFP}(M_8)}{\Gamma_4/\sqrt{R_4}}$$

or

$$\boxed{\frac{\sqrt{\tau_t}}{\pi_t} = \frac{A_8}{A_4}\frac{\text{MFP}(M_8)}{\Gamma_4/\sqrt{R_4}}} \tag{8-12a}$$

where

$$\boxed{\pi_t = \left(1 - \frac{1 - \tau_t}{\eta_t}\right)^{\gamma_t/(\gamma_t-1)}} \tag{8-12b}$$

For constant turbine efficiency η_t, constant values of R and Γ, constant areas at stations 4 and 8, and choked flow at station 8, Eqs. (8-12*a*) and (8-12*b*) can be satisfied only by constant values of the turbine temperature ratio τ_t and the turbine pressure ratio π_t. Thus we have

τ_t, π_t constant	for $M_8 = 1$ and constant A_4 and A_8

If the exhaust nozzle unchokes and/or its throat area is changed, then both τ_t and π_t will change. Consider a turbine with reference values of $\eta_t = 0.90$ and $\tau_t = 0.80$ when the exhaust nozzle is choked and the gas has $\gamma = 1.33$. From Eqs. (8-12*a*) and (8-12*b*), $\pi_t = 0.363174$ and $A_8/A_4 = 2.46281$ at reference conditions. Figure 8-7*a* shows plots of Eq. (8-12*a*) for different values of the area ratio A_8/A_4 times the mass flow parameter at station 8 [MFP(M_8)] and Eq. (8-12*b*). Because of the relative slopes of these equations, the changes of both τ_t and π_t with A_8 and M_8 can be found by using the following functional

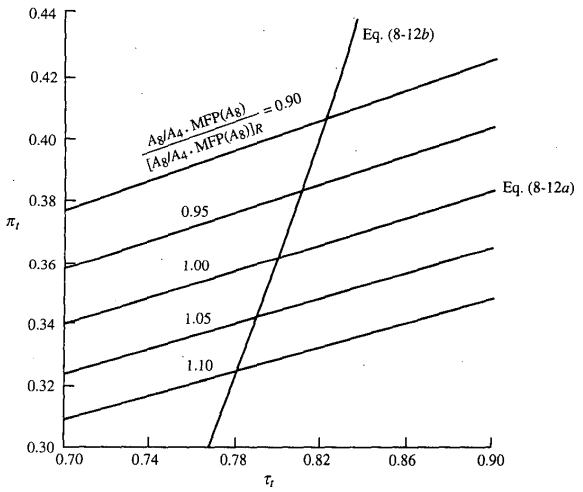

FIGURE 8-7*a*
Plot of turbine performance Eqs. (8-12*a*) and (8-12*b*).

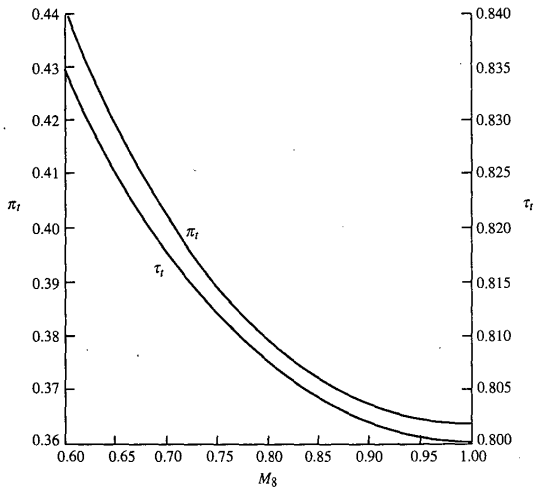

FIGURE 8-7*b*
Variation of turbine performance with exhaust nozzle Mach number.

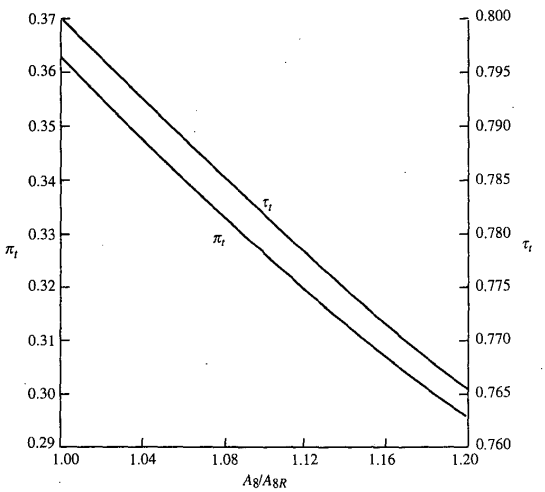

FIGURE 8-7*c*
Variation of turbine performance with exhaust nozzle area.

iteration scheme, starting with an initial value of τ_t: (1) solve for π_t, using Eq. (8-12*a*); (2) calculate a new τ_t, using Eq. (8-12*b*); (3) repeat steps 1 and 2 until successive values of τ_t are within a specified range (say, ± 0.0001). The results of this iteration, plotted in Figs. 8-7*b* and 8-7*c*, show that when the Mach number M_8 is reduced from choked conditions ($M_8 = 1$), both τ_t and π_t increase; and when the exhaust nozzle throat area A_8 is increased from its reference value, both τ_t and π_t decrease. A decrease in τ_t, with its corresponding decrease in π_t, will increase the turbine power per unit mass flow and change the pumping characteristics of the gas generator.

Compressor Operating Line

From a work balance between the compressor and turbine, we write

$$\dot{m}_2 c_{pc}(T_{t3} - T_{t2}) = \eta_m \dot{m}_2(1+f)c_{pt}(T_{t4} - T_{t5})$$

or

$$\tau_c = 1 + \frac{T_{t4}}{T_{t2}}\frac{c_{pt}}{c_{pc}}\eta_m(1+f)(1-\tau_t) \tag{8-13}$$

where

$$\pi_c = [1 + \eta_c(\tau_c - 1)]^{\gamma_c/(\gamma_c - 1)} \tag{ii}$$

Combining Eqs. (8-13) and (ii) gives

$$\pi_c = \left\{1 + \frac{T_{t4}}{T_{t2}}\left[\frac{c_{pt}}{c_{pc}}\eta_c\eta_m(1+f)(1-\tau_t)\right]\right\}^{\gamma_c/(\gamma_c-1)} \tag{8-14}$$

where the term in square brackets can be considered a constant when τ_t is constant. Solving Eq. (8-14) for the temperature ratio gives

$$\frac{T_{t4}}{T_{t2}} = C_2[(\pi_c)^{(\gamma_c-1)/\gamma_c} - 1]$$

where C_2 represents the reciprocal of the constant term within the square brackets of Eq. (8-14). Combining this equation with Eq. (8-10) gives an equation for the *compressor operating line* that can be written as

$$\boxed{\dot{m}_{c2} = \frac{\pi_c}{\sqrt{\pi_c^{(\gamma_c-1)/\gamma_c} - 1}}\frac{C_1}{\sqrt{C_2}} \quad \text{for constant } \tau_t} \tag{8-15}$$

We can plot the *compressor operating line,* using Eq. (8-15), on the compressor map of Fig. 8-6*a*, giving the compressor map with operating line

shown in Fig. 8-8. This compressor operating line shows that for each value of the temperature ratio T_{t2}/T_{t4} there is one value of compressor pressure ratio and corrected mass flow rate. One can also see that for a constant value of T_{t2}, both the compressor pressure ratio and the corrected mass flow rate will increase with increases in throttle setting (increases in T_{t4}). In addition, when at constant T_{t4}, the compressor pressure ratio and corrected mass flow rate will decrease with increases in T_{t2} due to higher speed and/or lower altitude (*note*: $T_{t2} = T_{t0} = T_0 \tau_r$). The curving of the operating line in Fig. 8-8 at pressure ratios below 4 is due to the exhaust nozzle being unchoked ($M_8 < 1$), which increases the value of τ_t (see Fig. 8-7*b*).

The compressor operating line defines the pumping characteristics of the gas generator. As mentioned earlier, changing the throat area of the exhaust nozzle A_8 will change these characteristics. It achieves this change by shifting the compressor operating line. Increasing A_8 will decrease τ_t (see Fig. 8-7*c*). This decrease in τ_t will increase the term within the square brackets of Eq. (8-14) which corresponds to the reciprocal of constant C_2 in Eq. (8-15). Thus an increase in A_8 will decrease the constant C_2 in Eq. (8-15). For a constant T_{t4}/T_{t2}, this shift in the operating line will increase both the corrected mass flow rate and the pressure ratio of the compressor, as shown in Fig. 8-9 for a 20 percent increase in A_8. For some compressors, an increase in the exhaust nozzle throat area A_8 can keep engine operation away from the surge.

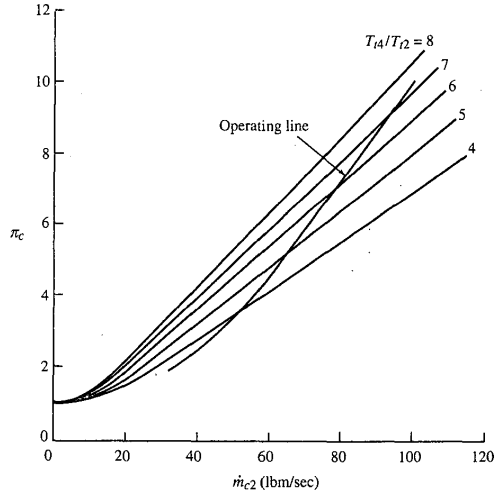

FIGURE 8-8
Compressor map with operating line.

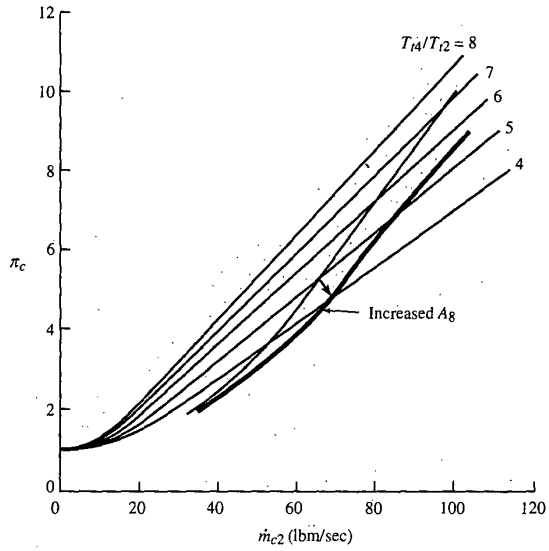

FIGURE 8-9
Effect of exhaust nozzle area on compressor operating line.

Engine Controls

The engine control system will control the gas generator operation to keep the main burner exit temperature T_{t4} and the compressor's pressure ratio π_c, rotational speed N, exit total pressure T_{t3}, and exit total pressure P_{t3} from exceeding specific maximum values. An understanding of the influence of the engine control system on compressor performance during changing flight conditions and throttle settings can be gained by recasting Eqs. (8-10) and (8-14) in terms of the dimensionless total temperature at station 0 (θ_0). We note that

$$T_{t0} = T_{\text{ref}} \frac{T_{t0}}{T_{\text{ref}}} = T_{\text{ref}} \theta_0$$

and

$$\theta_0 = \frac{T_0}{T_{\text{ref}}} \tau_r = \frac{T_0}{T_{\text{ref}}} \left(1 + \frac{\gamma - 1}{2} M_0^2\right) \tag{8-16}$$

Equation (8-16) and Figs. 8-10 and 8-11 show that θ_0 includes the influence of both the altitude (through the ambient temperature T_0) and the flight Mach number. Although Fig. 8-10 shows the direct influence of Mach number and altitude on θ_0, Fig. 8-11 is an easier plot to understand in terms of aircraft flight conditions (Mach number and altitude).

Using Eq. (8-16) and the fact that $T_{t2} = T_{t0}$, we can write Eq. (8-14) as

$$\boxed{\pi_c = \left(1 + \frac{T_{t4}}{\theta_0} K_1\right)^{\gamma_c/(\gamma_c - 1)}} \tag{8-17}$$

Example 8-7. The performance of an afterburning turbojet with a throttle ratio of 1 is considered. The engine performance, when the afterburner is operating at its maximum exit temperature, is commonly referred to as *maximum* or *wet.* This afterburning turbojet engine has a maximum thrust of 25,000 lbf. The terms *military* and *dry* refer to the engine's performance when the afterburner is off (not operating) and the engine core is at maximum operating conditions. The reference conditions and operating limits for the afterburning turbojet engine are as follows:

REFERENCE: Sea level static ($T_0 = 518.7°R$, $P_0 = 14.696$ psia), $\pi_c = 20$, $\pi_{cL} = 5$, $\pi_{cH} = 4$, $e_{cL} = 0.9$, $e_{cH} = 0.9$, $e_{tH} = 0.9$, $e_{tL} = 0.9$, $\pi_{d\,max} = 0.98$, $\pi_b = 0.96$, $\pi_n = 0.98$, $T_{t4} = 3200°R$, $c_{pc} = 0.24$ Btu/(lbm · °R), $\gamma_c = 1.4$, $c_{pt} = 0.295$ Btu/(lbm · °R), $\gamma_t = 1.3$, $\eta_b = 0.995$, $\eta_{mL} = 0.995$, $\eta_{mH} = 0.995$, $h_{PR} = 18{,}400$ Btu/lbm, $T_{t7} = 3600°R$, $c_{pAB} = 0.295$ Btu/(lbm · °R), $\gamma_{AB} = 1.3$, $\pi_{AB} = 0.94$, $\eta_{AB} = 0.95$, $\eta_{cL} = 0.8755$, $\eta_{cH} = 0.8791$, $\eta_{tH} = 0.9062$, $\eta_{tL} = 0.9050$, $\pi_{tH} = 0.5466$, $\tau_{tH} = 0.8821$, $\pi_{tL} = 0.6127$, $\tau_{tL} = 0.9033$, $M_8 = 1$, $M_9 = 1.85$, $f = 0.0358$, $f_{AB} = 0.0195$, $f_O = 0.0554$, $F = 25{,}000$ lbf, $S = 1.4473$ (lbm/hr)/lbf, $\dot{m}_0 = 181.57$ lbm/sec

OPERATION: Maximum $T_{t4} = 3200°R$ Maximum $T_{t7} = 3600°R$
Mach number: 0 to 2 Altitudes (kft): 0, 20, and 40

The wet and dry performances of this afterburning turbojet are compared in Figs. 8-43 and 8-44. Note that the wet thrust is about 20 percent greater than the dry thrust, and the thrust at 40-kft altitude is about 25 percent of its sea-level

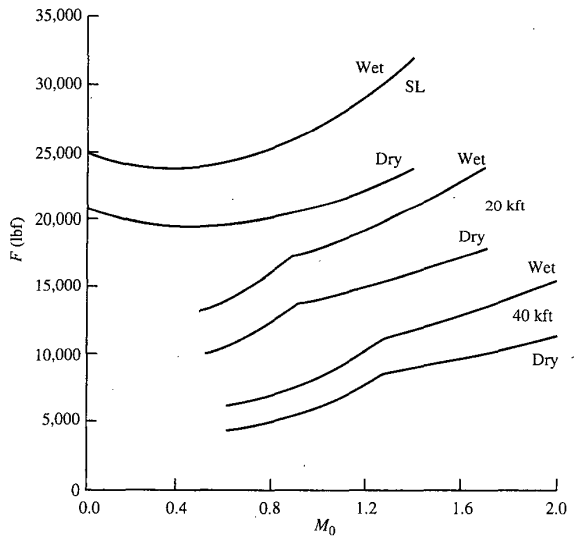

FIGURE 8-43
Maximum wet and dry thrust of afterburning turbojet.

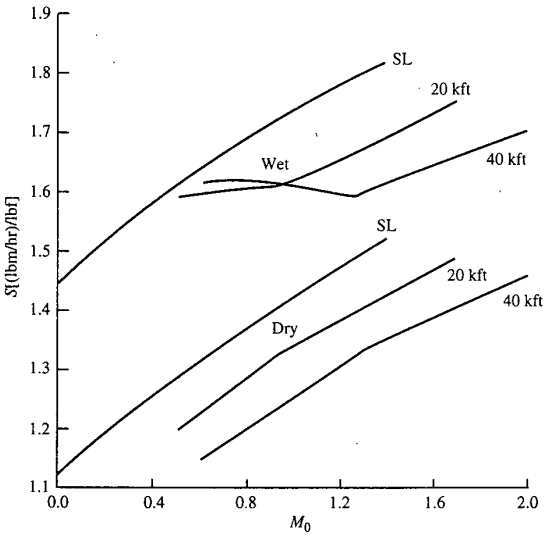

FIGURE 8-44
Maximum wet and dry thrust specific fuel consumption of afterburning turbojet.

value. The thrust specific fuel consumption at 40-kft altitude is much higher than expected for Mach numbers below about 1.3. This high S is due to the reduction in T_{t4} below maximum for $\theta_0 < \text{TR}$, which lowers the temperature of the gas entering the afterburner and increases the temperature rise across the afterburner.

The partial-throttle performance of the afterburning turbjoet is shown in Fig. 8-45 at flight conditions of sea-level static and Mach 1.5 at 40 kft. These curves are commonly called *throttle hooks* because of their shape. At sea level static conditions, the minimum thrust specific fuel consumption of about 1.02 (lbm/hr)/lbf occurs at a thrust of about 4300 lbf (about 20 percent of dry thrust). At partial-power levels this low, the change in component efficiency can cause the fuel consumption of a real engine to be very different from that predicted here. Since the engine models used to generate these curves are based on constant component efficiencies, the results at significantly reduced throttle settings can be misleading. Comparison of this figure with the partial-power performance of the advanced fighter engine of Fig. 1–14*e* shows that the trends are correct. The advanced turbofan engine of Fig. 1-14*e* has lower thrust specific fuel consumption mainly because it is a low-bypass-ratio turbofan engine.

8-5 TURBOFAN ENGINE—SEPARATE EXHAUSTS AND CONVERGENT NOZZLES

The turbofan engines used on commercial subsonic aircraft typically have two spools and separate exhaust nozzles of the convergent type, as shown in Fig.

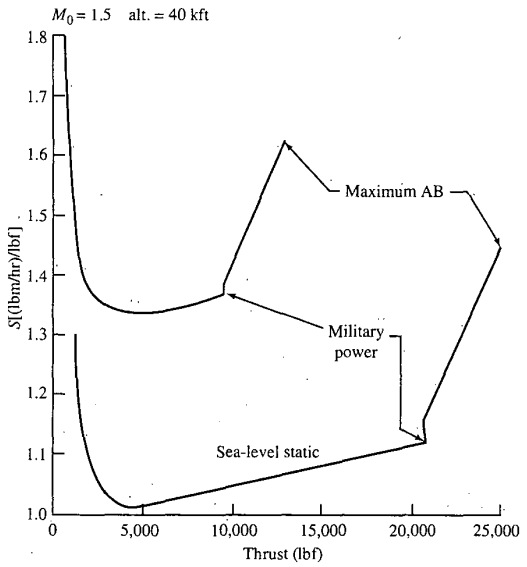

FIGURE 8-45
Partial-throttle performance of afterburning turbojet.

8-46. For ease of analysis, we will consider a turbofan engine whose fan exit state (13) is the same as the low-pressure compressor exit state (2.5). Thus

$$\tau_f = \tau_{cL} \quad \text{and} \quad \pi_f = \pi_{cL}$$

The exhaust nozzles of these turbofan engines have fixed throat areas

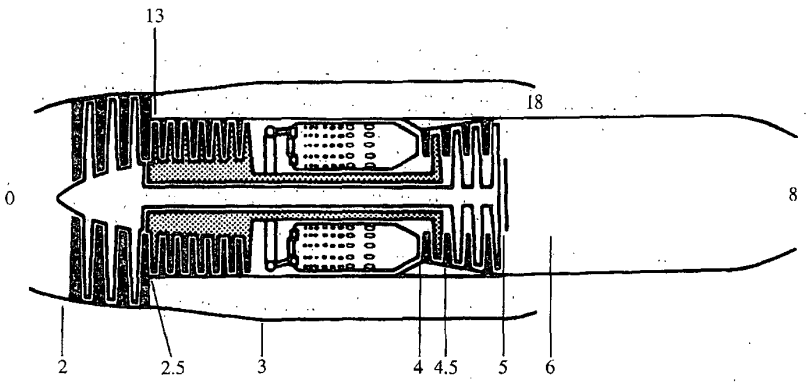

FIGURE 8-46
Turbofan engine with separate exhausts. (*Courtesy of Pratt & Whitney.*)

which will be choked when the exhaust total pressure/ambient static pressure ratio is equal to or larger than $[(\gamma+1)/2]^{\gamma/(\gamma-1)}$. When an exhaust nozzle is unchoked, the nozzle exit pressure equals the ambient pressure and the exit Mach number is subsonic.

Choked flow at stations 4 and 4.5 of the high-pressure spool during engine operation requires

$$\boxed{\text{Constant values of } \pi_{tH},\ \tau_{tH},\ \dot{m}_{c4}, \text{ and } \dot{m}_{c4.5}} \tag{8-36}$$

Since the exhaust nozzles have fixed areas, this gas turbine engine has 4 independent variables (T_{t4}, M_0, T_0, and P_0). We will consider the case when both exhaust nozzles may be unchoked, resulting in 11 dependent variables. The performance analysis variables and constants are summarized in Table 8-6.

LOW-PRESSURE TURBINE (τ_{tL}, π_{tL}). Equations (8-37) and (8-38) apply for the low-pressure turbine temperature and pressure ratios of this turbofan engine.

$$\boxed{\pi_{tL} = \pi_{tLR}\sqrt{\frac{\tau_{tL}}{\tau_{tLR}}}\,\frac{\text{MFP}(M_{9R})}{\text{MFP}(M_9)}} \tag{8-37}$$

TABLE 8-6
Performance analysis variables for separate-exhaust turbofan engine

	Variables		
Component	**Independent**	**Constant or known**	**Dependent**
Engine	M_0, T_0, P_0		$\dot{m}_0$, α
Diffuser		$\pi_d = f(M_0)$	
Fan			π_f, τ_f
High-pressure compressor			π_{cH}, τ_{cH}
Burner	T_{t4}	π_b, η_b	f
High-pressure turbine		π_{tH}, τ_{tH}	
Low-pressure turbine			π_{tL}, τ_{tL}
Core exhaust nozzle		π_n	M_9
Fan exhaust nozzle		π_{fn}	M_{19}
Total number	4		11

Since the flow is choked ($M_4 = 1$) and the area is constant ($A_4 = \text{constant}$) at station 4, the above equation can be rewritten for the core mass flow rate in terms of component pressure ratios as

$$\dot{m}_0 = \frac{P_0 \pi_r \pi_d \pi_c}{\sqrt{T_{t4}}} \left[\pi_b A_4 \frac{\text{MFP}(M_4)}{1+f} \right]$$

where the terms within the square brackets are considered constant. Equating the constants to reference values gives

$$\boxed{\dot{m}_0 = \dot{m}_{0R} \frac{P_0 \pi_r \pi_d \pi_c}{(P_0 \pi_r \pi_d \pi_c)_R} \sqrt{\frac{T_{t4R}}{T_{t4}}}} \tag{8-72}$$

Compressor (τ_c, π_c)

The power balance of the core spool between the high-pressure turbine and the compressor gives

$$\eta_m \dot{m}_4 c_{pt} (T_{t4} - T_{t4.5}) = \dot{m}_2 c_{pc} (T_{t3} - T_{t2})$$

Rewriting this equation in terms of temperature ratios, rearranging into variable and constant terms, and equating the constant to reference values give

$$\frac{\tau_r(\tau_c - 1)}{T_{t4}/T_0} = \eta_m (1+f)(1 - \tau_{tH}) = \left[\frac{\tau_r(\tau_c - 1)}{T_{t4}/T_0} \right]_R$$

Solving for τ_c gives

$$\boxed{\tau_c = 1 + \frac{T_{t4}/T_0}{(T_{t4}/T_0)_R} \frac{(\tau_r)_R}{\tau_r} (\tau_c - 1)_R} \tag{8-73}$$

From the definition of compressor efficiency, π_c is given by

$$\boxed{\pi_c = [1 + \eta_c(\tau_c - 1)]^{\gamma_c/(\gamma_c - 1)}} \tag{8-74}$$

Core Work Coefficient C_C

The expression for the core work coefficient C_C developed in Chap. 7 still applies and is given by Eq. (7-96)

$$\boxed{C_C = (\gamma_c - 1) M_0 \left[(1+f) \frac{V_9}{a_0} - M_0 + (1+f) \frac{R_t}{R_c} \frac{T_9/T_0}{V_9/a_0} \frac{1 - P_0/P_9}{\gamma_c} \right]} \tag{7-96}$$

where V_9/a_0 is given by Eq. (7-99) and T_9/T_0 is given by Eqs. (7-98*a*) and (7-98*b*).

Power (Low-Pressure) Turbine (τ_{tL}, π_{tL})

Equations (7-37) and (8-38) apply for the power (low-pressure) turbine temperature and pressure ratios of this turboprop engine. We write Eq. (8-37) in terms of the Mach number at station 9 as

$$\boxed{\pi_{tL} = \pi_{tL\,R}\sqrt{\frac{\tau_{tL}}{\tau_{tL\,R}}}\,\frac{\text{MFP}(M_{9\,R})}{\text{MFP}(M_9)}} \tag{8-75}$$

where

$$\boxed{\tau_{tL} = 1 - \eta_{tL}(1 - \pi_{tL}^{(\gamma_t - 1)/\gamma_t})} \tag{8-38}$$

If station 9 is choked at the reference condition and at all performance conditions of interest, then π_{tL} and τ_{tL} are constant.

The power balance of this spool was found in Chap. 7. It still applies, and Eq. (7-101) gives the propeller work coefficient C_{prop}:

$$\boxed{C_{\text{prop}} = \frac{\eta_{\text{prop}}\dot{W}_{\text{prop}}}{\dot{m}_0 c_{pc} T_0} = \eta_{\text{prop}}\eta_g\eta_{mL}(1+f)\tau_\lambda\tau_{TH}(1-\tau_{tL})} \tag{7-101}$$

Exhaust Nozzle

Two flow regimes exist for flow through the convergent exhaust nozzle (unchoked flow and choked flow). Unchoked flow will exist when

$$\frac{P_{t9}}{P_0} = \pi_r\pi_d\pi_c\pi_b\pi_{tH}\pi_{tL}\pi_n < \left(\frac{\gamma_t + 1}{2}\right)^{\gamma_t/(\gamma_t - 1)}$$

and choked flow will exist when

$$\frac{P_{t9}}{P_0} = \pi_r\pi_d\pi_c\pi_b\pi_{tH}\pi_{tL}\pi_n \geq \left(\frac{\gamma_t + 1}{2}\right)^{\gamma_t/(\gamma_t - 1)}$$

For unchoked flow, the exit static pressure P_9 is equal to the ambient pressure P_0, and the subsonic exit Mach number M_9 is given by

$$M_9 = \sqrt{\frac{2}{\gamma_t - 1}\left[\left(\frac{P_{t9}}{P_0}\right)^{(\gamma_t - 1)/\gamma_t} - 1\right]}$$

When the flow is choked, then

$$M_9 = 1, \qquad \frac{P_{t9}}{P_9} = \left(\frac{\gamma_t + 1}{2}\right)^{\gamma_t/(\gamma_t - 1)}, \qquad \text{and} \qquad \frac{P_0}{P_9} = \frac{P_{t9}/P_9}{P_{t9}/P_0}$$

Iteration Scheme for τ_{tL}, π_{tL}, and M_9

Determination of the conditions downstream of station 4.5 requires an iterative solution. The method used is as follows:

1. Initially assume that π_{tL} equals its reference value $\pi_{tL\,R}$.
2. Calculate τ_{tL}, using Eq. (8-38).
3. Calculate P_{t9}/P_0 and conditions at exit including M_9.
4. Calculate the new π_{tL}, using Eq. (8-75).
5. Compare the new π_{tL} to the previous value. If the difference is greater than 0.0001, then go to step 2.

Propeller Performance

The performance of the propeller can be simply modeled as a function of the flight Mach number (Ref. 12); one such model, which is used in the PERF computer program of this textbook, is shown in Fig. 8-71 and expressed

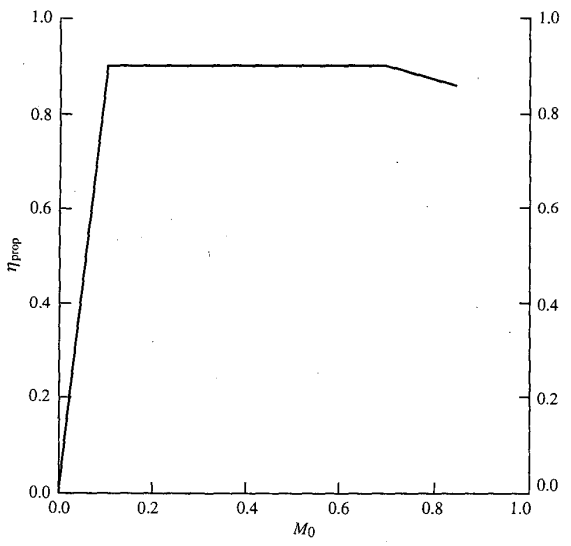

FIGURE 8-71
Variation in propeller efficiency with Mach number.

differential pressure change, or

$$e_c = \frac{dh_{ti}}{dh_t} = \frac{dT_{ti}}{dT_t} = \frac{dT_{ti}/T_t}{dT_t/T_t} = \frac{\gamma - 1}{\gamma} \frac{dP_t/P_t}{dT_t/T_t}$$

For a constant polytropic efficiency e_c, integration between states $t1$ and $t3$ gives

$$\boxed{e_c = \frac{\gamma - 1}{\gamma} \frac{\ln(P_{t3}/P_{t1})}{\ln(T_{t3}/T_{t1})}} \tag{9-11}$$

A useful expression for stage efficiency, in terms of the pressure ratio and polytropic efficiency, can be easily obtained by using Eqs. (9-10) and (9-11). Solving Eq. (9-11) for the temperature ratio and substituting into Eq. (9-10) give

$$\boxed{\eta_s = \frac{(P_{t3}/P_{t1})^{(\gamma-1)/\gamma} - 1}{(P_{t3}/P_{t1})^{(\gamma-1)/(\gamma e_c)} - 1}} \tag{9-12}$$

In the limit, as the pressure ratio approaches 1, the stage efficiency approaches the polytropic efficiency. The variation in stage efficiency with stage pressure ratio is plotted in Fig. 9-14*b* for constant polytropic efficiency.

The compressor polytropic efficiency is useful in preliminary design of compressors for gas turbine engines to predict the compressor efficiency for a given level of technology. The value of the polytropic efficiency is mainly a function of the technology level (see Table 6-2). Axial-flow compressors designed in the 1980s have a polytropic efficiency of about 0.88, whereas the compressors being designed today have a polytropic efficiency of about 0.9.

DEGREE OF REACTION. For compressible flow, the *degree of reaction* is defined as

$$\boxed{^\circ R_c = \frac{\text{rotor static enthalpy rise}}{\text{stage static enthalpy rise}} = \frac{h_2 - h_1}{h_3 - h_1}} \tag{9-13a}$$

For a calorically perfect gas, the static enthalpy rises in the equation become static temperature rises, and the degree of reaction is

$$\boxed{^\circ R_c = \frac{T_2 - T_1}{T_3 - T_1}} \tag{9-13b}$$

In the general case, it is desirable to have the degree of reaction in the vicinity of 0.5 because the rotor and stator rows then will "share the burden" of increasing the enthalpy of the flow. The degree of reaction for the stage data

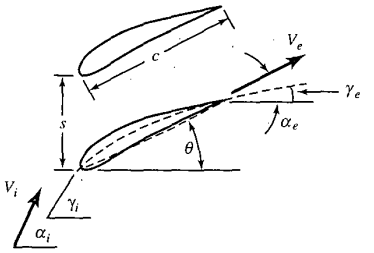

$\alpha_i - \alpha_e$ = turning angle
$\gamma_i - \gamma_e$ = airfoil camber angle
$\alpha_i - \gamma_i$ = incidence angle
$\alpha_e - \gamma_e = \delta_c$ = exit deviation
$\sigma = c/s$ = solidity
θ = stagger angle

FIGURE 9-15
Cascade airfoil nomenclature.

of Example 9-1 is approximately 0.28, which means the majority of the static temperature rise occurs in the stator.

CASCADE AIRFOIL NOMENCLATURE AND LOSS COEFFICIENT. Figure 9-15 shows the cascade airfoil nomenclature and the airfoil and flow angles. Subscripts i and e are used for the inlet and exit states, respectively. The ratio of the airfoil chord c to the airfoil spacing s is called the *solidity* σ, which typically is near unity. At design, the incidence angle is nearly zero. The exit deviation can be determined by using Carter's rule:

$$\boxed{\delta_c = \frac{\gamma_i - \gamma_e}{4\sqrt{\sigma}}} \tag{9-14}$$

The airfoil angles of both the rotor and the stator can be calculated from the flow angles, given the incidence angle and solidity for each. To obtain the exit airfoil angle, Eq. (9-14) is rearranged to give

$$\gamma_e = \frac{4\alpha_e\sqrt{\sigma} - \gamma_i}{4\sqrt{\sigma} - 1}$$

For the data of Example 9-1, we obtain the following airfoil angles, assuming a solidity of 1 and a zero incidence angle for both rotor and stator:

Rotor	$\gamma_i = 42.35°$	$\gamma_e = 17.71°$
Stator	$\gamma_i = 48.97°$	$\gamma_e = 37.01°$

Losses in cascade airfoils are normally quantified in terms of the drop in total pressure divided by the dynamic pressure of the incoming flow. This ratio is called the *total pressure loss coefficient* and is defined as

$$\boxed{\phi_c \equiv \frac{P_{ti} - P_{te}}{\rho V_i^2/(2g_c)}} \tag{9-15}$$

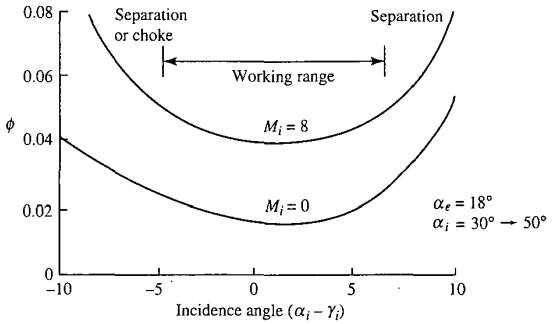

FIGURE 9-16
Compressor cascade experimental behavior.

Figure 9-16 shows the typical total pressure loss behavior of compressor airfoils obtained from cascade tests. Note that these losses increase with Mach number and incidence angle. The loss coefficients shown in Fig. 9-16 include only the two-dimensional or "profile" losses and must be increased in compressor stage design to account for end losses (e.g., tip leakage, wall boundary layer, or cavity leakage).

DIFFUSION FACTOR. The total pressure loss of a cascade depends upon many factors. The pressure and velocity distribution about a typical cascade airfoil is shown in Fig. 9-17. The upper (suction) side of the compressor blade

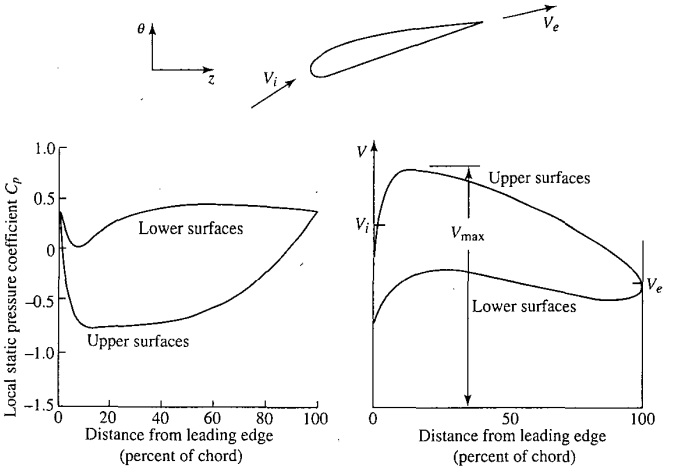

FIGURE 9-17
Compressor airfoil pressure and velocity distribution (Ref. 35).

TABLE 9-8*a*
Summary of eight-stage compressor design

Stage	1	2	3	4	5	6	7	8
M_1	0.600	0.560	0.528	0.500	0.476	0.456	0.438	0.422
π_s	1.497	1.430	1.379	1.338	1.306	1.279	1.256	1.237
P_{t1} (psia)	14.70	22.01	31.47	43.39	58.07	75.81	96.9	121.8
T_{t1} (°R)	518.7	589.6	660.5	731.4	802.3	873.1	944.0	1014.9
r_h (in)	14.03	14.80	15.32	15.67	15.93	16.12	16.27	16.38
r_t (in)	20.03	19.26	18.75	18.39	18.14	17.94	17.80	17.68
A_1 (in^2)	641.8	476.9	367.4	291.1	236.0	194.9	163.5	139.0

radius and hub radius at the inlet to the first stage are about 20 and 14 in, respectively, giving a first-stage hub/tip ratio of 0.7.

Example 9-7. *Preliminary design of mean line.* The COMPR program was used to perform the following analysis of a repeating-row, repeating-stage, mean-line design with a free-vortex swirl distribution. The following input data were entered:

Number of stages: 8
Rotor angular speed ω: 800 rad/sec
Inlet total temperature T_t: 518.7°R
Inlet Mach number M_1: 0.6
Solidity σ: 1.0
Rotor c/h: 0.6
Gas constant: 53.34 ft · lbf/(lbm · °R)
Mass flow rate: 150 lbm/sec
Inlet total pressure P_t: 14.70 psia
Inlet flow angle α_1: 36°
Diffusion factor D: 0.5
Polytropic efficiency e_c: 0.9
Stator c/h: 0.6
Ratio of specific heats γ: 1.4

The results from COMPR are summarized in Table 9-8*a* for the mean-line design. The mean radius is 17.032 in. and the flow angle at the entrance to the stator α_2 is 55.28°. A cross-sectional sketch of the eight stages as plotted by COMPR and captured on a laser printer is shown in Fig. 9-36*a*. The estimated

TABLE 9-8*b*
Number of blades with same c/h value for each row

Stage	1	2	3	4	5	6	7	8
Rotor								
c/h	0.60	0.60	0.60	0.60	0.60	0.60	0.60	0.60
Blades	56	71	87	106	128	151	177	206
Chord (in)	3.365	2.518	1.953	1.555	1.266	1.050	0.883	0.753
Stator								
c/h	0.60	0.60	0.60	0.60	0.60	0.60	0.60	0.60
Blades	48	64	81	102	124	149	176	206
Chord (in)	2.899	2.211	1.739	1.401	1.151	0.962	0.814	0.698

TABLE 9-8*c*
Number of blades with different c/h values for each row

Stage	1	2	3	4	5	6	7	8
Rotor								
c/h	0.60	0.60	0.63	0.73	0.83	0.93	1.03	1.13
Blades	56	71	83	88	92	98	104	110
Chord (in)	3.362	2.518	2.050	1.892	1.752	1.627	1.516	1.418
Stator								
c/h	0.60	0.60	0.60	0.70	0.80	0.90	1.00	1.10
Blades	48	64	81	87	93	99	106	113
Chord (in)	2.899	2.211	1.739	1.634	1.535	1.442	1.357	1.280

length of the compressor is 25.53 in. The resulting number of blades and blade chord lengths are given in Table 9-8*b* based on the input chord/height ratio of 0.6 for both the rotor and stator of all stages.

The number of blades in a rotor or stator now can be reduced by increasing its chord/height ratio. Since COMPR uses the same chord/height ratio for each

TABLE 9-8*d*
Material selection calculations for rotor blades, rims, and disks

Stage		1	2	3	4	5	6	7	8
AN^2	($\times 10^{10}$ in$^2 \cdot$ rpm^2)	3.2530	2.4598	1.9209	1.5389	1.2587	1.0474	0.88422	0.75579
σ_c/ρ	[ksi/(slug/ft^3)]*	2.7377	1.0702	1.6166	1.2951	1.0593	0.8815	0.7442	0.6361
T_{t1R}	(°R)	554	625	696	767	838	909	979	1050
T_{t1R}	(°F)	94	165	236	307	378	449	519	590
Blade material		←				Material 2			→
r_h	(in)	14.03	14.80	15.32	15.67	15.93	16.12	16.27	16.38
ωr_h	(ft/sec)	953.33	986.67	1021.3	1044.7	1062.0	1074.7	1084.7	1092.0
h_r†	(in)	3.362	2.518	2.050	1.892	1.752	1.627	1.516	1.418
r_r	(in)	10.668	12.282	13.270	13.778	14.178	14.493	14.754	14.962
Rim material		←				Material 2			→
σ_r/ρ	[ksi/(slug/ft^3)]	4	4	4	4	4	4	4	4
$\rho(\omega r)^2/\sigma_r$		1.5188	1.6901	1.8110	1.8947	1.9581	2.0050	2.0425	2.0702
W_{dr}/W_r‡		0.4578	0.3367	0.2856	0.2735	0.2616	0.2500	0.2395	0.2299
ωr_r	(ft/sec)	711.20	818.80	884.67	918.53	945.20	966.20	983.60	997.47
σ_d/ρ	[ksi/(slug/ft^3)]¶	0.8781	1.1639	1.3587	1.4648	1.5510	1.6207	1.6796	1.7273
Disk material		←				Material 2			→

* Based on Eq. (J-6) and a blade taper ratio of 1.0.

† Based on h_r equal to blade chord.

‡ Based on Eq. (J-10) and $\bar{\sigma}_{\text{blades}}/\sigma_r = 0.1$.

¶ Based on Eq. (J-12).

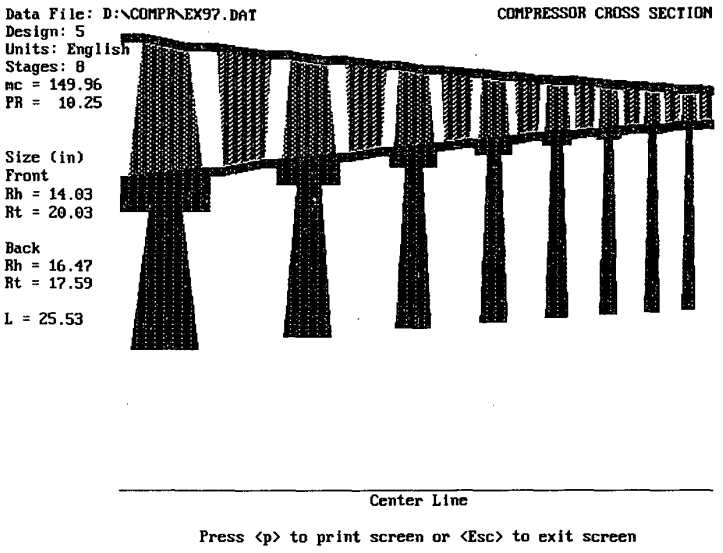

FIGURE 9-36*a*
Sketch of compressor cross section from COMPR with constant c/h.

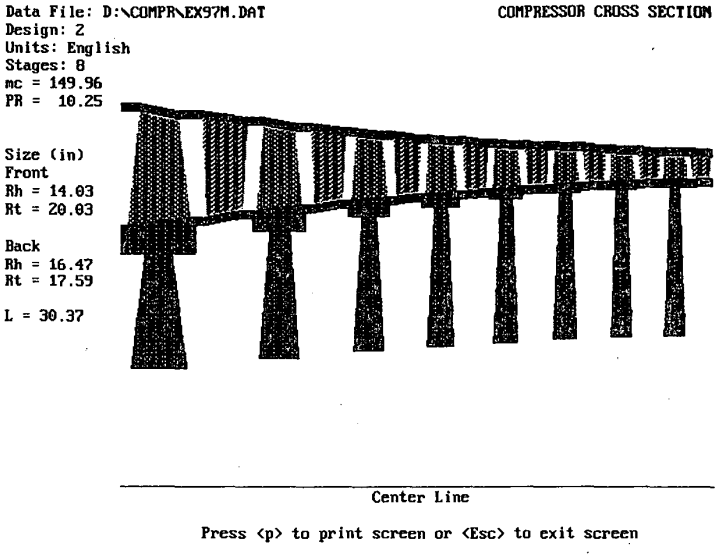

FIGURE 9-36*b*
Sketch of compressor cross section from COMPR with variable c/h.

flow rate by the valve. The inlet and exit conditions are measured along with the rotational speed and input power. These data are reduced to give the resulting compressor map.

CORRECTED QUANTITIES. For a compressor, the following four corrected quantities are normally used to map its performance:

Item	Symbol	Corrected	
Pressure	P_{ti}	$\delta_i = \frac{P_{ti}}{P_{\text{ref}}}$	where $P_{\text{ref}} = 14.696$ psia
Temperature	T_{ti}	$\theta_i = \frac{T_{ti}}{T_{\text{ref}}}$	where $T_{\text{ref}} = 518.7°\text{R}$
Rotational speed	$N = \text{RPM}$	$\frac{N}{\sqrt{\theta_i}}$	
Mass flow rate	$\dot{m}_i$	$\dot{m}_{ci} = \frac{\dot{m}_i\sqrt{\theta_i}}{\delta_i}$	

The corrected rotational speed is directly proportional to the ratio of the axial to rotational velocity. The corrected mass flow rate is directly proportional to the Mach number of the entering flow. We note that

$$\dot{m}_i = \frac{P_{ti}}{\sqrt{T_{ti}}} A_i \,\text{MFP}(M_i)$$

Then
$$\dot{m}_{ci} = \frac{\dot{m}_i\sqrt{T_{ti}}}{P_{ti}} \frac{P_{\text{ref}}}{\sqrt{T_{\text{ref}}}} = \frac{P_{\text{ref}}}{\sqrt{T_{\text{ref}}}} A_i \,\text{MFP}(M_i)$$

Therefore
$$\dot{m}_{ci} = f(M_i)$$

At engine station 2 (entrance to compressor or fan)

$$\dot{m}_{c2} = \frac{P_{\text{ref}}}{\sqrt{T_{\text{ref}}}} A_2 \,\text{MFP}(M_2) \tag{9-64}$$

Thus the corrected mass flow rate is directly proportional to the Mach number at the entrance to the compressor.

COMPRESSOR MAP. The performance of two modern high-performance fan stages is shown in Fig. 9-39. They have no inlet guide vanes. One has a low tangential Mach number (0.96) to minimize noise. The other has supersonic tip speed and a considerably larger pressure ratio. Both have high axial Mach numbers.

Variations in the axial-flow velocity in response to changes in pressure

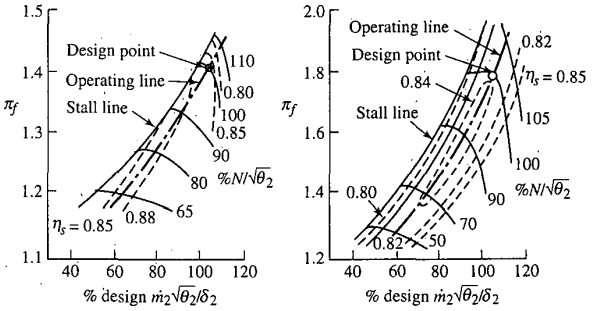

(*a*) Subsonic tangential Mach (*b*) Supersonic tangential Mach

FIGURE 9-39
Typical fan stage maps (Ref. 48).

cause the multistage compressor to have quite different mass flow versus pressure ratio characteristics from those of one of its stages. The performance map of a typical high-pressure-ratio compressor is shown in Fig. 9-40.

A limitation on fan and compressor performance of special concern is the stall or surge line. Steady operation above the line is impossible, and entering the region even momentarily is dangerous to the compressor and its application.

COMPRESSOR STARTING PROBLEMS. The cross section of a multistage compressor is shown in Fig. 9-41. Also shown (in solid lines) at three locations

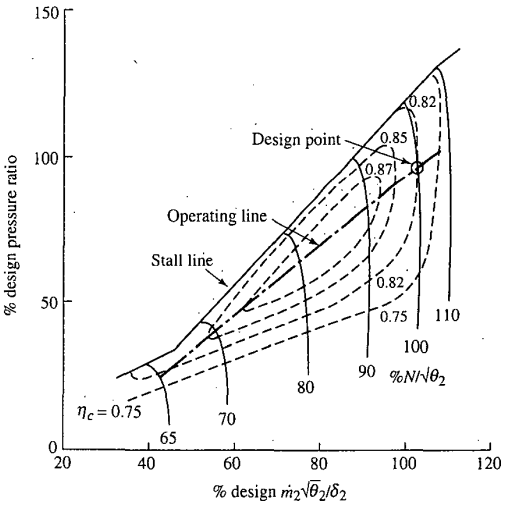

FIGURE 9-40
Typical compressor map.

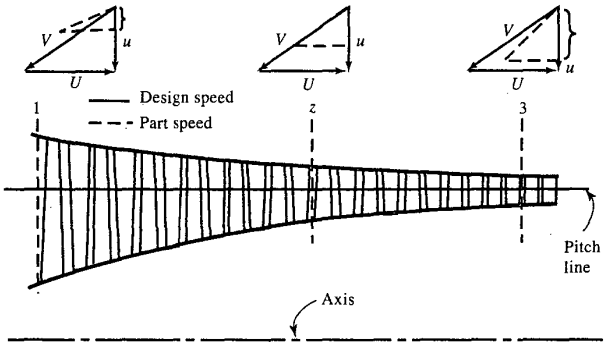

FIGURE 9-41
Cross section of a multistage compressor. Rotor-inlet velocity diagrams are shown for inlet, middle, and exit stages.

in the machine are mean-line rotor inlet velocity diagrams for on-design operation. The design shown here has a constant mean radius, a constant axial velocity, and zero swirl at the rotor-inlet stations.

Let us apply the continuity equation, which states that the mass flow rate is the same at all stations in the compressor. Then, at the inlets to the first and last stages,

$$\dot{m} = \rho_1 A_1 u_1 = \rho_3 A_3 u_3$$

or

$$\frac{u_1}{u_3} = \frac{\rho_3 A_3}{\rho_1 A_1} \tag{9-65}$$

At the design point, since $u_3 = u_1$, then $\rho_3/\rho_1 = A_1/A_3$. When the compressor is operating at a lower speed, however, it is not able to produce as high a density ratio (or pressure ratio) as at design speed; and since the area ratio remains fixed, it follows from Eq. (9-65) that the inlet/outlet axial velocity ratio must have a value less than that at design. In Fig. 9-41, the velocity diagrams shown (in dashed lines) indicate the rotor inlet conditions at partial speed. For each of the three stages represented, the blade speed is the same, but the inlet stage axial velocity is shown less than that for the outlet stage in accordance with Eq. (9-65). Because of the varying axial velocity, it is possible for only one stage near the middle of the machine (called the *pivot stage*) to operate with the same angle of attack at all speeds. At lower speeds, the blading forward of the pivot stage is pushed toward stall, and the blading aft of the pivot stage is windmilling with a tendency toward choking. At speeds higher than the design value, these trends are reversed.

Several techniques have been utilized to reduce the low-speed and starting effects:

$$v_{1Rt} = \frac{d_{1t}}{d_2} U_t = \frac{30}{50}(436.8) = 262.1 \text{ m/sec}$$

$$\beta_{1h} = \tan^{-1} \frac{v_{1Rh}}{u_1} = 44.6°$$

$$\beta_{1t} = \tan^{-1} \frac{v_{1Rt}}{u_1} = 63.1°$$

$$T_{t3} = T_{t2} = T_{t1} + \frac{\epsilon U_t^2}{g_c c_p} = 288.16 + \frac{0.9 \times 436.8^2}{1004} = 459.19 \text{ K}$$

$$\eta_c = \frac{(P_{t3}/P_{t1})^{\gamma/(\gamma-1)} - 1}{T_{t3}/T_{t1} - 1} = \frac{4^{1/3.5} - 1}{459.19/288.16 - 1} = 81.9\%$$

$$v_2 = \varepsilon U_t = 0.9 \times 436.8 = 393.1 \text{ m/sec}$$

$$w_2 = u_1 = 132.8 \text{ m/sec}$$

$$V_2 = \sqrt{w_2^2 + v_2^2} = \sqrt{132.8^2 + 393.1^2} = 414.9 \text{ m/sec}$$

$$\alpha_2 = \tan^{-1} \frac{w_2}{v_2} = 18.67°$$

$$M_2 = \sqrt{\frac{2}{\gamma - 1}\left[\frac{T_{t2}}{T_{t2} - V_2^2/(2g_c c_p)} - 1\right]}$$

$$= \sqrt{5\left(\frac{459.19}{459.19 - 85.73} - 1\right)} = 1.071$$

$$\frac{P_{t3s}}{P_{t1}} = \left(\frac{T_{t3}}{T_{t1}}\right)^{\gamma/(\gamma-1)} = 5.108$$

$$\frac{P_{t2}}{P_{t3s}} = \frac{P_{t3}}{P_{t2}} = \sqrt{\frac{P_{t3}/P_{t1}}{P_{t3s}/P_{t1}}} = 0.8849$$

$$P_{t2} = 0.8849 \times 5.108 \times 101.3 = 457.9 \text{ kPa}$$

$$P_{t3} = 4.0 \times 101.3 = 405.2 \text{ kPa}$$

$$\text{MFP}(M_2) = \frac{\text{MFP}(M_2)\sqrt{R/g_c}}{\sqrt{R/g_c}} = \frac{0.618966}{16.9115} = 0.040326$$

$$A_2 = \frac{\dot{m}\sqrt{T_{t2}}}{P_{t2}\,\text{MFP}(M_2)(\cos \alpha_2)} = \frac{8\sqrt{459.19}}{457{,}900 \times 0.040326 \times 0.9474} = 0.0098 \text{ m}^2$$

$$b = \frac{A_2}{\pi d_2} = \frac{0.0098}{\pi \times 0.5} = 0.624 \text{ cm}$$

$$M_3 = \sqrt{\frac{2}{\gamma - 1}\left[\frac{T_{t3}}{T_{t3} - V_3^2/(2g_c c_p)} - 1\right]}$$

$$= \sqrt{5\left(\frac{459.19}{459.19 - 4.034} - 1\right)} = 0.2105$$

TABLE 9-10
Results for Example 9-8 centrifugal compressor

Property		Station 1	1*R*	2*R*	2	3
T_t	(K)	**288.16**	296.70/322.36 (hub/tip)	383.23	459.19	459.19
T	(K)	279.37	279.37	272.50	373.50	455.16
P_t	(kPa)	**101.3**	112.2/150.0	243.1	457.9	**405.2**
P	(kPa)	90.9	90.9	222.2	222.2	392.9
M		0.3966	0.557/0.877	0.361	1.071	0.2105
V	(m/sec)	132.8	186.54/293.82	139.8	414.9	**90**
u/w	(m/sec)	132.8	132.8	132.8	132.8	
v	(m/sec)	0	131.0/262.1	43.7	393.1	
r	(cm)		**15/30**	**50.0**	**50.0**	
α	(deg)	0	—	—	18.67	
β	(deg)	—	44.6/63.1	69.1	—	

$$\text{MFP}(M_3) = \frac{\text{MFP}(M_3)\sqrt{R/g_c}}{\sqrt{R/g_c}} = \frac{0.242559}{16.9155} = 0.014343$$

$$A_3 \cos \alpha_3 = \frac{\dot{m}\sqrt{T_{t3}}}{P_{t3}\,\text{MFP}(M_3)} = \frac{8\sqrt{459.196}}{405{,}200 \times 0.014343} = 0.0295 \text{ m}^2$$

The results of this example are summarized in Table 9-10. Note that different values of flow properties are listed for the hub and tip at station 1*R* and that M_2 is supersonic while M_{2R} is subsonic.

9-5 AXIAL-FLOW TURBINE ANALYSIS

The mass flow of a gas turbine engine, which is limited by the maximum permissible Mach number entering the compressor, is generally large enough to require an axial turbine (even for centrifugal compressors). The axial turbine is essentially the reverse of the axial compressor except for one essential difference: The turbine flow operates under a favorable pressure gradient. This permits greater angular changes, greater pressure changes, greater energy changes, and higher efficiency. However, there is more blade stress involved because of the higher work and temperatures. *It is this latter fact that generally dictates the blade shape.*

Conceptually, a turbine is a very simple device since it is fundamentally no different from a pinwheel which spins rapidly when air is blown against it. The pinwheel will turn in one direction or the other, depending on the direction of the impinging air, and a direction can be found for the air which causes no rotation at all. Thus it is important to properly direct the airstream if the desired motion and speed are to be obtained.

A modern turbine is merely an extension of these basic concepts.

Considerable care is taken to establish a directed flow of fluid of high velocity by means of stator blades, and then similar care is used in designing the blades on the rotating wheel (the vanes on the pinwheel) so that the fluid applies the required force to these rotor blades most efficiently. Conceptually, the turbine is a cousin to the pinwheel, but such an analogy gives no appreciation for the source of the tremendous power outputs which can be obtained in a modern turbine. The appreciation comes when one witnesses a static test of the stator blades which direct a gas stream to the rotor of a modern aircraft gas turbine. Such a stream exhausting into the quiescent air of a room will literally rip the paint off the wall at a point 6 ft away in line with the jet direction. When blades of the rotating element are pictured in place immediately at the exit of these directing blades, it then becomes difficult to imagine that the rotor could be constrained from turning and producing power.

Terminology can be a problem in the general field of turbomachinery. Compressor development grew out of aerodynamics and aircraft wing technology, while turbines have historically been associated with the mechanical engineers who developed the steam turbine. The symbols as well as the names used in these two fields differ, but for consistency and to minimize problems for the reader, the turbine will be presented using the nomenclature already established in the beginning of this chapter. Where a term or symbol is in such common use that to ignore it would mean an incomplete education, it will be indicated as an alternate. Thus turbine stator blades are usually called *nozzles* and rotor blades are *buckets.*

In the gas turbine, the high-pressure, high-temperature gas from the combustion chamber flows in an annular space to the stationary blades (called *stators, vanes,* or *nozzles*) and is directed tangentially against the rotating blade row (called *rotor blades* or *buckets*). A simple single-stage turbine configuration with nomenclature is shown in Fig. 9-48*a*. It is convenient to "cut" the blading on a cylindrical surface and look at the section of the stator and rotor blades in two dimensions. This leads to the construction of a vector

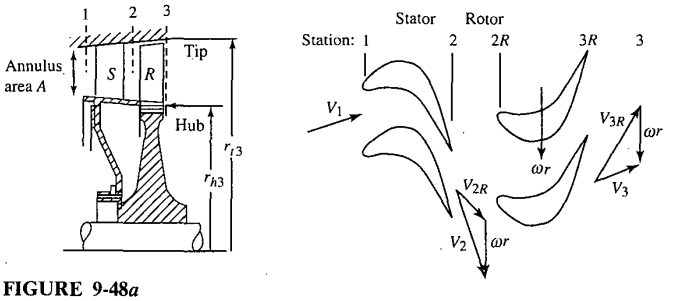

FIGURE 9-48*a*
Typical single-stage turbine and velocity diagram.

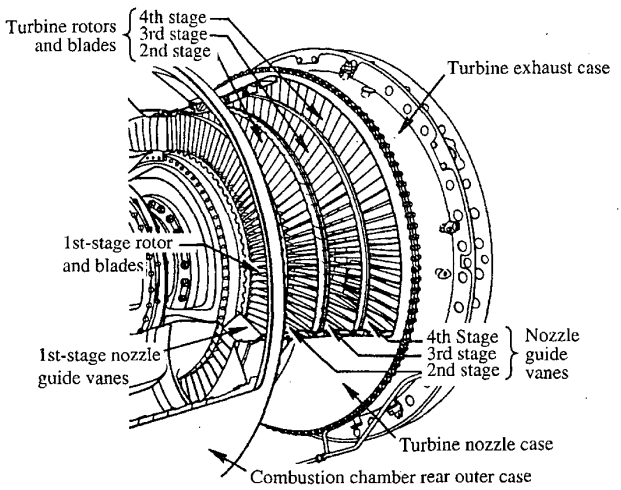

FIGURE 9-48*b*
Isometric section of multistage turbine.

or velocity diagram for the stage (see Fig. 9-48*a*) which shows the magnitude and direction of the gas velocities within the stage on the cylindrical surface.

In the stator or nozzle, the fluid is accelerated while the static pressure decreases and the tangential velocity of the fluid is increased in the direction of rotation. The *rotor* decreases the tangential velocity in the direction of rotation, tangential forces are exerted by the fluid on the rotor blades, and a resulting torque is produced on the output shaft. The absolute velocity of the fluid is reduced across the rotor. Relative to the moving blades, typically there is acceleration of the fluid with the associated decrease in static pressure and static temperature. A multistage turbine is made up of consecutive stages, each stage consisting of first a nozzle row followed by a rotor row. Figure 9-48*b* shows an isometric section of the four-stage turbine for a two-spool, low-bypass-ratio turbofan engine.

The following analysis of the axial-flow turbine stage is performed along the mean radius with radial variations being considered. In many axial-flow turbines, the hub and tip diameters vary little through a stage, and the hub/tip ratio approaches unity. There can be no large radial components of velocity between the annular walls in such stages, there is little variation in static pressure from root to tip, and the flow conditions are little different at each radius.

For these stages of high hub/tip ratio, the two-dimensional analysis is sufficiently accurate. The flow velocity triangles are drawn for the mean-radius condition, but these triangles are assumed to be valid for the other radial

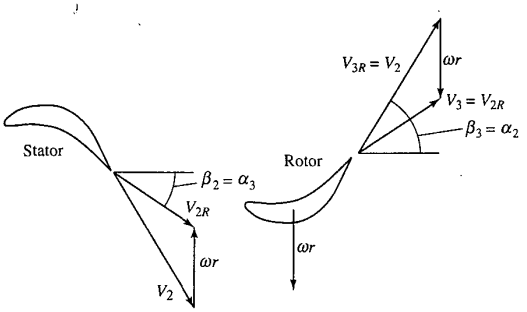

FIGURE 9-60
Diagram of 50 percent reaction turbine velocity.

Then, $\alpha_2 = \beta_3$, $\alpha_3 = \beta_2$, and

$$\tan \beta_3 - \tan \beta_2 = \tan \alpha_2 - \tan \alpha_3 = \frac{\omega r}{u_2} = \frac{1}{\Phi}$$

The stage loading coefficient for this turbine with constant axial velocity is

$$\boxed{\psi = \frac{\Delta v}{\omega r} = 2\Phi \tan \alpha_2 - 1 = 2\Phi \tan \beta_3 - 1} \tag{9-85}$$

Again, α_2 should be high but is limited to less than 70°. For *zero exit swirl*

$$\tan \beta_3 = \tan \alpha_2 = \frac{\omega r}{u} \qquad \beta_2 = 0 \qquad \boxed{\psi = 1} \tag{9-86}$$

Thus, for the same ωr and $v_3 = 0$, the work per unit mass from a zero-reaction turbine is twice that from the 50 percent reaction turbine [compare Eqs. (9-84) and (9-86)].

General zero-swirl case (constant axial velocity). If the exit swirl is to be zero (Fig. 9–61), then $\alpha_3 = 0$, $v_3 = 0$, and $\tan \beta_3 = \omega r/u$. From Eq. (9-82), the

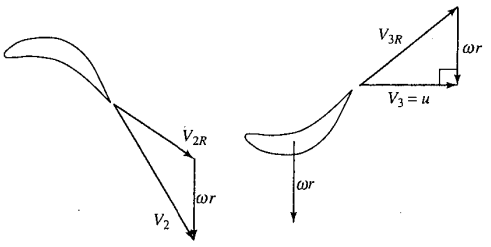

FIGURE 9-61
Zero-exis-swirl turbine.

reaction is then

$$^{\circ}R_t = \frac{u}{2\omega r}\left(\frac{\omega r}{u} - \tan\beta_2\right) = \frac{1}{2} - \frac{u\tan\beta_2}{2\omega r} = 1 - \frac{v_2}{2\omega r}$$

$$\boxed{^{\circ}R_t = 1 - \frac{v_2}{2\omega r} = 1 - \frac{\psi}{2}} \tag{9-87}$$

This equation can be rewritten as

$$\boxed{\psi = 2(1 - {}^{\circ}R_t)} \tag{9-88}$$

Thus high stage loadings give a low degree of reaction. In aircraft gas turbine engines, engine weight and performance must be balanced. Weight can be reduced by increasing stage loading (reduces the number of turbine stages), but this normally leads to a loss in stage efficiency (see Fig. 9-53).

TURBINE AIRFOIL NOMENCLATURE AND DESIGN METAL ANGLES. The nomenclature for turbine airfoil cascades is presented in Fig. 9-62. The situation in unchoked turbines is similar to that in compressors except that the deviations are markedly smaller owing to the thinner boundary layers. Hence

$$\boxed{\delta_t = \frac{\gamma_i + \gamma_e}{8\sqrt{\sigma}}} \tag{9-89}$$

is a good estimate of the turbine exit deviation. More importantly, however,

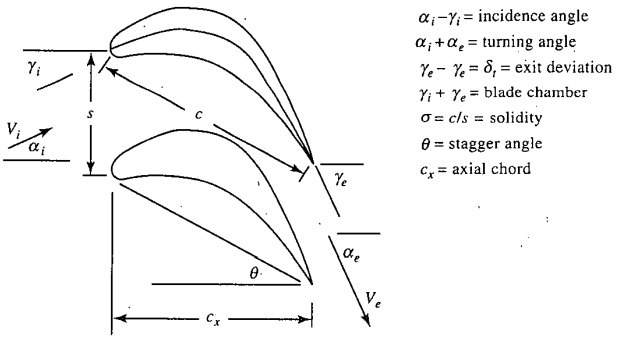

FIGURE 9-62
Turbine airfoil nomenclature.

when the turbine airfoil cascade exit Mach number is near unity, the deviation is usually negligible because the cascade passage is similar to a nozzle. In fact, the suction (or convex) surface of the airfoils often has a flat stretch before the trailing edge, which evokes the name *straight-backed.* Finally, the simple concept of deviation loses all meaning at large supersonic exit Mach numbers because expansion or compression waves emanating from the trailing edge can dramatically alter the final flow direction. This is a truly fascinating field of aerodynamics, but one that requires considerable study.

STAGE TEMPERATURE RATIO τ_s. The stage temperature ratio ($\tau_s = T_{t1}/T_{t3}$) can be expressed as follows, by using the definition of the stage loading coefficient:

$$\tau_s = \frac{T_{t3}}{T_{t1}} = 1 - \psi \frac{(\omega r)^2}{g_c c_p T_{t1}} \tag{9-90}$$

Thus, for a given T_{t1} and ωr, the zero-reaction turbine stage will have the lower stage temperature ratio (greater work output per unit mass) than a 50 percent reaction turbine stage.

STAGE PRESSURE RATIO π_s. Once the stage temperature ratio, flow field, and airfoil characteristics are established, several avenues are open to predict the stage pressure ratio. The most simple and direct method is to employ the polytropic efficiency e_t. Recall that the polytropic efficiency is

$$e_t = \frac{dh_t}{dh_{t\,\text{ideal}}} = \frac{\gamma}{\gamma - 1} \frac{dT_t/T_t}{dP_t/P_t}$$

Integration with constant γ and e_t yields the following equation for the stage pressure ratio

$$\pi_s = \frac{P_{t3}}{P_{t1}} = \left(\frac{T_{t3}}{T_{t1}}\right)^{\gamma/[(\gamma-1)e_t]} = \tau_s^{\gamma/[(\gamma-1)e_t]} \tag{9-91}$$

where the stage temperature ratio can be obtained from the total temperatures or an equation like Eq. (9-90).

Another approach involves the use of experimental or empirical cascade loss correlations, such as those shown in Figs. 9-63 and 9-64, to the stator and rotor in order to determine the total pressure loss. The *total pressure loss coefficient* for turbine cascade data is defined as

$$\phi_t \equiv \frac{P_{ti} - P_{te}}{P_{te} - P_e} \tag{9-92}$$

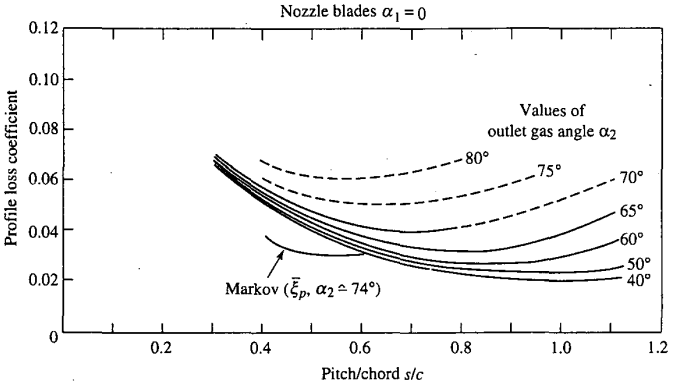

FIGURE 9-63
Turbine stator cascade loss coefficient ($\alpha_1 = 0$). (*From J. H. Horlock,* Axial Flow Turbines, *Ref. 34, by courtesy of Butterworth-Heinmann Limited.*)

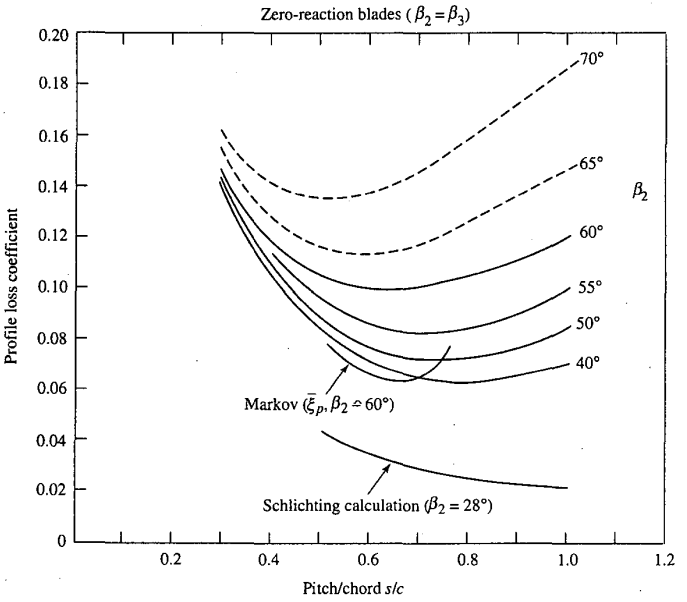

FIGURE 9-64
Turbine rotor cascade loss coefficient ($\beta_2 = \beta_3$). (*From J. H. Horlock,* Axial Flow Turbines, *Ref. 34, by courtesy of Butterworth-Heinmann Limited.*)

where subscripts i and e refer to the inlet and exit states, respectively. This equation can be rewritten for the cascade total pressure ratio as

$$\boxed{\frac{P_{te}}{P_{ti}} = \frac{1}{1 + \phi_t(1 - P_e/P_{te})}} \tag{9-93}$$

where P_e/P_{te} depends only upon the usually known airfoil cascade exit Mach number M_e. Note that the total pressure loss coefficient for the rotor is based on the relative total states. The stage total pressure ratio can be written as

$$\boxed{\frac{P_{t3}}{P_{t1}} = \left(\frac{P_{t2}}{P_{t1}}\right)_{\phi_{t\,\text{stator}},\, M_2} \frac{P_{t2R}}{P_{t2}} \left(\frac{P_{t3R}}{P_{t2R}}\right)_{\phi_{t\,\text{rotor}},\, M_{3R}} \frac{P_{t3}}{P_{t3R}}} \tag{9-94}$$

where $\phi_{t\,\text{stator}}$ and $\phi_{t\,\text{rotor}}$ are the loss coefficients for the stator and rotor, respectively, and the subscripted total pressure ratios are obtained from Eq. (9-93) and cascade data. Additional losses are associated with tip leakage, annulus boundary layers, and secondary flows. Then, with all the stator, rotor, and stage properties computed, the stage efficiency can be computed from Eq. (9-76).

BLADE SPACING. The momentum equation relates the tangential force of the blades on the fluid to the change in tangential momentum of the fluid. This force is equal and opposite to that which results from the difference in pressure between the pressure side and the suction side of the airfoil. Figure 9-65 shows the variation in pressure on both the suction and pressure surfaces of a typical turbine airfoil from cascade tests. On the pressure surface, the pressure is nearly equal to the inlet total pressure for 60 percent of the length before the fluid is accelerated to the exit pressure condition. However, on the suction surface, the fluid is accelerated in the first 60 percent of the length to a low pressure and then is decelerated to the exit pressure condition. The deceleration on the suction surface is limited and controlled since it can lead to boundary-layer separation.

Enough airfoils must be present in each row that the sum of the tangential force on each is equal to the change in tangential momentum of the fluid. A simple expression for the relationship of the blade spacing to the fluid flow angles is developed in this section based on an incompressible fluid. This same expression correlates to the required blade spacing in a turbine stator or rotor row.

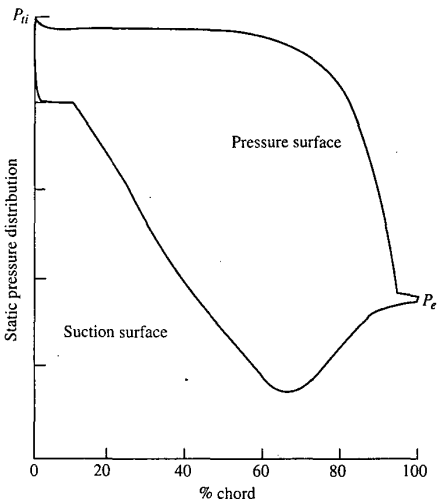

FIGURE 9-65
Pressure distribution on a turbine cascade airfoil.

Referring to the cascade nomenclature in Fig. 9-62, we see that the tangential force per unit depth of blades spaced a distance s apart is

$$F_t = \frac{\rho u_i s(v_i + v_e)}{g_c} = \frac{\rho u_i^2 s}{g_c}\left(\tan \alpha_i + \frac{u_e}{u_i}\tan \alpha_e\right) \tag{9-95}$$

Zweifel (Ref. 47) defines a tangential force coefficient that is the ratio of the force given by Eq. (9-95) to the maximum tangential force $F_{t\,\max}$ that can be achieved efficiently. And $F_{t\,\max}$ is obtained when

1. The pressure on the pressure surface is maintained at the inlet total pressure and drops to the exit static pressure at the trailing edge.
2. The pressure on the suction surface drops to the exit static pressure at the leading edge and remains at this value.

Thus the maximum tangential force is $F_{t\,\max} = (P_{ti} - P_e)c_x$, where c_x is the axial chord of the blade (see Fig. 9-62). For reversible flow of an incompressible fluid, $F_{t\,\max}$ can be written as

$$F_{t\,\max} = \frac{\rho V_e^2 c_x}{2g_c} = \frac{\rho u_e^2 c_x}{2g_c \cos^2 \alpha_e} \tag{9-96}$$

The *Zweifel tangential force coefficient* Z is defined as

$$\boxed{Z \equiv \frac{F_t}{F_{t\,\max}}} \tag{9-97}$$

From Eqs. (9-95) and (9-96), the equation of Z for a cascade airfoil becomes

$$Z = \frac{2s}{c_x}(\cos^2 \alpha_e)\left(\tan \alpha_i + \frac{u_e}{u_i}\tan \alpha_e\right)\left(\frac{u_i}{u_e}\right)^2$$

For the stator, we write

$$\boxed{Z_s = \frac{2s}{c_x}(\cos^2 \alpha_2)\left(\tan \alpha_1 + \frac{u_2}{u_1}\tan \alpha_2\right)\left(\frac{u_1}{u_2}\right)^2} \qquad (9\text{-}98a)$$

Likewise for the rotor, we write

$$\boxed{Z_r = \frac{2s}{c_x}(\cos^2 \beta_3)\left(\tan \beta_2 + \frac{u_3}{u_2}\tan \beta_3\right)\left(\frac{u_2}{u_3}\right)^2} \qquad (9\text{-}98b)$$

Since suction surface pressures can be less than the exit static pressure along the blade (see Fig. 9-65), *Z values near unity are attainable.* By using Eq. (9-98), lines of constant $Z_r c_x/s$ are plotted in Fig. 9-66 versus the relative rotor angles β_2 and β_3. High β_2 and zero reaction (high stage loading ψ, see Fig. 9-57) give high values of $Z_r c_x/s$ (see Fig. 9-66) and require high values of solidity [$\sigma = c/s = (c_x/s)/\cos \theta$]. High solidity at high β_2 and zero reaction can lead to high total pressure losses (see Fig. 9-64). For no exit swirl ($\alpha_3 = 0$), the

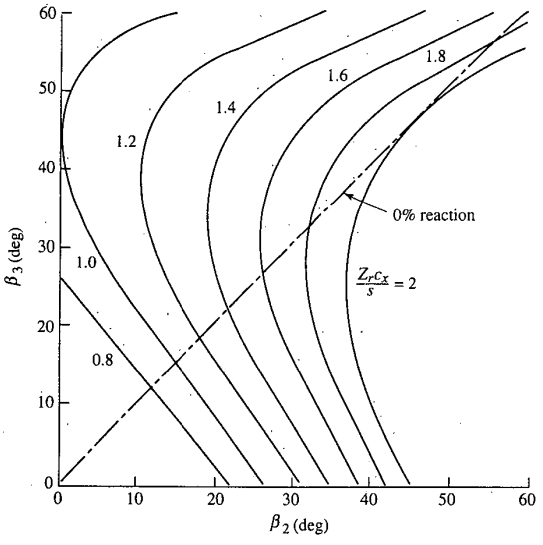

FIGURE 9-66
Zc_x/s of rotor versus β_2 and β_3.

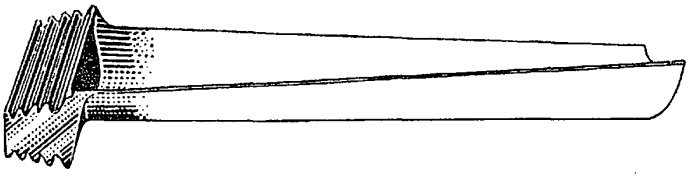

FIGURE 9-67
Low-pressure turbine rotor blade (Ref. 46).

50 percent reaction stage ($\psi = 1$) corresponds to $\beta_2 = 0$, the required solidity is low (Fig. 9-66), and the total pressure losses are low (Fig. 9-64). Thus the turbine design for aircraft engines will be a balance between the number of stages (stage loadings) and the turbine efficiency (total pressure losses).

RADIAL VARIATIONS. Since the mass flow rate per unit area [that is, $\dot{m}/A = P_t/(\text{MFP}\sqrt{T_t})$] is higher in turbines than in compressors, turbine airfoils are correspondingly shorter. The result is little radial variation of aerodynamic properties from hub to tip except in the last few stages of the low-pressure turbine. Figure 9-67 is the rotor blade of a low-pressure turbine which shows radial variation from hub to tip. Typically, the degree of reaction varies from near zero at the hub to about 40 percent at the tip.

If the aerodynamic design of these stages began as free vortex, the swirl distribution with radius is the same as for compressors, given by

$$\boxed{v = v_m \frac{r_m}{r}} \tag{9-44}$$

For constant axial velocity ($u_2 = u_3$), the degree of reaction is

$$^{\circ}R_t = \frac{T_2 - T_3}{T_{t1} - T_{t3}} = \frac{T_2 - T_3}{T_{t2} - T_{t3}} = 1 - \frac{V_2^2 - V_3^2}{2g_c c_p (T_{t1} - T_{t3})} = 1 - \frac{v_2^2 - v_3^2}{2\omega r (v_2 + v_3)}$$
$$= 1 - \frac{v_2 - v_3}{2\omega r}$$

Substituting Eq. (9-44), we write the degree of reaction at any radius in terms of the degree of reaction at the mean radius as

$$^{\circ}R_t = 1 - \frac{v_{m2} - v_{m3}}{2\omega r}\frac{r_m}{r} = 1 - \frac{v_{m2} - v_{m3}}{2\omega r_m}\left(\frac{r_m}{r}\right)^2$$

$$\boxed{^{\circ}R_t = 1 - (1 - {}^{\circ}R_{tm})\left(\frac{r_m}{r}\right)^2} \tag{9-99}$$

This is the same result as for compressors [Eqs. (9-51) and (9-52)]. Consequently, the most difficult airfoil contours to design would be at the hub of the rotating airfoils and at the tips of the stationary airfoils where the degree of reaction is low. It is, therefore, possible to find portions of some airfoils near the rear of highly loaded (i.e., high work per stage), low-pressure turbines where the static pressure actually rises across the cascade and boundary-layer separation is hard to avoid. In these cases, turbine designers have used their computers to develop nonfree or controlled vortex machines without these troublesome regions in order to maintain high efficiency at high loading.

Due to radial variations, the degree of reaction is lowest at the hub. Hence the Zweifel tangential force coefficient of the rotor Z_r times c_x/s will be maximum at the hub. Although the blade spacing varies directly with radius, $Z_r c_x/s$ is greatest at the hub and decreases faster than $1/r$ with increasing radius. Thus the value of $Z_r c_x/s$ at the rotor hub determines the spacing and number of rotor blades. For the stator, $Z_s c_x/s$ will be greatest at the tip, and its value determines the spacing and number of stator blades.

VELOCITY RATIO VR. The *velocity ratio* (VR) is defined as the ratio of the rotor speed ($U = \omega r$) to the velocity equivalent of the change in stage total enthalpy, or

$$\boxed{\text{VR} \equiv \frac{U}{\sqrt{2g_c\,\Delta h_t}} = \frac{\omega r}{\sqrt{2g_c\,\Delta h_t}}} \tag{9-100}$$

The velocity ratio is used by some turbine designers rather than the stage loading coefficient ψ, and one can show that

$$\boxed{\text{VR} = \frac{1}{\sqrt{2\psi}}} \tag{9-101}$$

The VR at the mean radius ranges between 0.5 and 0.6 for modern aircraft gas turbine engines. This range corresponds to stage loading coefficients ψ between 1.4 and 2.

Axial-Flow Turbine Stage

ANALYSIS. Consider the flow through a single-stage turbine as shown in Fig. 9-68. For generality, we will allow the axial velocity to change from station 2 to 3. The flows through the nozzle (stator) and rotor are assumed to be adiabatic. For solution, we assume that the following data are known: M_2, T_{t1}, T_{t3}, ωr, α_3, c_p, γ, and u_3/u_2. We will develop and write the equations for a general axial-flow turbine based on these known data.

indeed do, pass through a single point. This fact may be verified by equating the numerator and denominator on the right side of the equals sign in Eq. (9-124), and this reveals that $M_{3R} = M_2$ is independent of either M_2 or τ_s provided only that

$$\psi^2 - 1 = \frac{\gamma - 1}{2}(2\psi - \psi^2)M_2^2$$

Hence, for each γ, there are two values of ψ that satisfy this condition. When $M_{3R} = M_2 = 1.0$ and $\gamma = 1.3$, they are 1.072 and -0.82, the former obviously being the one that appears in Fig. 9-75 and the latter having no practical use. For $M_{3R} = M_2 = 1.2$ and $\gamma = 1.3$, they are 1.102 and -0.746. The physical meaning of this convenient convergence is clear enough, namely, that near $M_{3R} = M_2$, where the stator and rotor airfoil exit conditions are similar, the stage loading parameter ψ must be near unity regardless of the other stage parameters.

MULTISTAGE TURBINE DESIGN. When the required stage loading coefficient ψ for a design is greater than 2.0, a single-stage design would require a hopeless negative reaction [Eq. (9-87)] and would be impossible to design with high aerodynamic efficiency. A desirable multistage design would have the total temperature difference distributed evenly among the stages:

$$(\Delta T_t)_{\text{turbine}} = (\text{number of stages}) \times (\Delta T_t)_{\text{stage}}$$

This would result in stages with the same stage loading coefficients [Eq. (9-20)] and same degree of reaction [Eq. (9-87)] for the same rotor speed U. For a three-stage design, we get

$$\psi_{s1} = \psi_{s2} = \psi_{s3} \qquad \text{and} \qquad (^\circ R_t)_{s1} = (^\circ R_t)_{s2} = (^\circ R_t)_{s3}$$

To obtain the choked flow in the first-stage stator (nozzle), the Mach number entering the rotor M_2 is slightly supersonic. The Mach numbers in the remaining stages are kept subsonic. The net result is that the stage loading of the first stage is larger than the loading of any of the other stages. For a three-stage design, the stage loading coefficient and degree of reaction of the second and third stages are nearly equal.

Shaft Speed

The design rotational speed of a spool (shaft) having stages of compression driven by a turbine is initially determined by that component which limits the speed because of high stresses. For a low-pressure spool, the first stage of compression, since it has the greatest AN^2, normally dictates the rotational speed. The first stage of turbine on the high-pressure spool normally

TABLE 9-16*a*
Range of axial-flow turbine design parameters

Parameter	Design range
High-pressure turbine	
Maximum AN^2	$4–5 \times 10^{10}$ in$^2 \cdot$ rpm^2
Stage loading coefficient	1.4–2.0
Exit Mach number	0.40–0.50
Exit swirl angle (deg)	0–20
Low-pressure turbine	
Inlet corrected mass flow rate	40–44 lbm/(sec $\cdot$ ft^2)
Hub/tip ratio at inlet	0.35–0.50
Maximum stage loading at hub	2.4
Exit Mach number	0.40–0.50
Exit swirl angle (deg)	0–20

determines that spool's rotational speed because of its high AN^2 or high disk rim speed at elevated temperature.

Design Process

The design process requires both engineering judgment and knowledge of typical design values. Table 9-16a gives the range of design parameters for axial-flow turbines that can be used for guidance. The comparison of turbines

TABLE 9-16*b*
Comparison of Pratt & Whitney engines

Parameter	JT3D	JT9D
Year of introduction	1961	1970
Engine bypass ratio	1.45	4.86
Engine overall pressure ratio	13.6	24.5
Core engine flow (lb/sec)	187.7	272.0
High-pressure turbine		
Inlet temperature (°F)	1745	2500
Power output (hp)	24,100	71,700
Number of stages	1	2
Average stage loading coefficient	1.72	1.76
Coolant plus leakage flow (%)	2.5	16.1
Low-pressure turbine		
Inlet temperature (°F)	1410	1600
Power output (hp)	31,800	61,050
Number of stages	3	4
Average stage loading coefficient	1.44	2.47
Coolant plus leakage flow (%)	0.7	1.4

TABLE 9-18
Results for Example 9-14 single-stage axial-flow turbine design

Property		Station 1h	1m	1t	2h	2m	2t	2Rm	3Rm	3h	3m	3t
T_t	(°R)	3200	3200	3200	3200	3200	3200	2909	2909	2750	2750	2750
T	(°R)	3125	3125	3125	2665	2708	2745	2708	2621	2620	2621	2622
Pt	(psia)	143.1	143.1	143.1	138.8	138.8	138.8	91.8	87.0	68.3	68.3	68.3
P	(psia)	129.1	129.1	129.1	62.8	67.4	71.5	67.4	55.4	55.4	55.4	55.5
M		0.400	0.400	0.400	1.157	1.100	1.051	0.702	0.855	0.574	0.572	0.571
V	(ft/sec)	1057	1057	1057	2823	2705	2602	1727	2069	1389	1385	1381
u	(ft/sec)	1057	1057	1057	1353	1353	1353	1353	1353	1353	1353	1353
v	(ft/sec)	0	0	0	2477	2343	2222	1073	1566	316	296	278
α	(deg)	0	0	0	61.36	60.00	58.67	—	—	13.14	12.33	11.61
β	(deg)	—	—	—	—	—	—	38.42	49.17	—	—	—
Radii	(in)	18.25	19.05	19.85	18.02	19.05	20.08	19.05	19.05	17.83	19.05	20.27

Hub: $^{\circ}R_t = 0.0990$ $A_1 = 190.78\ \text{in}^2$

Mean: $^{\circ}R_t = 0.1939$ $A_2 = 247.52\ \text{in}^2$

Tip: $^{\circ}R_t = 0.2746$ $A_3 = 291.11\ \text{in}^2$

$M_{3Rt} = 0.875$ $\tau_s = 0.8593$ $\pi_s = 0.4770$ $\psi = 2.0776$ $\Phi = 1.0652$

$\eta_s = 89.57\%$ AN^2 at $2 = 1.44 \times 10^{10}\ \text{in}^2 \cdot \text{rpm}^2$

Computer calculations yield the single-stage turbine summarized in Table 9-18 with hub and tip tangential velocities based on free-vortex swirl distribution. This is a viable single-stage design with moderate exit swirl α_3, positive reaction, and subsonic M_{3R} at the tip.

This design gives a blade AN^2 of $1.44 \times 10^{10}\ \text{in}^2 \cdot \text{rpm}^2$ and hub speed of 1201 ft/sec. This AN^2 value is well within the limits of cooled turbine materials, and the low hub speed is below the limiting speed of turbine disk materials.

A cross-sectional sketch of the single-stage turbine designed above and plotted by the computer program TURBN is shown in Fig. 9-76. Note that this sketch does not show the required exit guide vanes that will turn the flow back to axial. The estimated axial length L shown in Fig. 9-76 is based on the input values of Z and c/h for the stator and rotor blades and the scaling relationships of Fig. 9-69. For the input values of Z and c/h, the resulting solidity at the mean radius, number of blades, and chord length for the stator and rotor are as follows:

	Solidity	Number of blades	Chord (in)
Stator	0.979	64	1.831
Rotor	1.936	103	2.250

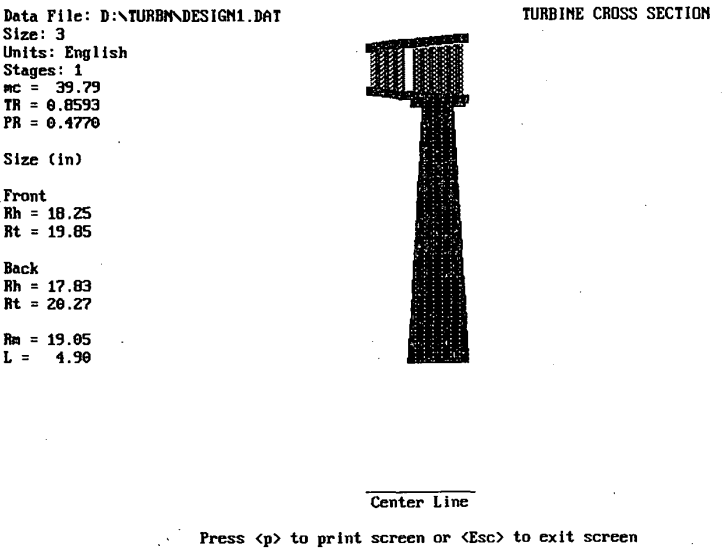

FIGURE 9-76
Sketch of cross section for single-stage turbine design.

The selected axial chord and number of blades for the stator or rotor depend on many factors (e.g., flow through the blades, vibration, blade attachment). Figure 9-77 shows the computer sketch of the blades at the mean radius, using C4 base profiles.

TWO-STAGE DESIGN. In a two-stage design, the stage loading coefficients ψ are lower and the temperature ratios τ_s are higher than those for a single-stage design. This results in higher reactions, less turning of the flow, and lower loss coefficients. For good flow control of the turbine, the first-stage stator (nozzle) should be choked which requires that M_2 for this stage be supersonic. Inspection of Fig. 9-75 shows that at low ψ and high τ_s, the value of M_{3R} is a little less than M_2—thus, we will want to select a low supersonic value of M_2 (about 1.05) for the first stage. A balanced design would have about the same α_2 values for both stages with the first-stage M_{3Rt} below 0.9.

The two-stage turbine will be designed with a 17.04 in mean radius (same as multistage compressor) at an rpm of 7640 ($\omega = 800$ rad/sec), giving a mean rotor speed $U_m = \omega r_m$ of 1136 ft/sec. An initial starting point for the design of this two-stage turbine is constant axial velocity through the rotor ($u_3 = u_2$), zero exit swirl ($\alpha_3 = 0$), and a second-stage M_2 of 0.7. The stage loading

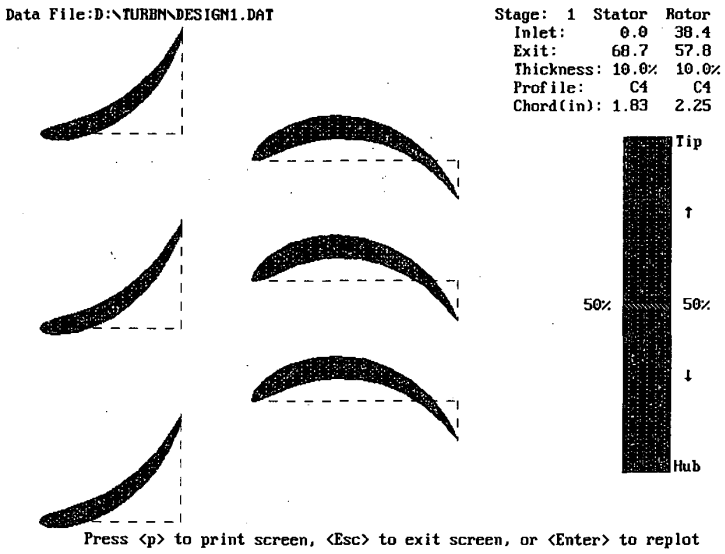

FIGURE 9-77
Sketch of blades for single-stage turbine design.

coefficients and other flow properties depend on the split in temperature drop between the stages. Calculations were performed by using the computer program TURBN with α_2 unknown at different values of the temperature leaving the first-stage turbine. The resulting α_2 and M_{3Rt} values are listed in Table 9-19. An interstage temperature of 2925°R gives a balance design for α_2 values with the first stage M_{3Rt} above 0.9. The value of M_{3Rt} can be reduced by selecting a value for the axial velocity ratio u_3/u_2 less than unity.

TABLE 9-19
Variation of stage parameters with interstage temperature for Example 9-14 two-stage design

← Stage 1 →					← Stage 2 →		
T_{t3} (°R)	ψ	τ_s	α_2 (deg)	M_{3Rt}	ψ	τ_s	α_2 (deg)
2875	1.8750	0.8984	55.0	0.7774	1.0034	0.9565	28.61
2900	1.7307	0.9063	49.12	0.8467	0.8659	0.9482	34.90
2925	1.5865	0.9141	43.88	0.9068	1.0102	0.9401	41.65
2950	1.4423	0.9219	39.06	0.9587	1.1544	0.9322	49.13
2975	1.2981	0.9297	34.55	1.0034	1.2986	0.9243	57.90

One advantage of the variable-area exhaust nozzle is that it improves the starting of the engine. Opening the nozzle throat area to its maximum value reduces the backpressure on the turbine and increases its expansion ratio. Thus the necessary turbine power for starting operation may be produced at a lower turbine inlet temperature. Also, since the backpressure on the gas generator is reduced, the compressor may be started at a lower engine speed, which reduces the required size of the engine starter.

EXHAUST NOZZLE AREA RATIO. Maximum engine thrust is realized for ideal flow when the exhaust nozzle flow is expanded to ambient pressure ($P_e = P_0$). When the nozzle pressure ratio is above choking, supersonic expansion occurs between aft-facing surfaces. A small amount of underexpansion is less harmful to aircraft and engine performance than overexpansion. Overexpansion can produce regions of separated flow in the nozzle and on the aft end of the aircraft, reducing aircraft performance.

The exhaust nozzle pressure ratio P_{te}/P_0 is a strong function of flight Mach number. Whereas convergent nozzles are usually used on subsonic aircraft, convergent-divergent nozzles are usually used for supersonic aircraft. When afterburning engine operation is required, complex variable-geometry nozzles must be used (see Fig. 10-52). Most of the nozzles shown in Fig. 10-54 are convergent-divergent nozzles with variable throat and exit areas. The

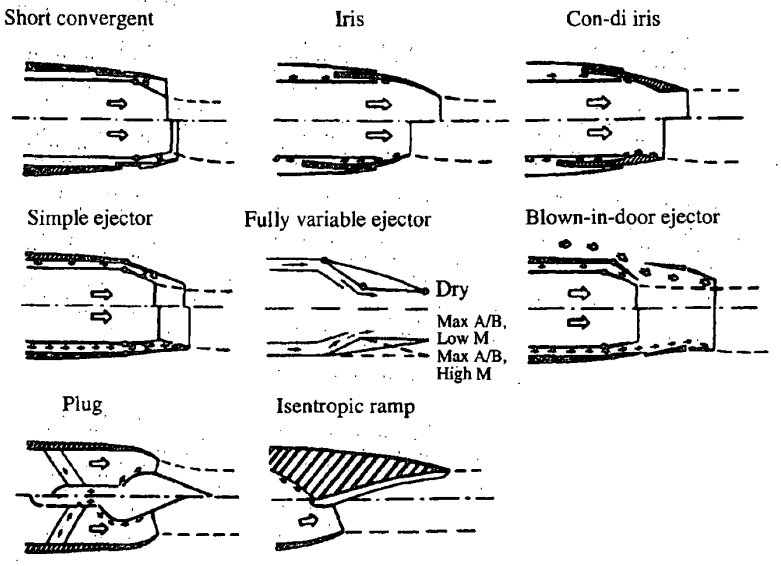

FIGURE 10-54
Typical nozzle concepts for afterburning engines (Ref. 62).

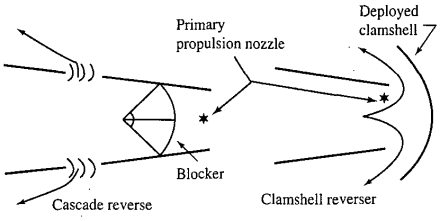

FIGURE 10-55
Thrust reversers (Ref. 62).

throat area of the nozzle is controlled to satisfy engine backpressure requirements, and the exit area is scheduled with the throat area. The sophisticated nozzles of the F-15 and B-1 aircraft have two schedules: a low-speed mode and a high-speed mode (Ref. 62).

THRUST REVERSING AND THRUST VECTORING. The need for thrust reversing and thrust vectoring is normally determined by the required aircraft and engine system performance. Thrust reversers are used on commercial transports to supplement the brakes. In-flight thrust reversal has been shown to enhance combat effectiveness of fighter aircraft (Ref. 62).

Two basic types of thrust reversers are used: the cascade-blocker type and the clamshell type (Fig. 10-55). In the cascade-blocker type, the primary nozzle exit is blocked off, and cascades are opened in the upstream portion of the nozzle duct to reverse the flow. In the clamshell type, the exhaust jet is split and reversed by the clamshell. Since both types usually provide a change in effective throat area during deployment or when deployed, most reversers are designed such that the effective nozzle throat area increases during the brief transitory period, thus preventing compressor stall.

The exhaust system for the Concorde is shown in Fig. 10-56. There are two nozzles, a primary nozzle and a secondary nozzle. The secondary nozzle is positioned as a convergent nozzle for takeoff and as a divergent nozzle for supersonic cruise. The modes of operation for this exhaust system are shown in Fig. 10-49 along with the inlet.

Development of thrust vectoring nozzles for combat aircraft has increased in the last decade. Vectoring nozzles have been used on vertical takeoff and landing (VTOL) aircraft, such as the AV-8 Harrier, and are proposed for future fighters to improve maneuvering and augment lift in combat. Thrust vectoring at augmented power settings is being developed for use in future fighters. However, cooling of the nozzle walls in contact with the hot turning or stagnating flows is very difficult and will require increased amounts of nozzle-cooling airflow. The operation of the Pratt & Whitney F119-PW-100 augmented turbofan engine's thrust vectoring nozzle is shown in Fig. 10-57. This two-dimensional nozzle was developed for use in the F-22 Advanced Tactical Fighter.

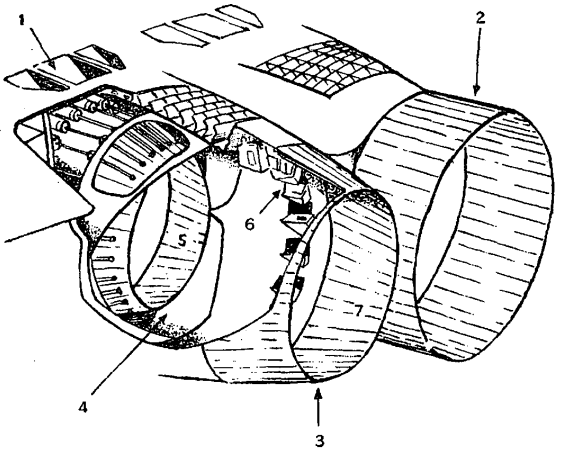

Details of the exhaust system: (1) tertiary doors; (2) nozzle in supersonic configuration; (3) subsonic configuration; (4) thrust reverse buckets; (5) primary nozzle; (6) silencer lobes; (7) secondary nozzle

FIGURE 10-56
Concorde exhaust system.

Figure 10-58 shows the schematic of a two-dimensional convergent-divergent nozzle with thrust vectoring of ±15° and thrust reversing. This is typical of the capabilities sought for use in future fighter aircraft.

Nozzle Coefficients

Nozzle performance is ordinarily evaluated by two dimensionless coefficients: the gross thrust coefficient and the discharge or flow coefficient. Figure 10-59 shows a convergent-divergent exhaust nozzle with the geometric parameters used in the following definitions of nozzle coefficients. Only total pressure losses downstream of station 8 are included in the gross thrust coefficient.

GROSS THRUST COEFFICENT. The *gross thrust coefficient* C_{fg} is the ratio of the actual gross thrust $F_{g\,\text{actual}}$ to the ideal gross thrust $F_{g\,\text{ideal}}$, or

$$C_{fg} \equiv \frac{F_{g\,\text{actual}}}{F_{g\,\text{ideal}}} \tag{10-17}$$

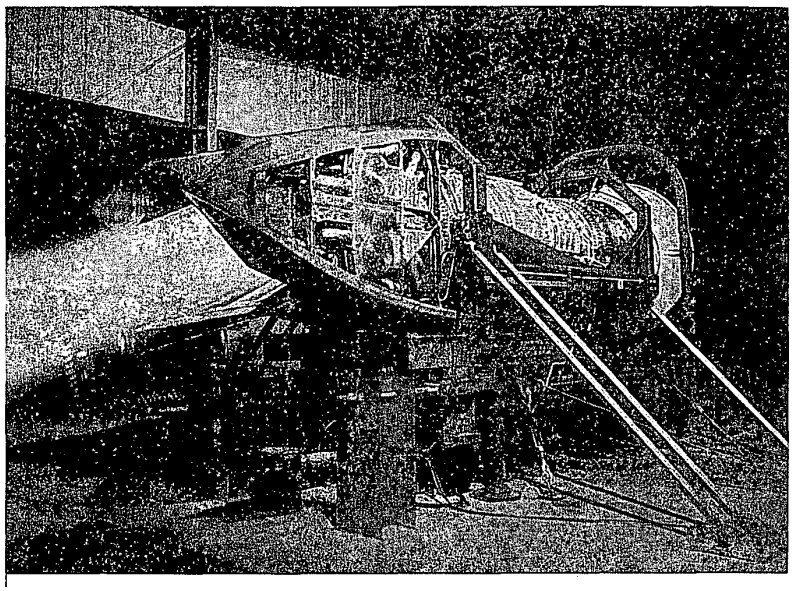

FIGURE 10-57
Pratt & Whitney F119-PW-100 turbofan engine with two-dimensional thrust vectoring nozzle. (*Courtesy of Pratt & Whitney.*)

Empirically derived coefficients are applied to Eq. (10-17) to account for the losses and directionality of the actual nozzle flow. Each engine organization uses somewhat different coefficients, but each of the following basic losses is accounted for:

- Thrust loss due to exhaust velocity vector angularity
- Thrust loss due to the reduction in velocity magnitude caused by friction in the boundary layers
- Thrust loss due to loss of mass flow between stations 7 and 9 from leakage through the nozzle walls
- Thrust loss due to flow nonuniformities

DISCHARGE OR FLOW COEFFICIENT. The ratio of the actual mass flow $\dot{m}_8$ to the ideal mass flow $\dot{m}_{8i}$ is called the *discharge coefficient* C_D:

$$C_D \equiv \frac{\dot{m}_8}{\dot{m}_{8i}} \tag{10-18}$$

A can system consists of one or more cylindrical burners, each contained in a burner case. Because of its modular design, the can system was used during the early development of the turbojet engine. The cannular system consists of a series of cylindrical burners arranged within a common annulus—hence, the name *cannular*. This burner type was the most common in the aircraft turbine engine population, but has been replaced with the annular type in most modern engines. Most modern main burner systems employ the annular design wherein a single burner having an annular cross section supplies gas to the turbine. The improved combustion zone uniformity, design simplicity, reduced linear surface area, and shorter system length provided by the common combustion annulus have made the annular burner the leading contender for all future propulsion systems.

Main Burner Components

The turbine engine main burner system consists of three principal elements: the inlet diffuser, the dome and snout or cowl, and the liner. In addition, important subcomponents are necessary: the fuel injector, igniter, burner case, and primary swirler, if used. The term *combustion zone* is used to designate that portion of the main burner within the dome and liner. These elements are illustrated in Fig. 10-76.

The purpose of the inlet diffuser is to reduce the velocity of the air exiting the compressor and deliver the air to the combustion zone as a stable, uniform flow field while recovering as much of the dynamic pressure as possible. The inlet diffuser represents a design and performance compromise relative to required compactness, low-pressure loss, and good flow uniformity. Early inlet

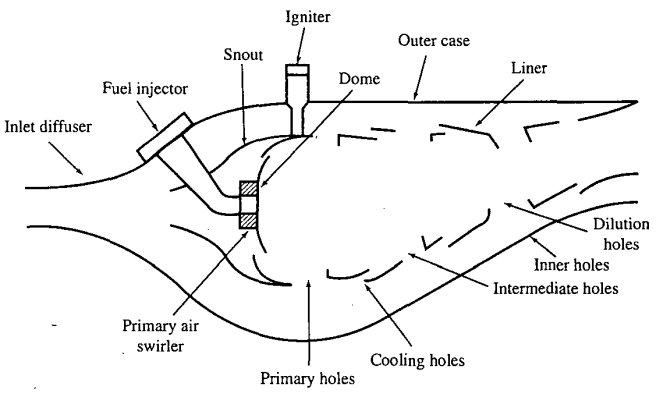

FIGURE 10-76
Main burner components (Ref. 62).

diffuser designs were of the smooth curved wall or contoured wall type. Because of the wide variations in the characteristics of the flow field exiting the compressor, however, the curved wall diffuser cannot always provide uniform, nonseparated flow at all operating conditions. This can become a critical problem in the short-length diffusers required of many current systems. Consequently, a trend toward dump, or combination curved wall and dump, diffuser designs is occurring. Although this design results in somewhat higher total pressure losses, it provides a known and constant point of flow separation at the dump plane, which prevents stalled operation at all diffuser entrance conditions.

The snout divides the incoming air into two streams: primary air and the other airflows (intermediate, dilution, and cooling air). The snout streamlines the combustor dome and permits a larger diffuser divergence angle and reduced overall diffuser length.

The combustor dome is designed to produce an area of high turbulence and flow shear in the vicinity of the fuel nozzle to finely atomize the fuel spray and promote rapid fuel/air mixing. There are two basic types of combustor domes: bluff body and swirl-stabilized. The bluff-body domes were used in early main burners, but swirl-stabilized domes are used in most modern main burners.

The combustion process is contained by the liner. The liner also allows introduction of intermediate and dilution airflow and the liner's cooling airflow. The liner must be designed to support forces resulting from pressure drop and must have high thermal resistance capable of continuous and cyclic high-temperature operation. This requires use of high-strength, high-temperature, oxidation-resistant materials (e.g., Hastalloy X) and cooling air.

Fuel injectors can be classified into four basic types according to the injection method utilized: pressure-atomizing, air blast, vaporizing, and premix/prevaporizing. The first two methods are the most common and are described below, but the reader is directed to other references (e.g., Ref. 32) for a description of the other two methods. In past main burner designs, the most common method of fuel injection was pressure atomizing, which can provide a large flow range with excellent fuel atomization when fuel system pressures are high (500 psi above main burner pressure). The pressure-atomized system is susceptible to fuel leaks (due to high fuel pressures) and plugging of orifices from fuel contaminants. Most modern main burner designs incorporate the air-blast atomizing fuel injector which achieves fuel atomization and mixing through the use of primary air momentum with strong swirling motion. The air-blast atomizing fuel injector requires lower fuel pressures (50 to 200 psi above main burner pressure) than the pressure-atomizing type.

Spark igniters, similar to automotive spark plugs, are used to ignite the cold, flowing fuel/air mixture in main burners. These spark igniters produce 4 to 12 J of ignition energy and require several thousand volts at the plug tip. Main burner starting redundancy is typically provided by use of at least two spark lighters.

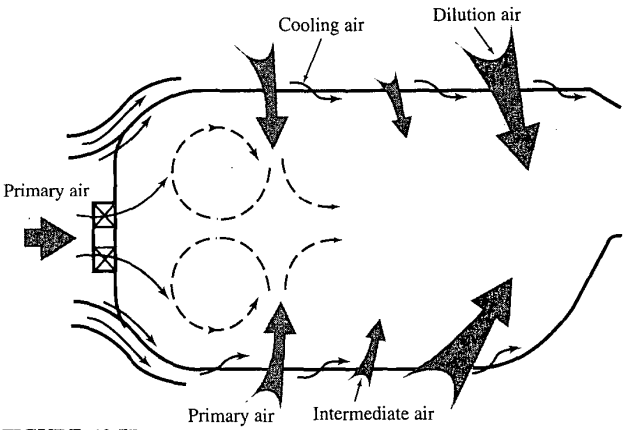

FIGURE 10-77
Main burner airflow distribution (Ref. 62).

Airflow Distribution and Cooling Air

This section identifies and briefly describes the airflow distribution terminology in, around, and through the main burner, resulting in the four basic airflow regions illustrated in Fig. 10-77. Effective control of this air distribution is vital to the attainment of complete combustion, stable operation, correct burner exit temperature profile, and acceptable liner temperatures for long life.

Primary air is the combustion air introduced through the dome or head plate of the burner and through the first row of liner airholes. This air mixes with the incoming fuel, producing the locally near-stoichiometric mixture necessary for optimum stabilization and operation. To complete the reaction process and consume the high levels of primary zone CO, H^-, and unburned fuel, intermediate air is introduced through a second row of liner holes. The reduced temperature and excess oxygen cause CO and H^- concentrations to decrease. In contemporary systems, the dilution air is introduced at the rear of the burner to reduce the high temperature of the combustion gases. The dilution air is used to carefully tailor exit temperature radial and circumferential profiles to ensure acceptable turbine durability and performance. This requires minimum temperatures at the turbine root (where stresses are highest) and at the turbine tip (to protect seal materials). However, modern and future main burner exit temperature requirements are necessitating increased combustion air in the primary and intermediate zones; thus, dilution zone airflow is necessarily reduced or eliminated to permit these increases.

Cooling air must be used to protect the burner liner and dome from the high radiative and convective heat loads produced within the burner. This air is normally introduced through the liner such that a protective blanket or film of

TABLE B-2
Data for some military turbofan engines

	Max./mil. power @ SLS				Maximum						
Model no.	Thrust (lb)	TSFC [(lbm/hr)/lbf]	Airflow (lb/sec)	OPR π_c	D (in)	L (in)	Weight (lb)	TIT (°F)	FPR π_f	BR α	Remarks
F100-PW-229	29,000/17,800	2.05/0.74	248	23.0	47	191	3,036	2,700	3.8	0.4	F-15, F16
F101-GE-102	30,780/17,390	2.460/0.562	356	26.8	55.2	180.7	4,448	2,550	2.31	1.91	B-1B
F103-GE-101	51,711	0.399	1,476	30.2	86.4	173	8,768	2,490	—	4.31	KC-10A
F107-WR-101	635	0.685	13.6	13.8	12	48.5	141	—	2.1	1.0	Air Launch Cruise Missile
F108-CF-100	21,634	0.363	785	23.7	72	115.4	4,610	2,228	1.5	6.0	KC-135R
F110-GE-100	28,620/18,330	2.08/1.47	254	30.4	46.5	182	3,895	—	2.98	0.80	F-16
F117-PW-100	41,700	0.33	—	31.8	84.5	146.8	7,100	—	—	5.8	(PW2040) C-17A
F118-GE-100	19,000	—	—	—	—	—	—	—	—	—	B-2
F404-GE-FID	10,000	—	—	25	34.5	87	1,730	—	—	—	F-117A
F404-GE-400	16,000	—	—	25	35	159	—	—	—	0.34	F-18, F-5G
JT3D-3B	18,000	0.535	458	13.6	53	136.4	4,300	1,600	1.74	1.37	(TF33-102) EC/RC-135
JT8D-7B	14,500	0.585	318	16.9	45	123.7	3.252	1,076	—	1.03	C-22, C-9, T-43A
TF30-P-111	25,100/14,560	2.450/0.686	260	21.8	49	241.7	3,999	2,055	2.43	0.73	F-111F
TF33-P-3	17,000	0.52	450	13.0	53	136	3,900	1,600	1.7	1.55	B-52H
TF33-P-7	21,000	0.56	498	16.0	54	142	4,650	1,750	1.9	1.21	C-141
TF34-GE-100	9,065	0.37	333	20.0	50	100	1,421	2,234	1.5	6.42	A-10
TF39-GE-1	40,805	0.315	1,549	26.0	100	203	7,186	2,350	1.56	8.0	C-5A
TF41-A-1B	14,500	0.647	260	20.0	40	114.5	3,511	2.165	2.45	0.76	A-7D, K
TFE731-2	3,500	0.504	113	17.7	40	50	625	—	1.54	2.67	C-21A

OPR = overall pressure ratio FPR = fan pressure ratio TSFC = thrust specific-fuel consumption TIT = turbine inlet temperature BR = bypass ratio.
Sources: Reference 86 and manufacturers' literature.

TABLE B-3
Data for some civil gas turbine engines

		Takeoff				Cruise				
Model no.	**Manufacturer**	**Thrust (lb)**	**BR**	**OPR π_c**	**Airflow (lb/sec)**	**Alt. (kft)**	**M_0**	**Thrust (lb)**	**TSFC [(lbm/hr)/lbf]**	**Aircraft application**
CF6-50C2	General Electric	52,500	4.31	30.4	1,476	35	0.80	11,555	0.630	DC10-10, A300B, 747-200
CF6-80C2	General Electric	52,500	5.31	27.4	1.650	35	0.80	12,000	0.576	767-200, −300, −200ER
GE90-B4	General Electric	87,400	8.40	39.3	3.037	35	0.80	17,500	—	777
JT8D-15A	Pratt & Whitney	15,500	1.04	16.6	327	30	0.80	4,920	0.779	727, 737, DC9
JT9D-59A	Pratt & Whitney	53,000	4.90	24.5	1.639	35	0.85	11,950	0.646	DC10-40, A300B, 747-200
PW2037	Pratt & Whitney	38,250	6.00	27.6	1.210	35	0.85	6,500	0.582	757-200
PW4052	Pratt & Whitney	52,000	5.00	27.5	1,700					767, A310-300
PW4084	Pratt & Whitney	87,900	6.41	34.4	2,550	35	0.83		—	777
CFM56-3	CFM International	23,500	5.00	22.6	655	35	0.85	4,890	0.667	737-300, −400, −500
CFM56-5C	CFM International	31,200	6.60	31.5	1.027	35	0.80	6,600	0.545	A340
RB211-524B	Rolls Royce	50,000	4.50	28.4	1.513	35	0.85	11,000	0.643	L1011-200, 747-200
RB211-535E	Rolls Royce	40,100	4.30	25.8	1.151	35	0.80	8,495	0.607	757-200
RB211-882	Rolls Royce	84,700	6.01	39.0	2.640	35	0.83	16,200	0.557	777
V2528-D5	International Aero Engines	28,000	4.70	30.5	825	35	0.80	5,773	0.574	MD-90
ALF502R-5	Textron Lycoming	6,970	5.70	12.2		25	0.70	2,250	0.720	BAe 146-100, -200
TFE731-5	Garrett	4,500	3.34	14.4	140	40	0.80	986	0.771	BAe 125-800
PW300	Pratt & Whitney Canada	4,750	4.50	23.0	180	40	0.80	1,113	0.675	BAe 1000
FJ44	Williams Rolls	1,900	3.28	12.8	63.3	30	0.70	600	0.750	
Olympus 593	Rolls Royce/SNECMA	38,000	0	*11.3	410	53	2.00	10,030	1.190	Concorde

OPR = overall pressure ratio TSFC = thrust specific fuel consumption BR = bypass ratio.

* At cruise.

Sources: Reference 87 and manufacturers' literature.

TABLE B-4
Temperature/pressure data for some engines

Engine: Type: Exhaust:	Pegasus Turbofan Separate	J57 Turbojet	JT3D Turbofan Separate	JT8D Turbofan Mixed	JT9D Turbofan Separate	F100-PW-100 Turbofan Mixed w/AB
P_{t2} (psia)	14.7	14.7	14.7	14.7	14.7	13.1
T_{t2} (°F)	59	59	59	59	59	59
$P_{t2.5}$ (psia)	36.1	54	63	60	32.1	
$T_{t2.5}$ (°F)	242	330	360	355	210	
P_{t13} (psia)	36.5		26	28	22.6	39.3
T_{t13} (°F)	257		170	190	130	297
P_{t3} (psia)	216.9	167	200	233	316	316
T_{t3} (°F)	708	660	715	800	880	1,014
P_{t4} (psia)		158	190	220	302	304
T_{t4} (°F)	1,028	1,570	1,600	1,720	1,970	2,566
P_{t5} or P_{t6} (psia)	29.3	36			20.9	38.0
T_{t5} or T_{t6} (°F)	510	1,013			850	1,368
P_{t16} (psia)						36.8
T_{t16} (°F)						303
P_{t6A} (psia)				29		37.5
T_{t6A} (°F)				890		960
P_{t7} (psia)		31.9	28	29	20.9	33.8
T_{t7} (°F)		2,540	890	890	850	3,204
P_{t17} (psia)	36.5		26		22.4	
T_{t17} (°F)	257		170		130	
Bypass ratio α	1.4	n/a	1.36	1.1	5.0	0.69
Thrust (lb)	21,500	16,000	18,000	14,000	43,500	23,700
Airflow (lb/sec)	444	167	460	315	1,495	224

Sources: Reference 88 and manufacturers' literature.

M	$4c_f L^*/D$	I/I^*	T/T^*	P_t/P_t^*	P/P^*	M
3.00	0.522159	1.236568	0.428571	4.234568	0.218218	3.00
3.02	0.525162	1.238290	0.424917	4.315989	0.215847	3.02
3.04	0.528125	1.239993	0.421301	4.398950	0.213512	3.04
3.06	0.531048	1.241677	0.417723	4.483475	0.211214	3.06
3.08	0.533932	1.243343	0.414182	4.569587	0.208951	3.08
3.10	0.536777	1.244989	0.410678	4.657311	0.206723	3.10
3.12	0.539584	1.246618	0.407210	4.746670	0.204529	3.12
3.14	0.542353	1.248228	0.403779	4.837689	0.202368	3.14
3.16	0.545086	1.249820	0.400384	4.930393	0.200240	3.16
3.18	0.547783	1.251394	0.397025	5.024808	0.198144	3.18
3.20	0.550444	1.252951	0.393701	5.120957	0.196080	3.20
3.22	0.553070	1.254490	0.390411	5.218868	0.194046	3.22
3.24	0.555661	1.256012	0.387157	5.318566	0.192043	3.24
3.26	0.558218	1.257517	0.383936	5.420078	0.190069	3.26
3.28	0.560741	1.259005	0.380749	5.523429	0.188125	3.28
3.30	0.563232	1.260477	0.377596	5.628647	0.186209	3.30
3.32	0.565690	1.261932	0.374476	5.735759	0.184321	3.32
3.34	0.568116	1.263371	0.371388	5.844792	0.182460	3.34
3.36	0.570510	1.264794	0.368333	5.955774	0.180626	3.36
3.38	0.572874	1.266201	0.365310	6.068734	0.178819	3.38
3.40	0.575207	1.267592	0.362319	6.183699	0.177038	3.40
3.42	0.577510	1.268968	0.359359	6.300698	0.175282	3.42
3.44	0.579783	1.270328	0.356430	6.419760	0.173552	3.44
3.46	0.582027	1.271674	0.353532	6.540915	0.171845	3.46
3.48	0.584242	1.273004	0.350664	6.664192	0.170163	3.48
3.50	0.586429	1.274320	0.347826	6.789621	0.168505	3.50
3.52	0.588588	1.275621	0.345018	6.917231	0.166870	3.52
3.54	0.590720	1.276907	0.342239	7.047055	0.165258	3.54
3.56	0.592825	1.278180	0.339489	7.179122	0.163668	3.56
3.58	0.594903	1.279438	0.336768	7.313463	0.162100	3.58
3.60	0.596955	1.280682	0.334076	7.450111	0.160554	3.60
3.62	0.598981	1.281913	0.331411	7.589097	0.159029	3.62
3.64	0.600982	1.283130	0.328774	7.730452	0.157524	3.64
3.66	0.602957	1.284334	0.326165	7.874211	0.156041	3.66
3.68	0.604909	1.285524	0.323583	8.020404	0.154577	3.68
3.70	0.606836	1.286701	0.321027	8.169066	0.153133	3.70
3.72	0.608739	1.287866	0.318498	8.320230	0.151709	3.72
3.74	0.610618	1.289018	0.315996	8.473930	0.150303	3.74
3.76	0.612474	1.290157	0.313519	8.630199	0.148917	3.76
3.78	0.614308	1.291283	0.311068	8.789073	0.147549	3.78
3.80	0.616119	1.292398	0.308642	8.950585	0.146199	3.80
3.82	0.617908	1.293500	0.306241	9.114772	0.144867	3.82
3.84	0.619675	1.294590	0.303865	9.281668	0.143552	3.84
3.86	0.621421	1.295669	0.301514	9.451309	0.142255	3.86
3.88	0.623145	1.296735	0.299186	9.623732	0.140974	3.88
3.90	0.624849	1.297791	0.296883	9.798973	0.139710	3.90
3.92	0.626532	1.298834	0.294603	9.977069	0.138463	3.92
3.94	0.628195	1.299867	0.292346	10.15806	0.137231	3.94
3.96	0.629838	1.300888	0.290113	10.34197	0.136015	3.96
3.98	0.631461	1.301899	0.287902	10.52886	0.134815	3.98
4.00	0.633065	1.302899	0.285714	10.71875	0.133631	4.00

APPENDIX J

TURBOMACHINERY STRESSES AND MATERIALS

J-1 INTRODUCTION

Even though the focus of this textbook is the aerothermodynamics of the gas turbine engine, the importance of the engine structure is also very significant. Because of its importance, this appendix addresses the major stresses of the rotating components and the properties of materials used in these components. The rotating components of the compressor and turbine have very high momentum, and failure of one part can be catastrophic, with a resulting destruction of the engine and, in the extreme, the aircraft. This is especially true of the "critical" parts of the turbomachinery such as the long first-stage fan blades and the heavy airfoils and disks of the cooled high-pressure turbine.

Over their lives, the rotating parts must endure in a very harsh environment where the loads are very dependent on the engine use. For example, an engine developed for a commercial aircraft will not be subjected to as many throttle excursions as one developed for a fighter aircraft. As a result, the "hot section" [combustor and turbine(s)] of the fighter engine will be subjected to many more thermal cycles per hour of operation than that of the commercial aircraft.

The main focus of the analytical tools developed in this appendix is on the fundamental source of stresses in rotating components—the centrifugal force. To get some idea of the brutal climate in which these components must live, the centrifugal force experienced by an element of material rotating at 10,000 rpm with a radius of 1 ft (0.3 m) is equivalent to more than 34,000 g. Yet, there are many other forces at work that can consume the life of (or

destroy) rotating parts, all of which must be considered in the design process. Some of the most important include:

- Stresses due to bending moments like those due to the lift on the airfoils or pressure differences across disks.
- Buffeting or vibratory stresses that occur as the airfoils pass through nonuniform incident flows such as the wakes of upstream blades. This can be most devastating when the *blade passing* frequency coincides with one of the lower natural frequencies of the airfoils.
- Airfoil or disk flutter, an aeroelastic phenomenon in which a natural frequency is spontaneously excited, the driving energy being extracted from the flowing gas. This is most often found in fan and compressor rows, and once it has begun, the life of the engine is measured in minutes.
- Torsional stresses that result from the transfer of power from the turbine to the compressor.
- Temperature gradients that can give rise to very high stresses. These can be very extreme during throttle transients when the engine is moving from one power setting to another. These cyclic thermal stresses extract life from components, especially in the hot section of fighter engines. This is commonly called *thermal* or *low-cycle* fatigue.

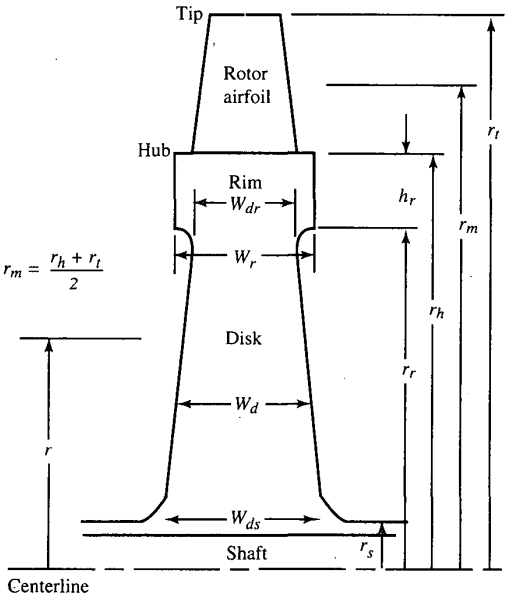

FIGURE J-1
Turbomachinery rotor nomenclature.

- Local stress concentrations which result from holes, slots, corners, and cracks—the most feared of all.
- Foreign object damage (FOD) and domestic object damage (DOD) that result from external and internal objects, respectively. The need to withstand FOD or DOD can dramatically impact the design. The use of lightweight, nonmetallic materials for large fan blades has been prevented for several decades due to requirement that they withstand bird strikes.

Each of the above areas and many others are included in the design of engine components and material selection. After these are accounted for, an *allowable working stress* is developed and commonly used for the principal tensile stresses alone.

The next section analyzes dominant stresses in the rotating components. Figure J-1 depicts a turbine rotor with its airfoils, rim, and disk. A compressor or fan rotor is constructed similarly. However, the portion of the airfoil stresses carried by the compressor or fan's rim is much greater than that of a turbine rotor; hence, its disk is either much smaller or nonexistent. We consider the principal stresses of each part, starting with the airfoils.

J-2 TURBOMACHINERY STRESSES

Rotor Airfoil Centrifugal Stress σ_c

We start by considering the force in an airfoil at a cross section (see Fig. J-2). At any radius r, the force must restrain the centrifugal force on all the material

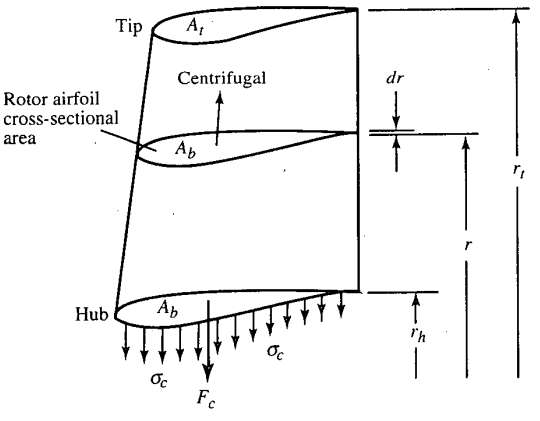

FIGURE J-2
Rotor airflow centrifugal stress nomenclature.

beyond it. Thus the hub or base of the airfoil must experience the greatest force. The total centrifugal force acting on A_h is

$$F_c = \int_{r_h}^{r_t} \rho\omega^2 A_b r\, dr \tag{J-1}$$

so that the principal tensile stress is

$$\sigma_c = \frac{F_c}{A_h} = \rho\omega^2 \int_{r_h}^{r_t} \frac{A_b}{A_h} r\, dr \tag{J-2}$$

The airfoil cross-sectional area usually tapers down or reduces with increasing radius, which, according to Eq. (J-2), has the effect of reducing σ_c. If the taper is *linear,* we can write

$$\frac{A_b}{A_h} = 1 - \left(1 - \frac{A_t}{A_h}\right)\left(\frac{r - r_h}{r_t - r_h}\right) \tag{J-3}$$

and Eq. (J-2) becomes

$$\sigma_c = \rho\omega^2 \left[\frac{A}{2\pi} - \left(1 - \frac{A_t}{A_h}\right)\int_{r_h}^{r_t} \left(\frac{r - r_h}{r_t - r_h}\right) r\, dr\right] \tag{J-4}$$

where A is the flow path annulus area $\pi(r_t^2 - r_h^2)$. Integration of Eq. (J-4) gives

$$\sigma_c = \frac{\rho\omega^2 A}{4\pi}\left[2 - \frac{2}{3}\left(1 - \frac{A_t}{A_h}\right)\left(1 + \frac{1}{1 + r_h/r_t}\right)\right] \tag{J-5}$$

Equation (J-5) has an upper limit (corresponding to $r_h/r_t = 1$) of

$$\boxed{\sigma_c = \frac{\rho\omega^2 A}{4\pi}\left(1 + \frac{A_t}{A_h}\right)} \tag{J-6}$$

This equation reveals the basic characteristic that σ_c is proportional to $\rho\omega^2 A$. It also shows that tapering can, at most, reduce the stress of a *straight* airfoil (i.e., $A_t = A_h$) by half (i.e., $A_t = 0$).

Common practice in the industry is to refer to $\omega^2 A$ as the term AN^2 because it is easy to calculate and use. The COMPR computer program calculates and outputs AN^2 for each stage for proper material selection. The TURBN computer program permits the turbine to be sized based on a user input value of AN^2. When another sizing criterion is used in TURBN, the value of AN^2 is calculated and output for each stage.

We note that

$$AN^2 = A\omega^2\left(\frac{30}{\pi}\right)^2 \tag{J-7}$$